VILNIUS UNIVERSITY

MARIUS DAGYS

FUNCTION OF MULTICOPPER OXIDASES ADSORBED ON GOLD NANOPARTICLES

Doctoral dissertation

Physical sciences, biochemistry (04P)

Vilnius, 2012

Doctoral dissertation was prepared during year 2007 – 2011 in the Institute of Biochemistry of Vilnius university, Lithuania.

Scientific supervisor:

Prof. habil. dr. Juozas Kulys, true member of Lithuanian Academy of Sciences (Institute of Biochemistry, Vilnius university, physical sciences, biochemistry – 04P).

VILNIAUS UNIVERSITETAS

MARIUS DAGYS

ADSORBUOTŲ ANT AUKSO NANODARINIŲ DAUGIAVARIŲ OKSIDAZIŲ FUNKCIJA

Daktaro disertacija

Fiziniai mokslai, biochemija (04P)

Vilnius, 2012

Disertacija rengta 2007 – 2011 metais Vilniaus Universiteto Biochemijos institute.

Mokslinis vadovas:

Prof. habil. dr. Juozas Kulys, LMA tikrasis narys

(Vilniaus Universiteto Biochemijos institutas, fiziniai mokslai, biochemija – 04P).

CONTENTS

ABBREVIATIONS

AU	Arbitrary unit(s)
ABTS	2,2'-azino-bis(3-ethylbenzthiazoline-6-sulphonic acid)
AuNP(s)	Gold nanoparticle(s)
CV	Cyclic voltammetry
DET	Direct electron transfer
DLS	Dynamic light scattering
EPR	Electron paramagnetic resonance
ET	Electron transfer
FCC	Face – centred cubic crystal lattice
HQU	Hydroquinone
IET	Internal electron trasnfer
K_M	Apparent Michaelis - Menten constant
K_i	Inhibition constant
k_{cat}	Catalytic constant
k_{obs}	Enzyme turnover constant
k_{ox}	Bimolecular enzyme and substrate reactivity constant
MET	Mediated electron transfer
NHE	Standard (normal) hydrogen electrode
NIR	Near infrared radiation
pI	Isoelectric point
PLL	Poly-L-lysine
PYR	Catechol
QCM-D	Quartz crystal microbalance with dissipation monitoring
RDE	Rotating disk gold electrode

R_s	Stokes radius
SEM	Scanning electron microscopy
SERS	Surface – enhanced Raman spectrophotometry
SYR	Syringaldazine

INTRODUCTION

In this work bioelectrocatalytic functions of multicopper oxidases are studied. Well-defined multicopper oxidases are laccase (benzenediol: oxygen oxidoreductase, EC 1.10.3.2), ascorbate oxidase (L-ascorbate: oxygen oxidoreductase, EC 1.10.3.3), and human ceruloplasmin (ferroxidase, iron(II): oxygen oxidoreductase, EC 1.16.3.1). A combination of detailed spectroscopic studies and X-ray crystallography has revealed that all multicopper oxidases contain at least one blue copper or T1 site and a T2/T3 trinuclear cluster as the minimal functional unit. Human ceruloplasmin is presently unique among the multicopper oxidases in that it possesses additional copper centres (Solomon, Sundaram et al. 1996). All multicopper oxidases couple the four - electron reduction of dioxygen to water, bypassing hydrogen peroxide formation, with the oxidation of substrate (Morozova, Shumakovich et al. 2007). In living organism these enzymes perform various functions involving oxidation of organic substances by different chemical mechanisms.

Multicopper oxidase, i.e. laccase due to its capability to oxidize numerous organic and inorganic substrates and reduce dioxygen directly to water without formation of reactive oxygen intermediates (Solomon, Sundaram et al. 1996) is the most interesting redox enzyme used for biosensors building (Kruus 2000; Duran, Rosa et al. 2002; Minussi, Pastore et al. 2002) and cathodes of biofuel cells (Yan, Su et al. 2007; Coman, Vaz-Dominguez et al. 2008; Gallaway, Wheeldon et al. 2008; Gallaway and Calabrese Barton 2009) It was discovered in the Japanese lacquer tree *Rhus vernicifera* in 1883 (Yoshida 1883). Laccases are found both in higher plants and fungi. Plant laccases are involved in lignin synthesis, catalysing polymerization of monomeric units (p-coumaryl, coniferyl, and synapyl alcohols), following the free radical mechanism while fungal laccases catalyse lignin degradation, fungus development and morphogenesis, pathogenesis, and detoxication (Thurston 1994; Zhao and Kwan 1999; Leonowicz, Cho et al. 2001).

Human ceruloplasmin (ferroxidase, iron(II):oxygen oxidoreductase, EC 1.16.3.1) is the most complex multicopper oxidase (Solomon, Sundaram et al. 1996). Its molecular structure is composed of six compact domains, with large loop insertions, and it contains six tightly bound copper atoms: three ions in the T2/T3 cluster and three coppers bound to the three T1-binding sites. In addition, human ceruloplasmin is a monomer with a significant amount of glycosylation (7-8%) (Lindley, Card et al. 1997).

Electron transfer is ubiquitous in biological and chemical systems. Thus, understanding and controlling this process comprise one of the broadest and most active research areas of science nowadays. Usually, electron transfer occurs in nature in connection with energy transduction. The theoretical framework of biological electron transfer is increasingly well understood, and several properties, such as redox enzymes and proteins carrying out many key reactions of biological and technological importance, make biological redox centres good systems for exploitation (Gilardi and Fantuzzi 2001). Particularly interesting is development of direct electron transfer (DET) bioelectrocatalytic systems between the redox - active biomolecule and the electrode surface (Freire, Pessoa et al. 2003). The first publications on DET for any large redox protein with enzymatic activity were concerned with a high potential laccase from the basidiomycetes *Trametes versicolor* (Berezin, Bogdanovskaya et al. 1978; Tarasevich, Yaropolov et al. 1979). The authors of these papers showed that in the presence of molecular oxygen, laccase modified carbon electrodes exhibited DET. The mechanism of DET between electrodes and multicopper oxidases associated with reduction of molecular oxygen and oxidation of substrates is not fully understood. The question is especially relevant for electrochemical investigations of high potential fungal laccases (Shleev, Christenson et al. 2005).

In this work DET between gold nanoparticle (AuNP) surface and active centres of multicopper oxidases, specifically laccases and human ceruloplasmin, are studied. AuNP exhibit optical and electronic properties that can be exploited in a variety of detection methodologies (Pong, Elim et al.

2007). Their inertness provides a basis for its characterization as a biocompatible material and a favourable environment for functionalization with macromolecules, namely immunoglobulins, enzymes, lectins, proteins, streptavidin, DNA, etc. (Katz, Willner et al. 2004; Yanez-Sedeno and Pingarron 2005; Pingarron, Yanez-Sedeno et al. 2008) Biomolecules combined with the surface of AuNP retain the biologic activity, where particularly proteins have more freedom in orientation (Liu, Leech et al. 2003). If multicopper oxidases would exhibit DET and DET – based oxygen bioreduction, this research, besides general fundamental knowledge of AuNP - enzyme electron transfer mechanisms, would contribute to construction of high current density biofuel cell biocathodes, as they require utilization of three-dimensional structures for higher current output (Bartlett 2008), what is achievable by AuNP multilayer assemblies.

Aim of work is to investigate bioelectrochemical DET systems containing multicopper oxidases and gold nanoparticles by using basic electrochemistry, quartz–crystal microbalance and surface enhanced Raman spectroscopy. As multicopper oxidases laccases from *Trametes hirsuta* and *Trichaptum abietinum* and human ceruloplasmin were used. The goals of the work had been set up:

- To establish biochemical properties of newly purified *Trichaptum abietinum* laccase, including redox potential of T1 copper site;

- to assemble DET bioelectrochemical systems containing AuNPs and multicopper oxidases covered gold electrodes, analyse them utilizing electrochemical and surface analysis techniques;

- to analyse multilayer AuNP – laccase systems by using quartz crystal microbalance sensor with dissipation monitoring.

Novelty of work:

- For the first time DET between gold nanoparticle and active centre of laccase has been reported. The current densities are comparable to current densities of carbon based biofuel cell cathodes.

- It has been established that T1 copper site traces are not detectable at close proximity to the surface of AuNP. A mixed type electron transfer (mediated and direct) mechanism is involved in these systems containing immobilized enzymes.

- For the first time it was revealed that laccase dependent oxygen reduction by DET speed depends on AuNP size; larger (70 – 90 nm) AuNPs facilitate slower heterogeneous electron transfer in comparison to medium sized (40 – 50 nm) AuNPs.

Defended statements:

1. Laccase from *Trichaptum abietinum* belongs to high redox potential laccase with the T1 copper site redox potential of 714 ± 12 mV *vs.* NHE.

2. Laccases from *Trametes hirsuta and Trichaptum abietinum*, also human ceruloplasmin, exhibit direct electron transfer between active centres of the enzyme and gold nanoparticles.

3. Laccases from *Trametes hirsuta and Trichaptum abietinum*, exhibit efficient direct electron transfer based oxygen bioreduction on gold nanoparticle.

4. *Trametes hirsuta* and *Trichaptum abietinum* laccases change orientation of gold nanoparticle surface when changing electrode potential, T1 copper site is not detectable near the gold nanoparticle surface by surface enhanced Raman spectroscopy measurements.

5. Heterogeneous electron transfer speed in gold nanoparticle - laccase bioelectrocatalytic systems depend on nanoparticle size. In general larger diameter (60 – 90 nm) AuNPs systems exhibit slower ET than medium sized (40 – 50 nm) AuNP systems. Heterogeneous ET constants can reach as high as

45 s^{-1} and 11 s^{-1} in *Trichaptum abietinum* and *Trametes hirsuta* laccase DET bioelectrocatalytic assays, respectively.

1. LITERATURE REVIEW

1.1. Multicopper oxidases

The multicopper oxidases belong to the group of enzymes that can be defined by their spectroscopy, sequence homology, and reactivity. The currently well-defined multicopper oxidases are laccase, ascorbate oxidase, and human ceruloplasmin. Other multicopper oxidases that have been isolated and characterized are phenoxazinone synthase (EC 1.10.3.4), bilirubin oxidase (EC 1.3.3.5), dihydrogeodin oxidase (EC 1.10.3.-) and sulochrin oxidase (EC 2.10.3.8). A combination of detailed spectroscopic studies and X-ray crystallography has revealed that all multicopper oxidases contain at least one blue copper or T1 site and a T2/T3 trinuclear cluster as the minimal functional unit. Ceruloplasmin is presently unique among the multicopper oxidases in that it possesses additional copper centres (Solomon, Sundaram et al. 1996). Functionally, all multicopper oxidases couple the four-electron reduction of dioxygen to water, bypassing hydrogen peroxide formation, with the oxidation of substrate, according to equation (Morozova, Shumakovich et al. 2007):

$$AH_2 + \tfrac{1}{2}\,O_2 \rightarrow A + H_2O \tag{1.1}$$

In the well-characterized enzymes (laccase, ascorbate oxidase, and ceruloplasmin), the substrate is oxidized by one electron. In the less well-characterized ones, it has not been established whether substrate oxidation occurs by two electrons or by two sequential one-electron oxidations (Solomon, Sundaram et al. 1996).

Spectroscopic studies combined with crystallography have provided significant insight into the mechanism of reduction of dioxygen by the multicopper oxidases (Fig. 1.1) (Shin, Sundaram et al. 1996). The fully reduced site reacts with O_2 to generate a peroxide-level intermediate, best described as a bridged hydroperoxide species. This is activated for further reduction (as compared to

reaction of the peroxide or reversible O_2 binding) to generate the „native intermediate" which is more appropriately described as a hydroxide product (one additional electron from the type 1 and another from the type 2) bridging the T2 and one of the T3 coppers in the trinuclear copper cluster. Thus, the reduction of O_2 by the fully reduced enzyme occurs in two, two-electron steps. The first is rate-determining and the second is fast.
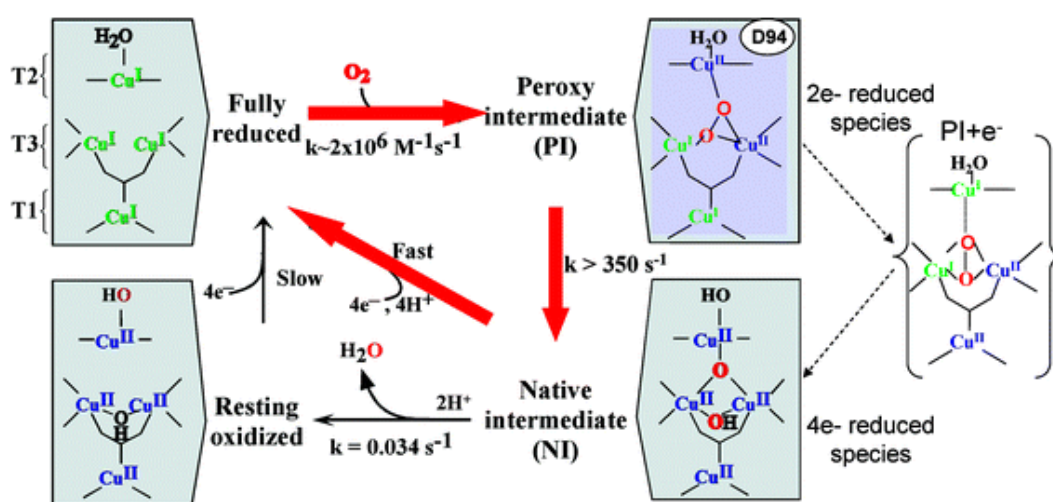
Fig. 1.1. Mechanism proposed for the four-electron reduction of O_2 to H_2O by the multicopper oxidases (Solomon, Sundaram et al. 1996).

1.1.1. Laccase functions

Laccase is among the few enzymes studied since the late 19th century. It was first discovered in the Japanese lacquer tree *Rhus vernicifera* (Yoshida 1883). This makes it one of the first enzymes ever described. Later, other plant laccases were found and partly described: *Rhus succedanea*, *Acer pseudoplatanus*, *Pinus taeda*, *Populus euramericana*, *Liriodendron tulipifera*, and *Nicotiana tabacum* (Sterjiades, Dean et al. 1992; Bao, O'Malley et al. 1993; Kiefer-Meyer, Gomord et al. 1996; LaFayette, Eriksson et al. 1999; Ranocha, McDougall et al. 1999; Sato, Wuli et al. 2001).

Laccases are also common in fungi (Baldrian 2006). Actually, they have been found in most of the higher fungi. They occur in fungal causative agents of soft

rots, in most bracket fungi causing white rot, in soil saprotrophs and plant pathogens, and in many agarics, including cultivated edible fungi: champignon, pleurotus, and medicinal shiitake *Lentinula edodes*. Other laccase producers are wood-degrading fungi: *Trametes (Coriolus) versicolor*, *Trametes hirsuta*, *Trametes ochracea*, *Trametes villosa*, *Trametes gallica*, *Cerrena maxima*, *Coriolopsis polyzona*, *Lentinus tigrinus*, *Pleurotus eryngii*, etc. Laccases occur in saprophytic ascomycetes inhabiting composts (*Myceliophthora thermophile* and *Chaetomium thermophile*) and in the soil hyphomycete *Mycelia sterlia* INBI 2-26. They appear to be involved in humification (Berka, Schneider et al. 1997; Chefetz, Chen et al. 1998; Vasil'chenko, Koroleva et al. 2000).

Not all laccase functions are known yet (Thurston 1994; Kiefer-Meyer, Gomord et al. 1996; Mayer and Staples 2002). It is believed that plant laccases are involved in lignin production, catalysing polymerization of monomeric units (p-coumaryl, coniferyl, and synapyl alcohols), following the free radical mechanism. The main physiological roles of fungal laccases are lignin degradation, fungus development and morphogenesis, pathogenesis, and detoxication (Thurston 1994; Zhao and Kwan 1999; Leonowicz, Cho et al. 2001).

Biochemical properties

All plant laccases are monomeric proteins with molecular weights within 90 - 130 kDa and high carbohydrate contents (22–45%). Little is known about higher plant laccases, probably because of their location in cell walls (Morozova, Shumakovich et al. 2007).

Current knowledge about the structure and physico - chemical properties of fungal proteins is based on the study of purified proteins. The laccase molecule, as an active holoenzyme form, is a dimeric or tetrameric glycoprotein, usually containing -per monomer- four copper (Cu) atoms bound to three redox sites (Type 1, Type 2 and Type 3 Cu pair). The molecular mass of the monomer ranges from about 50 to 100 kDa with acidic isoelectric point around pH 4.0. The high level of glycosylation (with covalently linked

carbohydrate moieties ranging from 10 - 50% of the total weight, depending on the species or the heterologous host) may contribute to the high stability of the enzyme (Durán, Rosa et al. 2002). Several laccase isoenzymes have been detected in many fungal species. More than one isoenzyme is produced in most white-rot fungi.

For the catalytic activity a minimum of four copper atoms per active protein unit is needed. Three types of copper can be distinguished using UV/visible and electronic paramagnetic resonance (EPR) spectroscopy. Type 1 Cu at its oxidised resting state is responsible for the blue colour of the protein at an absorbance of approximately 610 nm and is EPR detectable, Type 2 Cu does not confer colour but is EPR detectable and Type 3 Cu atoms consists of a pair of Cu atoms in a binuclear conformation that give a weak absorbance in the near UV region but no detectable EPR signal ((Morozova, Shumakovich et al. 2007) and citations therein). The Type 2 and Type 3 copper sites are close together and form a trinuclear centre that are involved in the catalytic mechanism of the enzyme (Thurston 1994).

The redox potential of the Type 1 site has been determined for many laccases using different mediators and varies from 430 mV (*vs*. NHE) for the laccase from *Rhus vernicifera* tree up to 780 mV for fungal laccase from *Polyporus versicolor* (Xu, Brown et al. 1996; Gianfreda, Xu et al. 1999). More specifically, from an electrochemical point of view based on the primary structures of the enzymes all laccases can be divided into three groups depending on the $E°'$ value of the T1 site: low, middle and high potential laccases. The low potential group includes laccases from trees, e.g., *Rhus vernicifera* with a potential of the T1 site of about 430 mV. The middle group includes laccases from basidiomycetes like *Myceliophthora thermophila* and *Coprinus cinereus*. These enzymes have a potential of the T1 site ranging from 470 to 710 mV versus NHE. The high potential laccases (e.g., those from *Trametes* (*Polyporus, Coriolus*) *hirsuta* (*hirsutus*), *T. versicolor*, *T. villosa*) all have a potential of the T1 site of about 780 mV versus NHE ((Shleev, Tkac et al. 2005) and citations therein). It was previously found that the catalytic

efficiency (k_{cat}/K_M) of laccases for some reducing substrates depended linearly on the redox potential of the Type 1 copper, in the sense that the higher the potential of the Type 1 site the higher the catalytic efficiency (Xu, Brown et al. 1996). That is why laccases with a high redox potential of the Type 1 site are of special interest in biotechnology, e.g., for bleaching and bioremediation.

Catalytic properties

To function, laccase depends on Cu atoms distributed among the three different binding sites. Cu atoms play an essential role in the catalytic mechanism. There are three major steps in laccase catalysis. The Type 1 Cu is reduced by a reducing substrate, which therefore is oxidized. The electron is then transferred internally from Type 1 Cu to a trinuclear cluster made up of the Type 2 and Type 3 Cu atoms (Fig. 1.2). The O_2 molecule is reduced to water at the trinuclear cluster ((Morozova, Shumakovich et al. 2007) and citations therein).
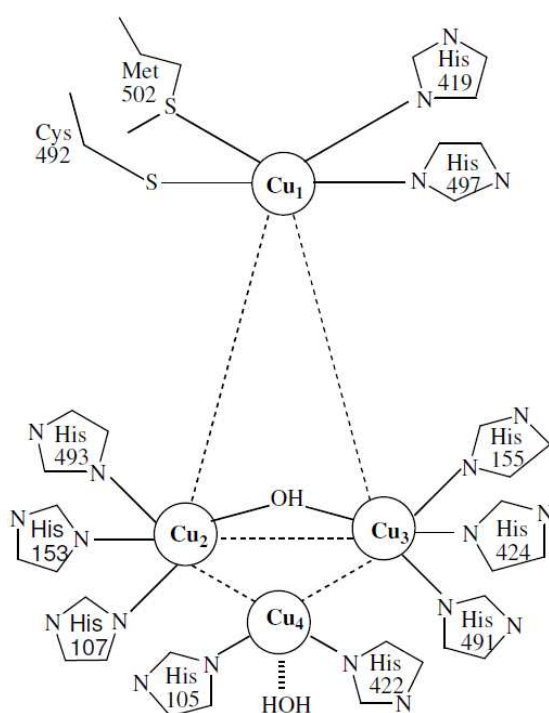

Fig. 1.2. Illustration of the active site of laccase showing the relative orientation of the copper atoms (Enguita, Martins et al. 2003).

The O_2 molecule binds to the trinuclear cluster for asymmetric activation and it is postulated that the O_2 binding pocket appears to restrict the access of

oxidizing agents other than O_2. H_2O_2 is not detected outside of laccase during steady state laccase catalysis indicating that a four electron reduction of O_2 to water is occurring. A one-electron substrate oxidation is coupled to a four-electron reduction of oxygen so the reaction mechanism cannot be straightforward. Laccase must operate as a battery, storing electrons from individual substrate oxidation reaction to reduce molecular oxygen. In fact, it appears that bound oxygen intermediates are also involved ((Gianfreda, Xu et al. 1999) and citations therein). Details of the O_2 reduction have not been fully elucidated and continue to be studied.

From a mechanistic point of view, the reactions catalysed by laccases for bioremediatory and biotechnological applications can be represented by one of the schemes shown in Fig. 1.3. The simplest case (Fig. 1.3a) is the one in which the substrate molecules are oxidized to the corresponding radicals by direct interaction with the copper cluster. Laccases use oxygen as the electron acceptor to remove protons from the phenolic hydroxyl groups. This reaction gives rise to radicals that can spontaneously rearrange, which can lead to fission of C-C or C-O bonds of the alkyl side chains, or to cleavage of aromatic rings. The radical can further undergo laccase-catalysed oxidation (e.g., to form quinone from phenol) or nonenzymatic reactions (e.g., hydration or polymerization).

Frequently, however, the substrates of interest cannot be oxidized directly by laccases, either because they are too large to penetrate into the enzyme active site or because they have high redox potential. By mimicking nature, it is possible to overcome this limitation with the addition of so-called "chemical mediators", which are suitable compounds that act as intermediate substrates for the laccase, whose oxidized radical forms are able to interact with the bulky or high redox-potential substrate targets (Fig. 1.3b) ((Kunamneni, Plou et al. 2008) and citations therein).
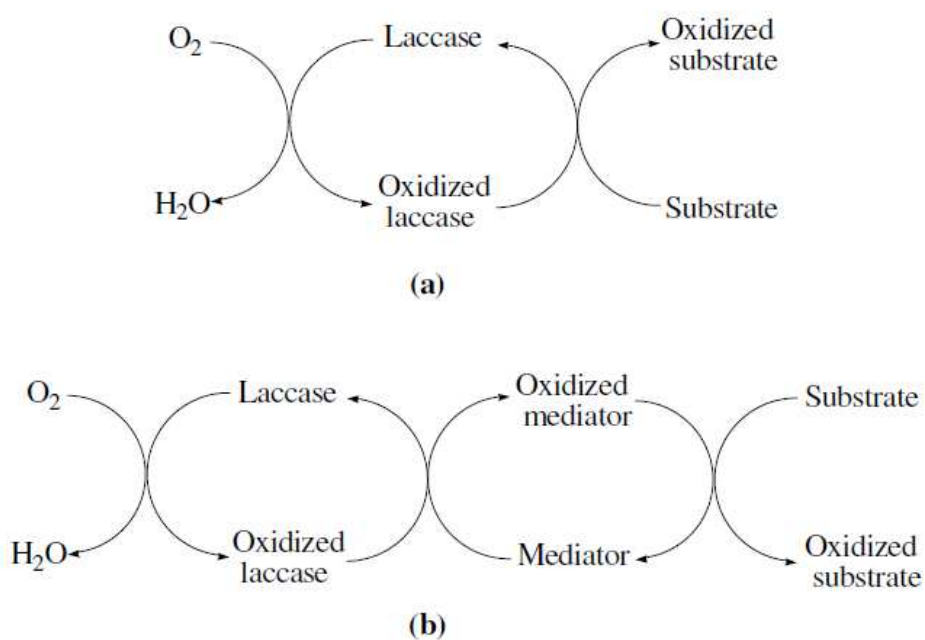
Fig. 1.3. Schematic representation of laccase – catalysed redox cycles for substrates oxidation in the absence **(a)** or presence **(b)** of chemical mediators (Kunamneni, Plou et al. 2008).
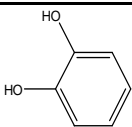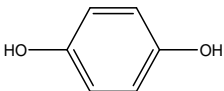
The reducing substrate spectrum for laccase is diverse (Yaropolov, Skorobogat'ko et al. 1994; Messerschmidt 1994; Thurston 1994), ranging from inorganic/organic metal complexes (such as $Fe(EDTA)^{2-}$ (Wherland, Holwerda et al. 1975), and ferrocyanide, anilines, benzenethiols, and phenols to other redox inorganic, organic, or biological compounds (Xu 1996). Phenols are typical laccase substrates because their redox potentials (ranging from 0.5 to 1.0 V *vs.* NHE) are low enough to allow electron abstraction by the Type 1 Cu. Commonly used phenolic substrates are syringaldazine, 2,6-dimethoxyphenol and guaiacol; however, laccases are also able to oxidize electron donor substrates such as ABTS [2,2′-azino-bis(3-ethylbenzothiazoline-6-sulfonic acid)] or ferrocyanide [$K_4Fe(CN)_6$] (Sakurai 1992; Yaropolov, Skorobogat'ko et al. 1994; Giardina, Palmieri et al. 1999). Phenolic substrates are oxidized to phenoxy radicals, which, depending on reaction conditions, can spontaneously polymerize via radical coupling or rearrange themselves leading to quinones (through disproportionation), alkyl–aryl cleavage, Cα oxidation, cleavage of Cα–Cβ bond or aromatic ring (Kawai, Umezawa et al. 1988). In general,

laccase has low specificity for these reducing substrates, in contrast to its strong preference for O_2 as the oxidizing substrate (Gianfreda, Xu et al. 1999). Laccase can be inhibited by various reagents. Small anions such as halides (excluding iodide (Xu 1996; Kulys, Bratkovskaja et al. 2005)), azide, cyanide, and hydroxide bind to the T2/T3 site (Koudelka and Ettinger 1988), resulting in an interruption of the internal electron transfer and activity inhibition. The inhibition order of $F^- > Cl^- > Br^-$ is attributed to limited accessibility of the T2/T3 copper atoms. Different laccases can have quite different tolerances toward inhibition by various halide species. If the inhibition is mainly limited by the size of the putative channel that leads to the T2/T3 site, then the observed variation in inhibition constant Ki indicates a significant difference among various laccases. While the plant *Rhus* laccase might have a "wide-open" channel leading to the T2/T3 site (as indicated by the similar Ki values for F^-, Cl^-, and Br^-), fungal laccases seem to have T2/T3 channels with a defined "cutoff diameter" that corresponds to the diameter of hydrated chloride or bromide ((Xu 1996) and citations therein). The halide inhibition study does not include iodide, because it reacts with the T1 site and serves as a substrate for laccase (Xu 1996). Laccase inhibition by OH^- can dominate catalysis at alkaline pH (Xu 1997). Other inhibitors include metal ions (e.g., Hg^{2+}), fatty acids, sulfhydryl reagents, hydroxyglycine and cationic quaternary ammonium detergents (Bollag and Leonowicz 1984; Banerjee and Vohra 1991; Coll, Tabernero et al. 1993; Yaropolov, Skorobogat'ko et al. 1994), whose reactions may involve amino acid residue modification, copper chelation, or conformational change. Laccases generally are more stable at alkaline pH than at acidic pH, probably due to the OH^- inhibition on autooxidation (Nishizawa, Nakabayashi et al. 1995; Xu, Brown et al. 1996). In addition to autooxidation, laccases can be inactivated by loss of Cu or other conditions (proteolysis, conformational denaturation, etc.) (Gianfreda, Xu et al. 1999).

1.1.2. Laccase from *Trametes hirsuta*

White rot basidiomycete *Trametes hirsuta* produces several laccase isoenzymes with different enzymatic and physico-chemical properties (Xu, Brown et al. 1996; Schneider, Caspersen et al. 1999; Shleev, Zaitseva et al. 2003). *Trametes hirsuta* laccase isoenzymes have molecular masses ranging from 55 to 82 kDa, a pI between 3.5 and 7.4, pH optima between 2.5 and 4.5, and a carbohydrate composition from 11 to 15%. The catalytic site of the laccase consists of four copper ions per enzyme molecule, which can be classified into three types: one type 1 (T1), one type 2 (T2) and two type 3 (T3) copper ions. Laccase has strong absorbance at 610 nm and 330 nm due to the T1 and T3 coppers respectively. The T3 copper shows fluorescence emission near 418 nm and an excitation maximum at 332 nm (Schneider, Caspersen et al. 1999).

The enzyme used in our research contained one form of the monomeric protein with a molecular weight of 69 kDa as determined by SDS-PAGE and HPLC (data not shown). Laccase has a pH-optimum of 3.5 – 4.5; the protein has significant carbohydrate content – $12 \pm 1\%$. It was found that the carbohydrate moieties of the enzyme consisted of mannose and N-acetylglucosamine. The laccase is highly stable retaining 50% of their initial activity after incubation at 50 °C for about 60 h. Afterwards kinetic investigations of the laccases were performed and the catalytic constants (k_{cat} and K_M) measured for some organic and inorganic compounds are (Shleev, Morozova et al. 2004):

Substrate	K_M, μM	k_{cat}, s^{-1}
$K_4[Fe(CN)_6]$	180 ± 20	400 ± 40
Catechol	140 ± 10	390 ± 40
Hydroquinone	61 ± 6	450 ± 40

It can be seen that *Trametes hirsuta* laccase possess large catalytic constants with respect to all organic substrates, as well as with inorganic substance $K_4[Fe(CN)_6]$.

The potential of the T1 copper was measured by direct redox titration using mediators. The reduction of the T1 copper was accompanied by the disappearance of the blue absorbance band at 610 nm. The redox potential of the laccase was estimated as 780 mV *vs.* NHE, as expected for high – potential laccases (Shleev, Morozova et al. 2004).

1.1.3. Human ceruloplasmin

Human ceruloplasmin (ferroxidase, iron(II):oxygen oxidoreductase, EC 1.16.3.1) is the most complex of multicopper oxidases (Solomon, Sundaram et al. 1996). Contrary to three-domain structures of other multicopper oxidases, such as ascorbate oxidase, bilirubin oxidase, and laccase containing four copper ions, ceruloplasmin composed of six compact domains, with large loop insertions, and it contains six tightly bound copper atoms (Fig. 1.4): three ions in the T2/T3 cluster and three coppers bound to the three T1-binding sites. In addition, human ceruloplasmin is a monomer with a significant amount of glycosylation (7-8%) (Lindley, Card et al. 1997). The three copper ions of the trinuclear cluster lie at the interface between the first and last domains, 1 and 6 respectively, possessing ligands from each domain, an arrangement also seen in the structures of ascorbate oxidase and laccase (Messerschmidt, Ladenstein et al. 1992; Piontek, Antorini et al. 2002) (Fig. 1.4). The remaining three copper atoms are mononuclear centres held by intra-domain sites; those located on domains 4 and 6 have a typical T1 copper environment with a set of four ligands, two histidines, one methionine and one cysteine (Fig. 1.4, $T1_{CysHis}$ and $T1_{Remote}$ copper sites), whereas the one (Fig. 1.4, $T1_{PR}$ site) located in domain 2 has a different structure in that it lacks the methionine, which is replaced in the amino acid sequence by a leucine residue, Leu329, analogous to the T1 site of some fungal laccases (Shleev, Jarosz-Wilkolazka et al. 2005). The $T1_{CysHis}$ centre is connected to the T2/T3 cluster *via* the highly conserved Cys-2His

electron transfer (ET) pathway, also found in the structures of ascorbate oxidase (Messerschmidt, Ladenstein et al. 1992) and laccase (Piontek, Antorini et al. 2002), across a distance of approximately 12–13 Å. It is believed that O_2 is bound and reduced to two H_2O molecules at the three-nuclear copper cluster, whereas the mononuclear $T1_{CysHis}$ site is able to accept electrons from reduced substrates of ceruloplasmin, *e.g.* Fe^{2+} (Solomon, Sundaram et al. 1996).
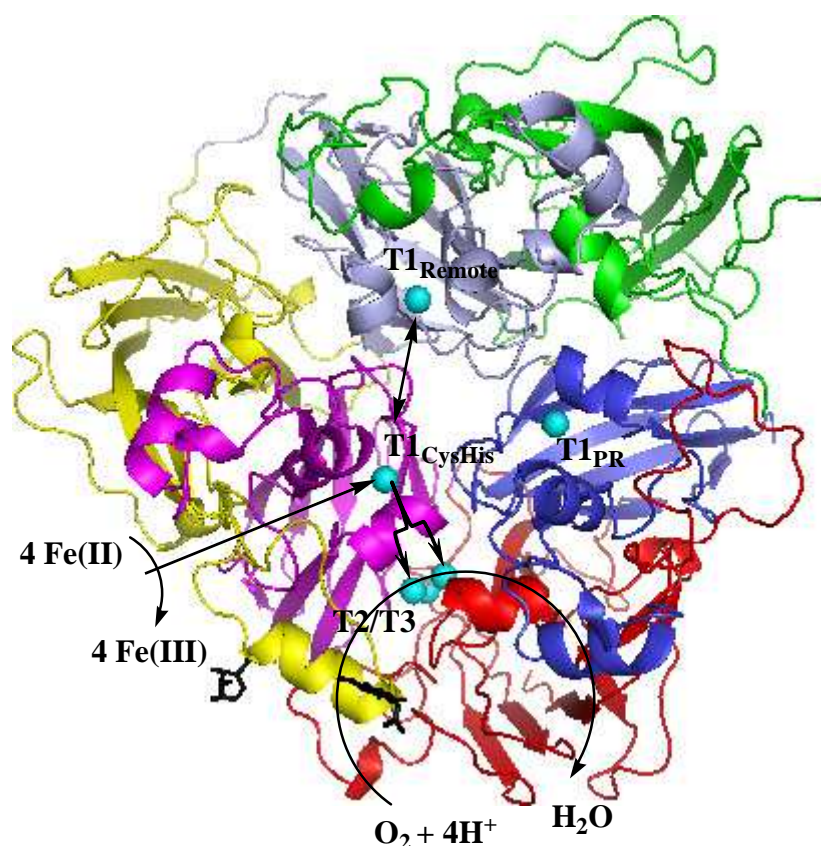
Fig 1.4. Proposed mechanisms of Fe(II) oxidation and O_2 reduction by human ceruloplasmin. The six domains are colour coded as red (1), blue (2), green (3), light blue (4), yellow (5), and purple (6). Six copper ions are shown in cyan and carbohydrates (*n*-acetil-*d*-glucosamine) are in black.

The redox potentials of the $T1_{CysHis}$ and $T1_{Remote}$ copper sites (E_{T1}) of human ceruloplasmin were measured by mediated redox titration and found to be 490 mV and 580 mV *vs*. NHE (Deinum and Vänngård 1973). As for the $T1_{PR}$ site, its E_{T1}-value was estimated to be very high, approximately 1000 mV *vs*. NHE (Machonkin and Solomon 2000).

The possibility of direct electron transfer (DET) between ceruloplasmins from different origins and electrodes were at focus in investigations in different laboratories (Kuznetsov, Mestechkina et al. 1977; Razumas, Vidugiris et al. 1986; Studničková, Pitřincová et al. 1991) due to the huge medical importance of this protein known since 1952 (Scheinberg and Gitlin 1952). However, no electrochemical contact between the enzyme and any electrode (Kuznetsov, Mestechkina et al. 1977) or just irreversible electrochemical activity from denaturized human and porcine ceruloplasmin (Razumas, Vidugiris et al. 1986; Studničková, Pitřincová et al. 1991) were observed until 1996, when the first and the last report of DET processes involving ceruloplasmin was published (Yaropolov, Kharybin et al. 1996). Small cathodic and anodic Faradaic currents corresponding to a reversible processes could be seen under anaerobic conditions with E_m values of approximately 340 and 410 mV vs. NHE for human ceruloplasmin adsorbed on a spectrographic graphite electrode (SPGE). However, these redox potentials are more negative than those of the redox potentials of the T1 copper sites of the enzyme (490 mV, 580 mV, and ≈ 1000 mV) (Deinum and Vänngård 1973; Machonkin and Solomon 2000). This difference was explained by a conformational transformation in the vicinity of the copper ions during adsorption of the enzyme or an overvoltage of the electrochemical redox reaction of the copper ions in the protein structure on the graphite electrode (Yaropolov, Kharybin et al. 1996). Knowledge of the redox properties of ceruloplasmin might give insights in the possible complex roles of this enzyme in human bodies.

1.1.4. Direct electron transfer of multicopper oxidases on electrodes

Electron transfer is ubiquitous in biological and chemical systems. Thus, understanding and controlling this process comprise one of the broadest and most active research areas of science nowadays. Usually, electron transfer occurs in nature in connection with energy transduction (Freire, Pessoa et al. 2003). The theoretical framework of biological electron transfer is increasingly

well understood, and several properties, such as redox enzymes and proteins carrying out many key reactions of biological and technological importance, make biological redox centres good systems for exploitation (Gilardi and Fantuzzi 2001). Enzyme or protein mediated electron transfer is a fundamental phenomenon, not only in cellular processes, but also in reactions of biotechnological interest.

Much progress has been made over the past ten years in understanding how the protein matrix finely tunes the parameters that are essential to the regulation of biological electron transfer. Undoubtedly, the protein matrix has a fundamental role in regulating redox functions, even in simple electron-transfer proteins, such as b-type and c-type cytochromes that contain the same heme iron. Physico - chemical investigations of direct electron transfer using redox enzyme/protein systems were the focus of intensive investigations during the last two decades.

The electronic coupling between redox enzymes and electrodes can be based on the electroactivity of the enzyme substrate or product (first generation); utilization of redox mediators, either free in solution or immobilized with the biomolecule (second generation), or direct electron transfer (DET) between the redox-active biomolecule and the electrode surface (third generation) (Freire, Pessoa et al. 2003).

The very first reports on DET with a redox active protein were published in 1977 when Eddowes and Hill (Eddowes and Hill 1977) and Yeh and Kuwana (Yeh and Kuwana 1977) independently showed that cytochrome *c* on bipyridyl modified gold and tin doped indium oxide electrodes, respectively, showed virtually reversible electrochemistry as revealed by cyclic voltammetry. The first publications on DET for any large redox protein with enzymatic activity were concerned with a high potential laccase from the basidiomycetes *Trametes versicolor* (Berezin, Bogdanovskaya et al. 1978; Tarasevich, Yaropolov et al. 1979). The authors of these papers showed that in the presence of molecular oxygen, laccase modified carbon electrodes exhibited DET. They found that addition of laccase into the electrochemical cell shifts

the equilibrium potential of the working electrode by 30 - 380 mV. The process was dependent on the electrode material, its method of preparation and the partial pressure of oxygen in the system. Moreover, in the presence of molecular oxygen a reduction current was recorded at the laccase modified carbon electrode due to DET between the electrode and the adsorbed enzyme. A second publication about the electroreduction of oxygen at laccase modified electrodes was published in 1984 (Lee, Gray et al. 1984). The electroreduction of oxygen using highly ordered pyrolytic graphite electrode coated with laccase from *Trametes* (*Polyporus*) *versicolor* (high potential fungal laccase) was shown. The potential at which the laccase begins to catalyse the electroreduction of oxygen (about 735 mV *vs.* NHE) is in the vicinity of the redox potential of the T1 site (780 mV *vs.* NHE). However, under anaerobic conditions the laccase modified graphite electrode exhibited CVs that were indistinguishable from the background voltammograms obtained in the absence of enzyme. In the presence of an electrochemically inactive promoter, 2,9-dimethylphenanthroline, an electrochemical response was, however, observed with an average of the peak potentials of 645 mV *vs.* NHE.

The characteristics of electroreduction of oxygen at laccase modified graphite/carbon electrodes depend on the origin and also on the amount of enzyme on the electrode surface (Yaropolov, Kharybin et al. 1996; Shleev, Christenson et al. 2005). Laccases from different sources (from *Rhus vernicifera* and *Trametes hirsuta*) catalyse the heterogeneous electroreduction of oxygen in very different potential regions. The pH dependence of the heterogeneous electrocatalytic currents for both enzymes adsorbed on electrodes was found to be very similar to that obtained for the corresponding enzyme reactions in homogeneous media (Yaropolov, Kharybin et al. 1996). The difference in the redox potential of the T1 site of the two laccases is most likely the major determinant of this behaviour with a similar mechanism operating for both homogeneous catalysis in solution and heterogeneous electrocatalysis at an electrode. A mechanism for the bioelectrocatalytic reduction of oxygen by laccase adsorbed on carbon electrode materials has

been proposed by Tarasevich et al (Tarasevich, Bogdanovskaya et al. 2001). At potentials close to the steady-state potential, the rate-determining step is proposed to be a concerted transfer of two electrons to the oxygen molecule. In the region of polarisation, where the current is essentially potential independent, the process is limited by the formation of "peroxide" intermediate. Further support for this was recently obtained for laccases from different basidiomycetes (Shleev, Zaitseva et al. 2003; Shleev, Jarosz-Wilkolazka et al. 2005). Three high potential laccases (having differences in the redox potential of the T1 site of only 50 mV) had the same electrocatalytic activity on graphite. In addition, the potential of electroreduction of oxygen correlated with the values of the redox potential of their T1 sites. This supports the belief that carbon electrodes act as the primary electron donor to the T1 site of the enzyme by DET. This would also explain the similar catalytic behaviour of laccases adsorbed on graphite electrodes with that in homogeneous solution in the presence of soluble electron donors (Christenson, Dimcheva et al. 2004). Experiments with carbon electrodes modified with laccases confirm that the T1 site is the primary electron acceptor from carbon electrodes during heterogeneous reduction under both aerobic and anaerobic conditions. The mechanistic scheme of this process is presented in Fig. 1.5. The electrons are transferred from the electrode to the T1 site of the adsorbed enzyme and then through an internal electron transfer (IET) mechanism to the T2/T3 cluster, where molecular oxygen is reduced to water (Shleev, Jarosz-Wilkolazka et al. 2005).
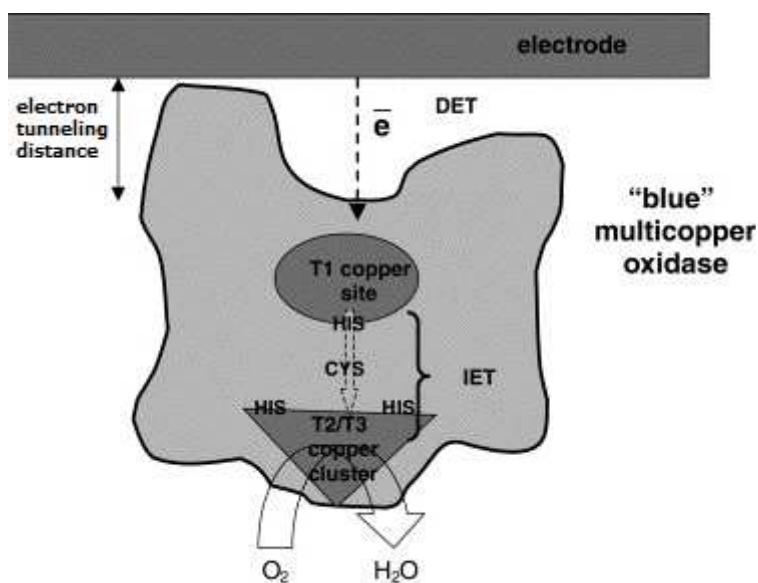
Fig. 1.5. Proposed scheme for electroreduction of oxygen at carbon electrodes with adsorbed multicopper oxidase (Shleev, Jarosz-Wilkolazka et al. 2005).

Gold is often used as electrode material due to its inertness, and it is important to achieve and understand electrochemical reactions of redox proteins on gold electrodes both for fundamental research and applications in biotechnology. As early as in 1978 it was shown for the first time that the presence of laccase shifted the steady-state potential of a bare gold electrode in oxygenated buffer to a value about 100 mV more positive than that without the enzyme (Berezin, Bogdanovskaya et al. 1978). However, only in 1997 was independent DET shown for *Rhus vernicifera* laccase (low potential enzyme) (Hyung, Jun et al. 1997). Laccase was adsorbed onto a mercaptopropionic acid modified gold electrode and under anaerobic conditions well-pronounced reversible CV peaks were obtained with a difference in potential between the anodic and cathodic peaks (ΔE_p) of around 60 mV and an E_m of about 330 mV *vs.* NHE. A subsequent paper on gold electrodes modified with laccase embedded in a polymeric film of an anion exchange resin (Santucci, Ferri et al. 1998) not only confirmed these results but also reported a reversible and diffusion - controlled electrochemical process with a ΔE_p of around 30 mV and an E_m of about 410 mV, which is very close to the potential of the T1 site of the enzyme (420 mV *vs.* NHE) (Shleev, Tkac et al. 2005).

The mechanism of DET between the high redox potential laccases and carbon and gold electrodes are very different. At carbon electrodes DET is observed

between the surface of the electrode and the T1 site, whereas in the case of gold another electrochemical process can be seen, suggesting the interaction of the T2 site of the enzyme with the electrode. The evidence to support such a suggestion have been presented in (Shleev, Christenson et al. 2005). Spectroelectrochemical (EPR and UV–Vis) titration studies using mediators as well as electrochemistry of a T2 depleted laccase on a bare gold electrode showed that not the T1 but rather the T2 site of the enzyme was in contact with the bare gold electrode (Shleev, Christenson et al. 2005). The electrochemical action mechanism of high redox potential laccase on a gold surface has been described in another article (Shleev, Jarosz-Wilkolazka et al. 2005) by a mechanism presented in Fig. 1.6.
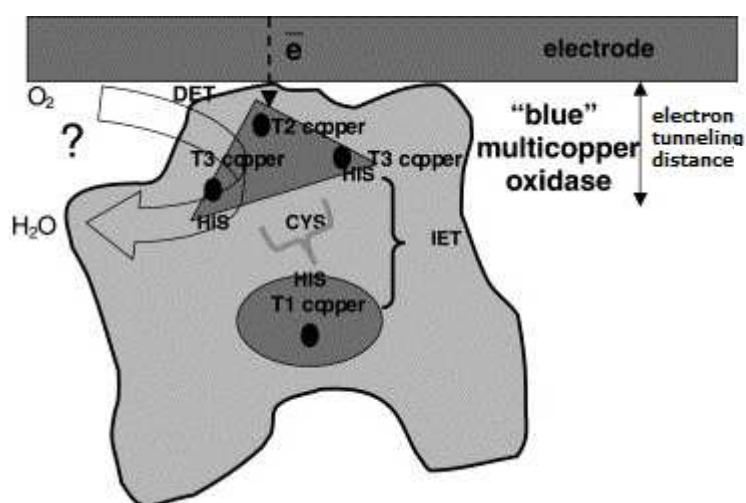
Fig. 1.6. Proposed scheme for electrocatalytic activity of laccases on the gold electrode (Shleev, Jarosz-Wilkolazka et al. 2005).

The mechanism of DET between electrodes and multicopper oxidases associated with reduction of molecular oxygen and oxidation of substrates is not fully understood as discussed in (Shleev, Christenson et al. 2005), since in many cases the DET processes recorded with CV or other voltammetric techniques do not coincide with the formal potential values evaluated with other techniques for the different copper sites. In a parallel study involving analysis of gold – bilirubin oxidase electrochemical systems, the experimental results indicated that under certain conditions the IET can be the rate - limiting step in bilirubin oxidase catalytic cycle and one of the catalytically relevant

intermediates formed during the catalytic cycle of bilirubin oxidase has a redox potential close to 400 mV *vs.* NHE, indicating an uphill IET process from the T1 copper site (0.7 V *vs.* NHE) to the T2/T3 site (Shleev, Andoralov et al. 2012). If these findings could relate to gold – laccase electrochemical systems, it would be another confirmation that T1 site is important in DET between T2/T3 site and gold surface, despite its orientation when adsorbed on gold surface (Fig. 1.6). In the light of studies done by different scientific groups, a demonstration of efficient DET based oxygen bioreduction catalysed by laccase adsorbed on gold surface would possibly lead to further insight into mechanisms of DET between electrodes and multicopper oxidases.

1.1.5. Applications of multicopper oxidases in biofuel cells

Fuel cells are electrochemical devices that convert chemical energy into electrical energy. Biofuel cells are a subset of fuel cells that employ biocatalysts. The main types of biofuel cells are defined by the type of biocatalyst. Microbial biofuel cells employ living cells to catalyse the oxidation of the fuel, whereas enzymatic biofuel cells use enzymes for this purpose. The current advantage to microbial biofuel cells is that they typically have long lifetimes (up to five years) (Kim, Chang et al. 2003; Moon, Chang et al. 2006) and are capable of completely oxidizing simple sugars to carbon dioxide (Bond and Lovley 2005). They are limited, however, by low power densities (i.e. the power generated per unit electrode surface area, typically in $\mu W/cm^2$) owing to slow transport across cellular membranes (Palmore and Whitesides George 1994). By contrast, enzymatic biofuel cells typically possess orders of magnitude higher power densities (although still lower than conventional fuel cells), but can only partially oxidize the fuel and have limited lifetimes (typically 7 – 10 days) owing to the fragile nature of the enzyme (Calabrese Barton, Gallaway et al. 2004; Kim, Jia et al. 2006). Enzymes have the added advantage of specificity, which can eliminate the need for a membrane separator.

Both microbial and enzymatic biofuel cells are also plagued by the lifetime and efficiency of their mediators. Mediators are those compounds that shuttle the electrons from the oxidized fuel to the electrode surface. These mediators are typically organic dyes or organometallic complexes, which are either in solution or immobilized at the electrode surface. Their lifetime and performance have proven to be as problematic as the enzymes themselves.

One of the most significant advances in biofuel cells has been the development of biocathodes and bioanodes that employ DET instead of mediated electron transfer. The importance of DET is that the electrons are transferred from the catalyst (enzyme) directly to the electrode and problems associated with the use of mediators are overcome. Although DET has been observed for several enzymes in electroanalytical applications, it was not employed in a biofuel cell until 2006 when researchers developed biocathodes for the reduction of oxygen using laccase (Yan, Zheng et al. 2006; Zheng, Li et al. 2006) and bioanodes employing glucose oxidase (Ivnitski, Branch et al. 2006).

A second key advance has been an increase in the active lifetime of the immobilized enzymes. Enzymes are proteins that typically have short lifetimes (8 h to 2 days) in buffer solution (Kim, Jia et al. 2006), although their active lifetimes can be extended to 7 - 20 days by immobilization on electrode surfaces via entrapment, chemical bonding, and crosslinking (Kim, Jia et al. 2006). Recently, active lifetimes have even been extended beyond 1 year through encapsulation in micellar polymers. These polymers physically confine the enzyme and prevent it from denaturing by providing a biocompatible hydrophobic nest and buffered pH micro chemical environment (Moore, Akers et al. 2004; Akers, Moore et al. 2005).
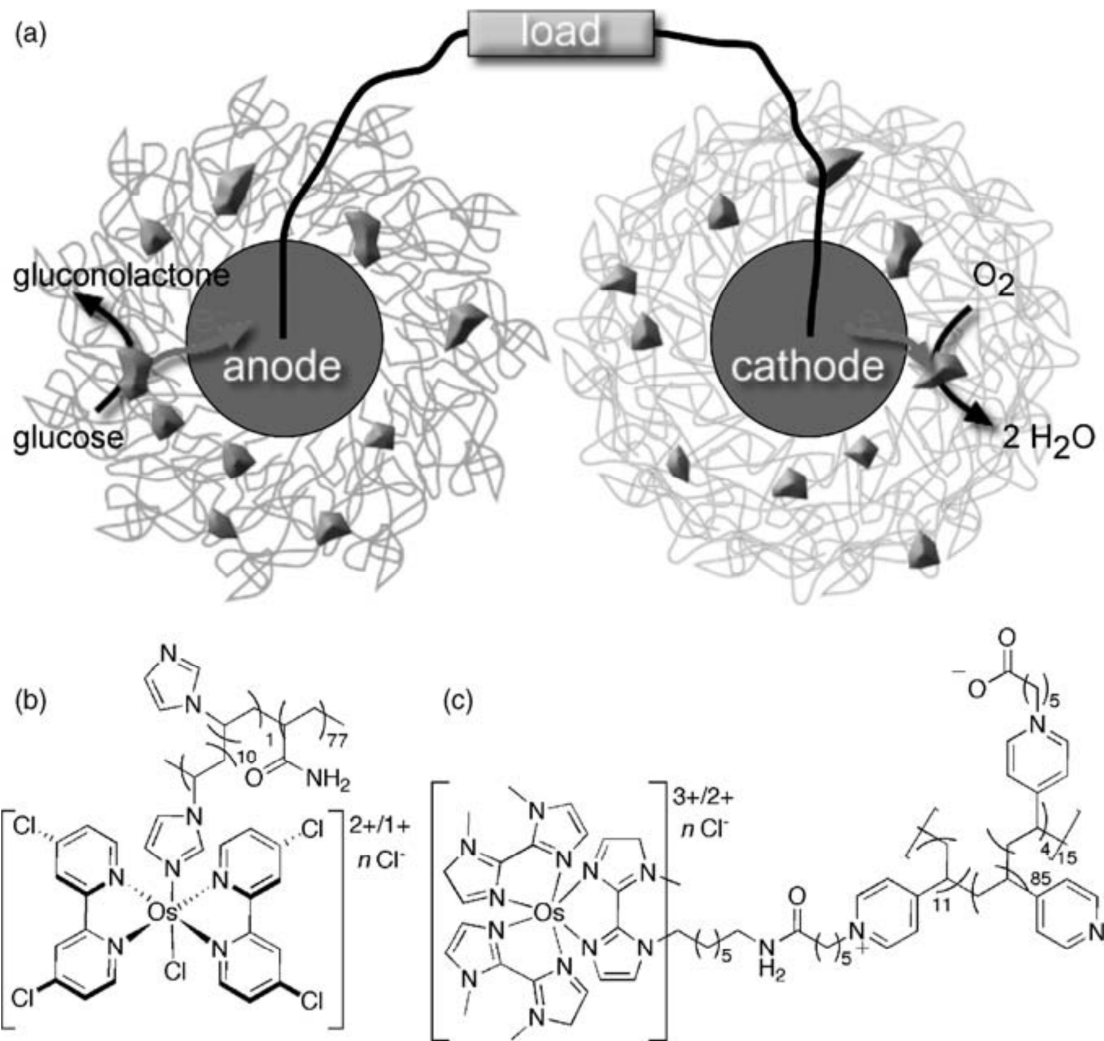
Fig. 1.7. (a) Configuration of a exemplary membraneless biofuel cell in which the anode and cathode consist of carbon fibers coated with redox-active polymers embedded with glucose oxidase and bilirubin oxidase, respectively. Molecular structure of redox-active polymer used in the (b) anode and (c) cathode (Palmore 2008).

The power density of typical biofuel cell is described by the following equation:

$$P = (V_{Cell}^o - I \times R_{Cell}) \times I = V_{Cell}^o \times I - I^2 \times R_{Cell} \tag{1.2}$$

where V^o_{Cell} is the open circuit equilibrium potential (V) and R_{Cell} is internal resistance of biofuel cell.

This equation suggests that for any given rate of operation in the fuel cell, there are two clear paths to achieve improved power density. The first, which is not affected by geometry, is the thermodynamic consideration as represented in the first term of Eq. 1.2, where the equilibrium potential of the cell V^o_{Cell} is governed by the cell chemistry through a judicious choice of the oxidation and reduction reactions at the anode and cathode, respectively. The second term, however, emphasizes the importance of kinetics where the cell internal resistance R_{Cell} is a crucial parameter in determining the power density in a cell reaction. R_{Cell} is a lump sum of various attributes, including charge transfer resistance of the electrode, electrode connections, membrane conductance, and the electrolyte conductance.

Fuel cells require porous anode and cathode structures that support fuel transport to the catalyst reaction sites. Enzymatic fuel cells are no different except that, if they are to compete against primary batteries as a power source, they will require anodes that maximize power density. This requirement demands a solution to three technical hurdles:

1. Biofuel cell anodes should be three-dimensional, as opposed to biosensors which are less sensitive to this requirement. They should be able to optimize the need for surface area, which generally means smaller pores that increase the reactive surface area and thus the current generated, and the need for larger pores, which generally supports the mass transport of liquid phase fuel. This could be achieved by employing gold nanoparticles (AuNPs) as a 3D structural building component of enzymatic biofuel cell.

2. The successful immobilization of multi enzyme systems that can completely oxidize the fuel to carbon dioxide is needed. Current enzymatic biofuel cells have low efficiency, as only a single type of enzyme is employed and can only partially oxidize the fuel.

3. The anode must support efficient charge transfer mechanisms, whether it be direct or mediated, and balance electron transfer with proton transfer. It is therefore crucial to understand this interplay between porosity (for fuel

delivery and effluent flow), surface area (for catalytic rate), and electronic and proton conductivity (to minimize resistive losses) (Bartlett 2008).

The field of research continues to move forward with new approaches being used in the development of biofuel cells. The continued interest in biofuel cells is premised on the idea that biology offers a range of enzymatic catalysts capable of all sorts of chemical transformations in a variety of environments, and that most of these catalysts are yet to be discovered and exploited for energy conversion. Knowledge gained from research on biofuel cells has high translational value to nanotechnology, in which control of chemical transformations at the interface between functional biology and engineered materials is crucial (Palmore 2008).

1.2. Gold nanoparticles

Gold nanoparticles (AuNPs) have become one of the most commonly studied metallic nanoparticles for the development of bioanalytic assays. This is due in part to the relative ease of synthesizing stable AuNP of controlled size with narrow size distribution. Also, AuNP exhibit optical and electronic properties that can be exploited in a variety of detection methodologies (Pong, Elim et al. 2007). Among metal molecules, AuNP are particularly extensively studied due to their utility in biological systems, particularly in labelling, drug delivery, heating sources, and sensors applications (Luo, Morrin et al. 2006; Bhattacharya and Mukherjee 2008; Sperling, Rivera Gil et al. 2008).

Besides that AuNPs are relatively easy to synthesize, at the same time they also remain colloidally stable with no corrosion indication (Sperling, Rivera Gil et al. 2008). Their inertness provides a basis for its characterization as a biocompatible material and a favourable environment for functionalization with macromolecules, namely immunoglobulins, enzymes, lectins, proteins, streptavidin, DNA, etc. (Katz, Willner et al. 2004; Yanez-Sedeno and Pingarron 2005; Pingarron, Yanez-Sedeno et al. 2008). Biomolecules combined with the surface of AuNP retain the biologic activity, where

particularly proteins have more freedom in orientation (Liu, Leech et al. 2003). Regular polycrystalline gold itself is a poor catalyst in a bulk, but nanometre size gold particles exhibit excellent catalytic activities due to their high surface area to volume ratio and the high surface energy.

The novel interesting usage of AuNPs comes from the wiring of enzymes where the particles become an electron pathway, which by direct connection decreases the distance between proteins and the electrode surface, enables to conduct and facilitate the electron transfer between prosthetic groups of redox proteins and the electrode surface (Xiao, Patolsky et al. 2003; Willner, Katz et al. 2006).

1.2.1. Synthesis of gold nanoparticles

Some of the interest in AuNPs is a prominent optical resonance in the visible range and their sensitivity on environmental changes, size, and shape of the particles as well as the local field enhancement of light interacting with the resonant system. Therefore, applications require synthesis protocols, which deliver well-defined shapes and sizes (Cushing, Kolesnichenko et al. 2004; Burda, Chen et al. 2005). Several classes of synthesis routes exist, which display different characteristics of the final products. Examples of widespread usage are the organic phase synthesis after Brust (Brust, Walker et al. 1994), involving a two phase process, or the single phase water based reduction of a gold salt by citrate, introduced by Turkevich et al (Turkevich, Stevenson et al. 1951; Turkevich 1985) and refined by Frens (Frens 1973), which produces almost spherical particles over a tuneable range of sizes (Fig. 1.8.).
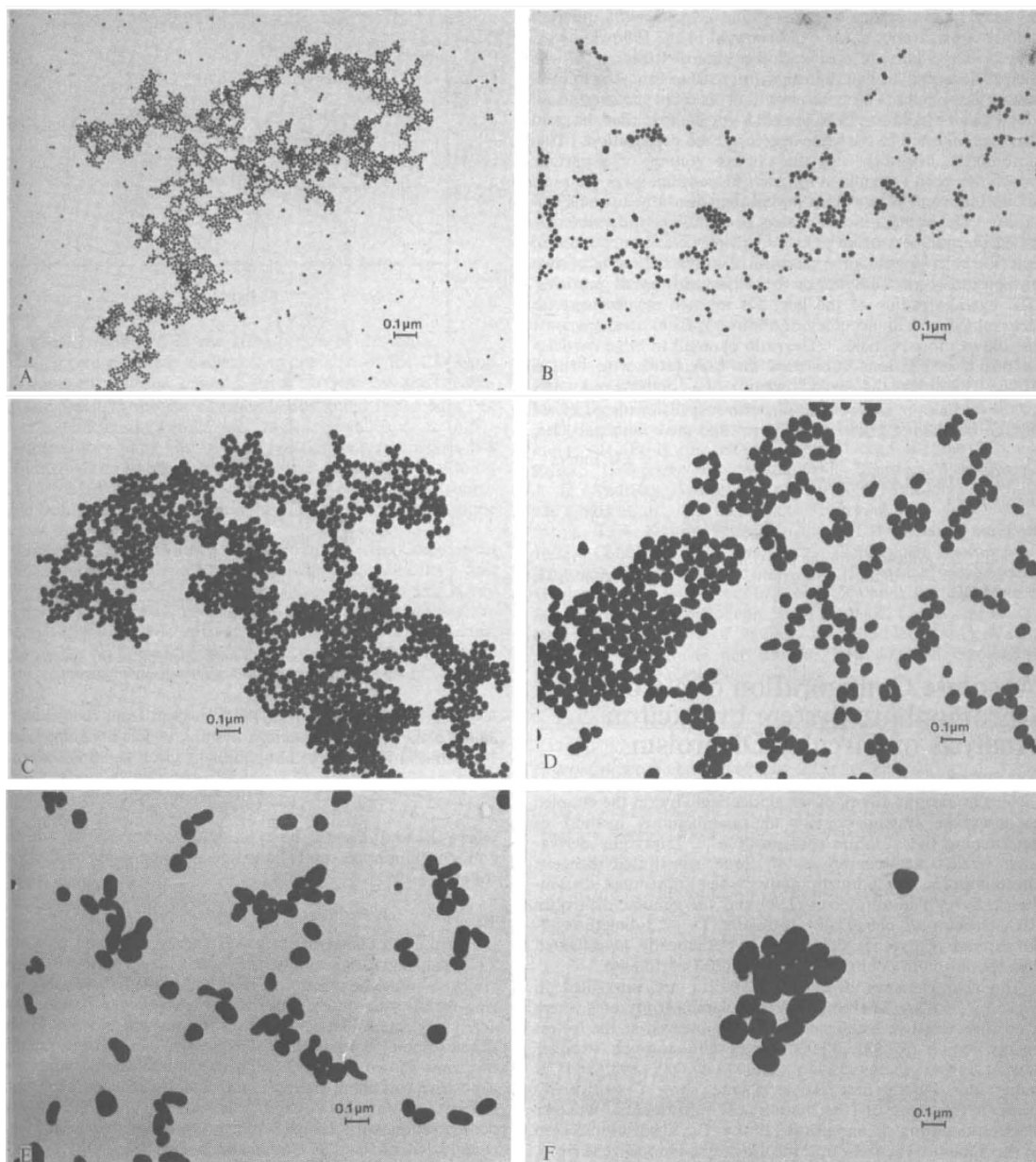
Fig. 1.8. Electron micrographs of the gold sols with sizes of 16 nm (A), 24.5 nm (B), 41 nm (C), 71.5 nm (D), 97.5 nm (E), 147 nm (F) (Frens 1973).

To create large-particle colloidal gold dispersions, an aqueous solution of tetrachloroauric acid is treated with trisodium citrate in aqueous solution. The colloidal gold will form because the citrate ions act as both a reducing agent, and a capping agent. This would result in particles sized 15 - 150 nm, the final range depending on the concentration of the citrate used in the reduction process. Medium-sized gold particles with diameters between 6 and 15 nm and an average size of 12 nm are formed by reducing the tetrachloroauric acid

37

solution with an aqueous sodium ascorbate solution. The smallest particles, measuring less than 5 nm in diameter, are produced by reduction with either white or yellow phosphorus in diethyl ether (Hayat 1989; Hermanson 1996).

In our works it was focused on the research of bioelectrocatalytic systems containing AuNPs produced by tetrachloroauric acid reduction by trisodium citrate, mainly because the size range of this method was projected as optimal and also because AuNPs with different coatings (polyethyleneimine – covered (Song, Du et al. 2010), chitosan – covered (Luo, Xu et al. 2004), also plain AuNPs obtained by laser ablation method (Mafuné, Kohno et al. 2001)) revealed to be unsuitable for construction of working bioelectrocatalytic systems. Such AuNP synthesis mechanism involves chemical reactions that are broadly classified as either homogeneous or heterogeneous. In a homogeneous reaction, all the reactants are miscible and form a homogeneous solution. The products that are formed from the reaction are also soluble; therefore, there is no phase separation at any time during the course of reaction. The rate of such a reaction depends on the concentration of the reactants and on the operating temperature. The temperature influences the rate constant of the reaction. Usually, a 10° rise in the operating temperature enhances the rate of reaction by a factor of two. In a heterogeneous reaction, more than one phase is present. The reaction might be gas-liquid, liquid-liquid, gas-solid, liquid-solid, gas-liquid-solid, or liquid-liquid-solid, or display some other progression of phases. Any solid involved could be a catalyst or a reactant. The relatively simple rules for controlling homogeneous reactions are not applicable to the control of heterogeneous reactions. In addition to concentrations and temperature, the physical shift of reactant from one phase to another assumes great importance in heterogeneous reactions.

The chemical reaction between an aqueous solution of tetrachloroauric acid and an aqueous solution of trisodium citrate is interesting in that the reaction begins as a homogeneous one, but then, within a minute, the reaction mixture becomes heterogeneous. This phase transition from homogeneous to heterogeneous occurs very rapidly, making the process difficult to monitor or

control effectively. Moreover, the reaction is completed so quickly that one does not have much time to take any corrective action necessary to ensure reproducible product (Hayat 1989).

The reaction model, described in (Chaudhuri and Raychaudhuri 2001), is as follows. Before the addition of the reducing agent, 100% gold ions exist in solution. Immediately after the reducing agent is added, gold atoms start to form in the solution, and their concentration rises rapidly until the solution reaches super saturation. Aggregation subsequently occurs, in a process called nucleation. Central icosahedral gold cores of 11 atoms are formed at nucleation sites. The formation of nucleation sites, in response to the super saturation of gold atoms in solution, occurs very quickly. Once it is achieved, the remaining dissolved gold atoms continue to bind to the nucleation sites under an energy-reducing gradient until all atoms are removed from solution (Fig 1.9.).
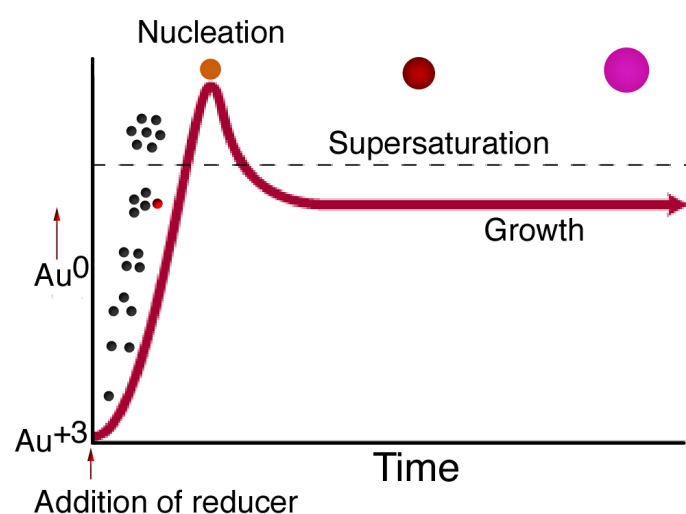
Fig. 1.9. AuNP synthesis reaction model illustration (McFarland, Haynes et al. 2004).

The number of nuclei formed initially determines how many particles finally grow in solution. At a fixed concentration of tetrachloroauric acid in solution, as the concentration of the reducing agent is increased the number of nuclei that form grows larger. The more nuclei, the smaller the gold particles produced. Finding the optimal concentration of the citrate in solution is therefore an important, even crucial, task. If manufacturing conditions are optimized, all nucleation sites will be formed instantaneously and

simultaneously, resulting in formation of final gold particles of exactly the same size (monodisperse gold). This is indeed difficult to achieve. Most manufacturing methods fail to accommodate this ideal and generate irreproducible gold (gold inconsistent from batch to batch) that gives unstable gold conjugates in most situations.

Gold colloids are composed of an internal core of pure gold that is surrounded by a surface layer of adsorbed $[AuCl]^{2-}$ ions. These negatively charged ions confer a negative charge to the colloidal gold and thus, through electrostatic repulsion, prevent particle aggregation. All colloidal gold suspensions are sensitive to electrolytes. Electrolytes compress the ionic double layer and thereby reduce electrostatic repulsion. This destabilizing effect results in particle aggregation, which is accompanied by a colour change and eventual sedimentation of the gold. The detrimental effect of chloride, bromide, and iodide electrolytes on the stability of the gold colloid is greatest for chlorides and least with iodides.
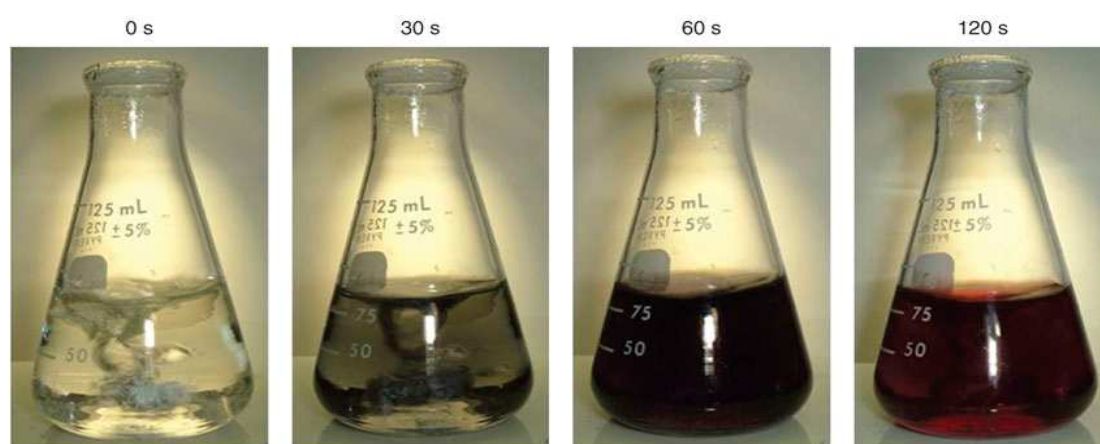
Fig. 1.10. A solution of 1mM $HAuCl_4$ is heated until it comes to a boil (far left). After a 1% sodium citrate solution is added, the formation of gold nanoparticles proceeds first as a faint blue color (30 s), followed by a dark violet appearance (60 s), and finally a brilliant orange red (120 s) (Kumar, Aaron et al. 2008).

All gold colloids display a single absorption peak in the visible range between 510 and 550 nm. With increasing particle size, the absorption maximum shifts to a longer wavelength, while the width of the absorption spectra relates to the size range (Fig. 1.11).
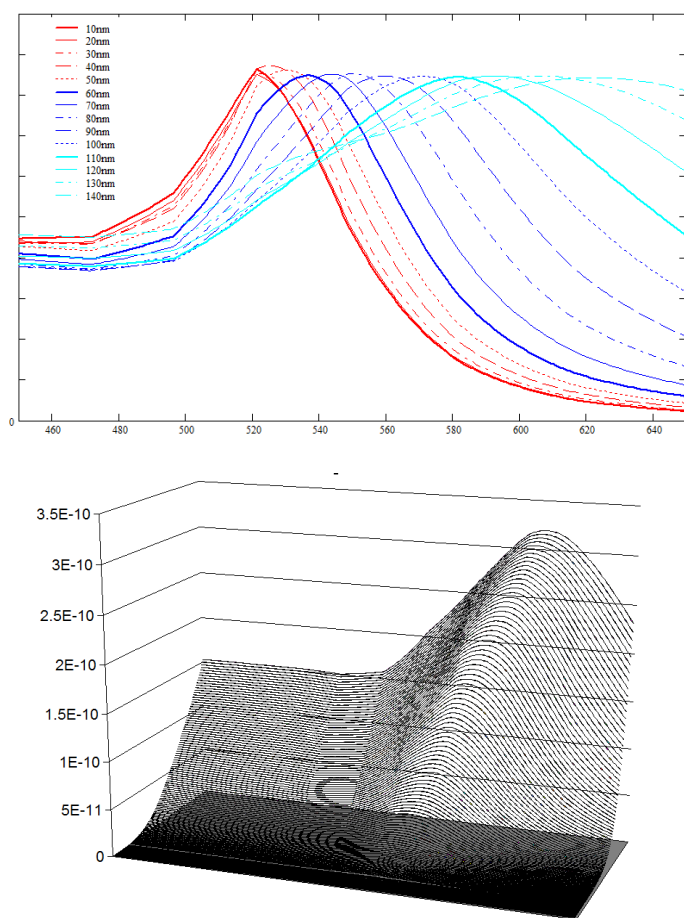
Fig. 1.11. Theoretical spectra of 10 – 140 nm AuNPs, when the peak maximum values are equalized (top) and without equalization (bottom). Spectra were generated by using *MiePlot* software from http://www.philiplaven.com/mieplot.htm.

The smallest gold colloids (2 - 5 nm) are yellow-orange, midrange particles (10 - 20 nm) are wine red, and larger particles (30 - 64 nm) are blue-green. Smaller gold particles are basically spherical, while particles in the range of 30 - 80 nm show more shape eccentricity related to the ratio of major to minor axes.

Researchers have observed several factors that affect the quality and stability of the gold colloid. An important consideration leading to the preparation of stable gold colloids is employment of thoroughly cleaned glass apparatus, micro filtered solutions, and, at least, triple-glass-distilled water (Hayat 1989). The use of ultrapure water is recommended. These precautions suggest the adverse effect that even trace contaminants have on the preparation of colloidal gold. Although the use of siliconized glassware is often recommended, good results have consistently been obtained without any special glassware.

The effect of the order of reagent addition - that is, adding citrate solution to the tetrachloroauric acid solution or vice versa - on the quality of the gold colloid formed has been noted by researchers. However, no clear indication of how addition order might relate to methods of manufacturing colloidal gold suspensions reproducibly has been given.

Researchers have not explicated the role of mixing in the formation of the suspension, nor have they mentioned the negative impact of the use of a stir bar (for laboratory-scale preparation) in a magnetically agitated system on the quality and stability of the gold sol. It must be kept in mind that it is not only the chemistry of the process that is important, but also its perhaps seemingly insignificant physical parameters. Small changes in process conditions can so adversely affect the quality of the product that its utility to users will be minimal (Chaudhuri and Raychaudhuri 2001).

1.2.2. Crystal structure of gold nanoparticles

Gold nanoparticles are typically heterogeneous as synthesized, and though their size distribution may be narrowed by fractionation or other means, atomically monodisperse preparation is very difficult. It is well known that a material's properties arise from collective atomic effects that are very sensitive to the atomic ordering, including the presence of local structural disorder (Liz-Marzán and Mulvaney 2003). The atomic disorder in gold nano-sized structures is seen as broadening in the electron density of states that leads to distinct optical responses for nanoparticles of different sizes and local structures (Schaaff, Shafigullin et al. 1997). A detailed knowledge of AuNP structure, including its imperfections, has been examined by several scientific groups. One study, described in (Petkov, Peng et al. 2005), utilizing pair distribution function technique, while examining nanoparticles with an average size of 3 nm, 15 nm, and 30 nm, clearly showed that the nanoparticles possess a well-defined atomic arrangement resembling the face-centred cubic (FCC) structure occurring in bulk gold. Also, they showed that the FCC – type

arrangement becomes more prominent with increasing nanoparticle size. According to authors, the models based on a fragment of a locally disordered FCC - type structure describe quite well the atomic arrangement in 15 nm and 30 nm nanoparticles. The atomic arrangement in 3 nm nanoparticles is best described by a model that takes into account the presence of extended structural defects and domains inside the nanoparticles.

More recent study, revealed in (Jadzinsky, Calero et al. 2007), investigated the chemistry of such AuNPs by creating a crystal of them - a huge achievement in itself - that could be investigated using X-ray crystallography. The particles they investigated consist of 102 gold atoms arranged in a ball and covered on the surface by a one-molecule-thick layer of 44 sulphur-containing *p*-mercaptobenzoic acid (*p*-MBA) molecules (Fig. 1.12.). A clear, three-dimensional picture of the structure of this monster molecule reveals that atoms in the core of this nanoparticle are arranged similarly to those in bulk gold, as expected. But this "grand core" is then surrounded by two caps, each with 15 slightly twisted gold atoms.
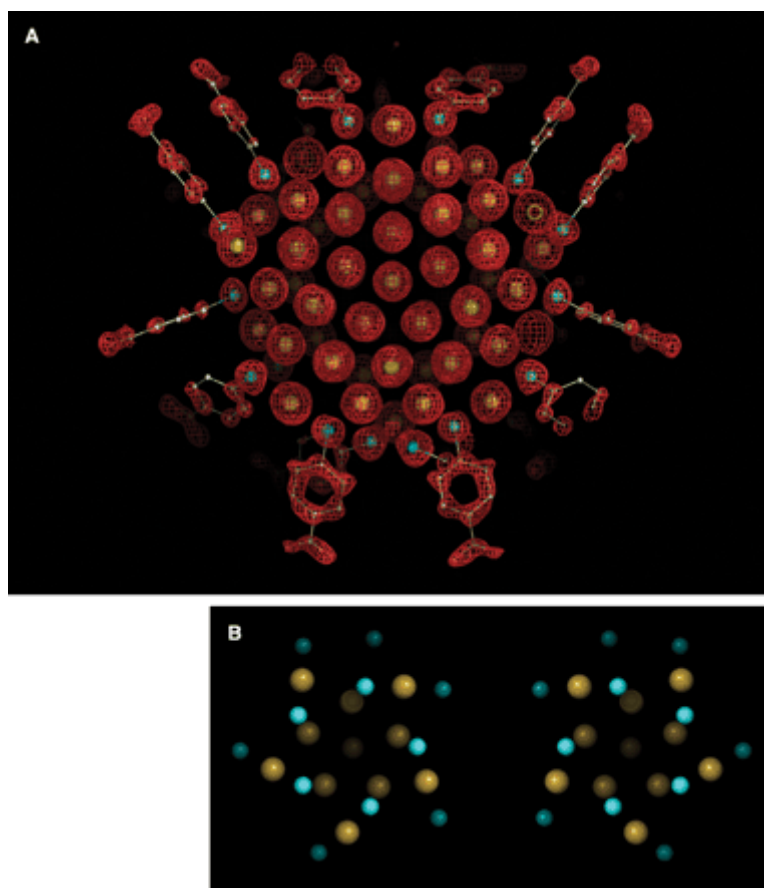
Fig. 1.12. X-ray crystal structure determination of the Au_{102}(p-MBA)$_{44}$ nanoparticle. (A) Electron density map (red mesh) and atomic structure (gold atoms depicted as yellow spheres, and p-MBA shown as framework and with small spheres [sulphur in cyan, carbon in grey, and oxygen in red]). (B) View down the cluster axis of the two enantiomeric particles. Colour scheme as in (A), except only sulphur atoms of p-MBA are shown (Jadzinsky, Calero et al. 2007).

The sulphur groups, rather than binding directly to the gold surface as predicted in some models, forms an alliance with the outermost shell of gold, which then interacts weakly with the grand core. In addition to that, the nanoparticle is chiral — it has a handedness — introduced by the arrangement of the gold atoms with the sulphur groups.

Another study, reported in (Heaven, Dass et al. 2008), reported the crystal structure of the thiolate gold nanoparticle [TOA$^+$][Au_{25}(SCH$_2$CH$_2$Ph)$_{18}^-$], where TOA$^+$ = N(C$_8$H$_{17}$)$^{4+}$. The crystal structure revealed three types of gold atoms: (a) one central gold atom whose coordination number is 12 (12 bonds to gold atoms); (b) 12 gold atoms that form the vertices of an icosahedron

around the central atom, whose coordination number is 6 (five bonds to gold atoms and one to a sulphur atom), and (c) 12 gold atoms that are stellated on 12 of the 20 faces of the Au_{13} icosahedron. The arrangement of the latter gold atoms may be influenced by aurophilic bonding. Together they form six orthogonal semi rings, or staples, of $-Au_2(SCH_2CH_2Ph)_3-$ in an octahedral arrangement around the Au_{13} core.

These studies suggest that AuNPs could be considered as FCC – type gold alloy particles in the core, while macro scale AuNPs with orderly crystal structure is difficult to synthesize for X-ray analysis. Such feat would be valuable, as our study reveals dependence of heterogeneous electron transfer rate between active centres of oxidoreductases and AuNP surface on AuNP size, and it would be very interesting to relate adsorbed enzyme kinetic properties with crystal structure differences of various size AuNPs.

1.2.3. Protein adsorption on gold nanoparticles

The utilization of AuNPs as a building block in the self-assembly of nanoscale functional devices has become important in both the electrochemistry of proteins and biosensing (Elghanian, Storhoff et al. 1997). Colloidal gold nanocrystals have been used to develop a new class of nanobiosensors to recognize and detect specific DNA sequences (Maxwell, Taylor et al. 2002). Application of AuNP systems has greatly expanded due to its good biocompatible action with a wide variety of macromolecules (immunoglobulins, enzymes, lectins, proteins, streptavidin, DNA, etc.). The biofunctionalized colloidal gold nanoparticles not only reveal extraordinary stability and regeneration properties, but also possess the undisturbed, specific recognition capabilities of the colloid - bound proteins, which allow the fabrication of devices such as sensors or bioelectrochemical devices with great control over selectivity, sensitivity, and functionality. The application of other molecular or biomolecular crosslinking units, e.g., chiral molecule, or antigen is anticipated to yield new functional nanoparticle electrodes exhibiting

chiroselectivity and immunoassay features. With the rapid development in biology and surface modification with nanoparticles, the emergence of many novel applications of these nanoparticle constructions in the near future is to be expected (Liu, Leech et al. 2003).

Nanoparticle films have been applied on various surfaces in order to improve stability and electron transport from enzyme active sides to the electrode. However it is difficult to obtain the formation of dense films of metal nanoparticles from the aqueous media as disperse solutions. It has been showed that the surface coverage of AuNP adsorbed from aqueous solutions onto solid substrates is less than 30% (Schmitt, Decher et al. 1997). In order to achieve close-packed films the following two methods have been applied. The one way to increase the surface concentration is to use linker molecules to bind extra nanoparticles to the surface (Hicks, Seok-Shon et al. 2002), however, the disadvantage of this method is that the typically covalently bound molecules will unfortunately affect the catalytic reactivity of the nanoparticles (Yu, Liang et al. 2003). The other solution is to increase the nanoparticle loading by building multilayers based on electrostatic interaction between metal particles and e.g. polyelectrolytes (Yu, Liang et al. 2003; Chirea, Garcia-Morales et al. 2005). It was shown that such a structure exhibits a great permeability of the layers allowing AuNP to be in contact with both the electrode surface as well as inter-contact with the particles present within the layers (Chirea, Pereira et al. 2007; Zhao, Bradbury et al. 2008).

Considering protein adsorbtion on AuNP surface, several strategies are available for conjugation of proteins to AuNPs. First, 'non-specific' adsorption can be employed: the nanoparticles are incubated with the protein, which adsorbs to the particles by electrostatic attraction if both partners are oppositely charged, by van der Waals forces, hydrogen bridges, gold - thiol bonds (from cysteine residues) or by hydrophobic interaction, e.g. when the pH is close to the pI of the protein or the nanoparticle so that the electrostatic repulsion is reduced. After adsorption, the protein can be irreversibly immobilized by those forces or a combination of them (Gole, Dash et al. 2001). Potentially, the

protein can get into intimate contact with the particle surface by partial or complete denaturation (Gao, Chan et al. 2002), giving rise e.g. to hydrophobic interaction of the inner part of the protein and/or an increased contact area between the binding partners. Electrostatic binding has been demonstrated e.g. for protease to 3-mercaptocarboxylic acid - modified quantum dots (Lin, Cui et al. 2003), and desorption of proteins can be triggered by increasing the electrolyte concentration that effectively shields the attractive electrostatic interaction (Bucak, Jones et al. 2003). Traditionally, these effects have been exploited for the preparation of the so - called immunogold (Geoghegan 1988), and small AuNPs conjugated with antibodies that have been used as labels for immunostaining in electron microscopy and have already been commercially available for many years (Sperling and Parak 2010).

Due to several protein adsorption on AuNP mechanisms involved, there are no clear guidelines for initial AuNP and enzyme preparation that could lead to definite and predictable enzyme orientation on AuNP surface, besides probably the introduction of protein side – chain amino acids by directed mutagenesis enzyme engineering, etc. In this work the only prerequisite that has been taken in consideration was that pH of the AuNP – enzyme solution would be lower than pI of the enzyme. This should had ensured that enzyme surface had positive charge, while AuNPs were covered by negatively charged citrate ions, thus ensuring that the electrostatic repulsion would be reduced.

2. MATERIALS AND METHODS

2.1. Equipment

Potentiostats:

a) Computer-assisted Autolab potentiostat from Metrohm Autolab;

b) Compact potentiostat Ivium CompactStat from Ivium Technologies B.V.;

Spectrophotometers:

a) Anthelie Advanced spectrophotometer;

b) Thermo Spectronics *Helios Beta* computer-assisted spectrophotometer;

Quarzt – crystal microbalance with dissipation monitoring equipment Q-Sense E4 with QWEM401 electrochemistry module from Q-Sense®, BiolinScientific AB, Sweden;

Echelle type spectrometer RamanFlex 400 from PerkinElmer, Inc., equipped with thermoelectrically cooled (-50 °C) CCD camera and fiber-optic cable for excitation and collection of the Raman spectra, used for surface enhanced Raman spectroscopy measurements. Equipment is paired with 785 nm laser as excitation source;

EVO® scanning electron microscopy platform Life Science LS10, produced by Carl Zeiss SMT, used with LaB_6 filament;

NICOMP^{TM} submicron particle sizer from Nicomp 380 ZLS, Santa Barbara, California, used in dynamic light scattering spectroscopy.

2.2. Reagents

All the chemicals were of analytical grade. The detailed list below provides information about the chemical reagents used in research regarding the sources of purchase:

Reagent	Source
2,2'-azino-bis(3-ethylbenzothiazoline-6-sulfonic acid) (ABTS)	Sigma – Aldrich

Citric acid monohydrate	Sigma - Aldrich
$HAuCl_4$ x 3 H_2O	Sigma - Aldrich
Nitric acid	Merck, Darmstadt, Germany
Polyethyleneimine, Mw 750kDa	Sigma - Aldrich
Poly-L-lysine	Sigma - Aldrich
Potassium fluoride	Merck, Darmstadt, Germany
Sodium fluoride	Merck, Darmstadt, Germany
Sodium chloride	Sigma - Aldrich
Sodium phosphate dihydrate, dibasic	Sigma – Aldrich
Sodium sulphate	Sigma – Aldrich
Sulphuric acid	Merck, Darmstadt, Germany
Trisodium citrate dihydrate	Riedel-de-Haën, Germany
Potassium octacyanomolibdate $K_4[Mo(CN)_8]$	Sigma - Aldrich
Potassium ferrocyanide	Reachim, Russia
Catechol (PYR)	Reachim, Russia
Hydroquinone (HQU)	Reachim, Russia
Syringaldazine (SYR)	Sigma - Aldrich

2.3. Solutions

Buffer and all other solutions were prepared using water (18 MΩ/cm) purified with a PURELAB UHQ II system from ELGA Labwater (High Wycombe, UK). When needed, anaerobic conditions were established using pressurized nitrogen (N_2) from AGA Gas AB (Sundbyberg, Sweden), or pressurized argon (Ar) from AGA (Vilnius) which was bubbled through the working solutions.

Main buffer solution used – 50 mM sodium phosphate, 100 mM sodium sulphate when pH was adjusted by controlled addition of citric acid. The pH was usually 4.0, but also buffer solutions adjusted at other pH (2.5, 3.0, 3.5, 4.0, 4.5, 5.0, 5.5, 6.0, 6.5, 7.0, 7.5, 8.0) were employed. Sodium phosphate and citric acid provided a system requiring but two compounds and covers a range

of from pH 2.2 to pH 8.0 without the need of several types of buffer solutions (McIlvaine 1921), and sodium phosphate was chosen to alleviate ionic strength differences in solutions at various pH.

2.4. Enzymes

2.4.1. Biochemical properties of enzymes

The homogeneous fungal laccase from *Trametes hirsuta* solution was kindly provided by dr. Sergey Shleev, and has been prepared as described in (Shleev, Morozova et al. 2004). The molecular weight and the carbohydrate moiety of the enzyme were 70 kDa and 12%, respectively (Haghighi, Jarosz-Wilkolazka et al. 2005). The concentration of the *Trametes hirsuta* laccase in the stock solutions was 14.4 - 17.9 mg/ml. A homogeneous preparation was stored frozen in 0.1 M phosphate buffer, pH 6.5, at -18°C. The stock and diluted enzyme solutions were kept at 4-8°C.

The homogeneous fungal laccase from *Trichaptum abietinum* was purified at the Department of Molecular Microbiology and Biotechnology of VU Institute of Biochemistry. The purified enzyme showed the specific activity about 1100 U/mg protein and appeared as a single band on 14 % SDS-PAGE (Fig. 2.1.). Activity of laccase was determined via the oxidation of ABTS. The 1 ml of reaction mixture consisted of 50 mM sodium citrate buffer, pH 3.5, 0.25 mM ABTS and 5 - 10 µl of laccase. The ABTS oxidation was monitored by the increase of absorbance at 420 nm ($\varepsilon = 36\ 000\ M^{-1}cm^{-1}$) (Childs and Bardsley 1975) at 30 °C. One unit of enzyme was defined as amount of enzyme that oxidized 1 µmol of ABTS per min. Specific activity was defined as the unit per mg of protein. Protein concentration was measured routinely by the method of Lowry, using bovine serum albumin as the standard (Lowry, Rosebrough et al. 1951). The concentration of the *Trichaptum abietinum* laccase in the stock solutions was 20.76 mg/ml.

The molecular mass was 51 ±2.5 kDa according to SDS-PAGE (Fig. 2.1). The molecular mass determined by gel filtration chromatography on Superdex 200

10/300 column was 55.6 ± 2.5 kDa. These results showed that the enzyme is a monomer (Fig. 2.1). A homogeneous preparation was stored frozen in 10 mM phosphate buffer, pH 7.0, at -18°C. The stock and diluted enzyme solutions were kept at 4-8°C.
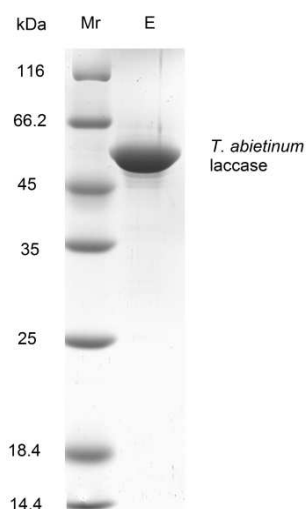

Fig. 2.1. SDS-PAGE of the purified laccase *Trichaptum abietinum* LAC2.

Human ceruloplasmin (Cp) was purchased from Sigma-Aldrich and used without further purification. The concentration of the enzyme in the stock solution was determined by the established method of Ehresmann (Ehresmann, Imbault et al. 1973).

2.4.2. Catalytic properties of enzymes

The kinetic reactions of laccases catalysing reactions between oxygen and various oxidized substrates were registered spectrophotometrically using the Anthelie Advanced (in Malmö University) or Thermo Spectronics *Helios Beta* computer-assisted (in Institute of Biochemistry) spectrophotometers. The kinetic curves were recorded at the wavelength which corresponds to the maximum of absorbance of electron-donor substrate ABTS (2,2'-azino-bis(3-ethylbenzthiazoline-6-sulphonic acid),which has the extinction coefficient 36000 $M^{-1}cm^{-1}$ at 420nm wavelength (Temp and Eggert 1999) (Childs and Bardsley 1975).

The maximal reaction rate was determined in air saturated buffer solution (oxygen concentration 0.25 mM (Koppenol and Butler 1985)) and 5 mM of ABTS, i.e. the concentration of oxygen and ABTS was the highest possible. The initial reaction rate speed was measured as the slope function of absorbance change over time curve at the beginning of the reaction. It was calculated as a slope of absorbance change at 10-30 s intervals. Then the observed reaction rate constant (k_{obs}) was calculated using this equation:

$$k_{obs} = \frac{slope \cdot V_t \cdot Mw}{ext \cdot m_{enz} \cdot 60}$$

(2.1)

where *slope* – initial rate (A/min), V_t – total volume of solution (µl), *Mw* – molecular weight of enzyme (kDa), *ext* – extinction coefficient of oxidized substrate at certain wavelength ($M^{-1}cm^{-1}$), m_{enz} – total mass of enzyme in solution (mg). Reaction rate constant k_{obs}, measured in s^{-1}, provides information about how many molecules of ABTS does one molecule of enzyme oxidize (single electron process) in one second.

For biochemical characterisation of *Trichaptum abietinum* laccase, the oxidation of the substrates was monitored spectrophotometrically in 50 mM sodium acetate buffer solution pH 5.5 or 50 mM potassium phosphate- citric acid buffer solution pH 4.0. The kinetic curves were recorded at the wavelength corresponding to the maximum of absorbance of oxidized substrate. The concentration of the oxidized substrates was calculated using the extinction coefficients: ε_{420} = 1.02 $mM^{-1}cm^{-1}$ for hexacyanoferrate(II) (Schellenberg and Hellerman 1958), ε_{530} = 65 $mM^{-1}cm^{-1}$ for syringaldazine (Harkin and Obst 1973), $\varepsilon_{410} = 0.74$ $mM^{-1}cm^{-1}$ for catechol (Shleev, Nikitina et al. 2007), ε_{248} = 17.5 $mM^{-1}cm^{-1}$ for hydroquinone (Minussi, Miranda et al. 2007).

Kinetics of the substrates oxidation also was recorded by using a homemade computer-assisted membrane oxygen electrode and 1.1 ml cell. The concentration of oxygen was assumed as 0.25 mM in air saturated 0.1 M buffer solution at 25ºC. The kinetic measurements were performed in 50 mM sodium

acetate buffer solution pH 5.5 or 50 mM potassium phosphate- citric acid buffer solution pH 4.0.

The initial rate (V) of the oxidation of the substrates was calculated by fitting the kinetic curves by linear functions. For the linear dependence the initial rate was calculated as a slope. To analyse the dependence of V on the substrate concentration and determine the apparent kinetic parameters V_{max} and K_M of the reactions, the Michaelis – Menten equation was used. Catalytic constant (k_{cat}) was calculated as ratio V_{max} and [E] - the total enzyme concentration. Bimolecular enzyme and substrate reactivity constant (k_{ox}) was calculated as a ratio of catalytic constant (k_{cat}) and K_M.

Effect of addition of inhibitors, specifically NaF and NaCl, to the solution where the reaction of substrate oxidation by oxygen catalysed by either laccase takes place was studied. NaF was considered as non-competitive (Koudelka and Ettinger 1988; Shleev, Christenson et al. 2005) and NaCl – competitive inhibitor (Ali and Varfolomeev 1981).

2.5.Electrochemical methods

2.5.1. Cyclic voltammetry

Cyclic voltammetry (CV) is a type of potentiodynamic electrochemical measurement, during which the working electrode potential is ramped linearly versus time. The current at the working electrode is plotted versus the applied voltage to give the cyclic voltammogram trace. CV is generally used to study the electrochemical properties of an analyte in solution. CV has the further attraction of providing information not only on the thermodynamics of redox processes but also on the kinetics of heterogeneous electron-transfer reactions and coupled chemical reactions (Heinze 1984).

In our research CV was performed in an electrochemical cell containing 20 ml of solutions. Saturated calomel electrode (Hg|HgCl|satKCl (242 mV *vs.* NHE, provided in received electrode data sheet)) was used as a reference electrode and a platinum wire as a counter electrode. Computer-assisted Autolab

potentiostat from Metrohm Autolab was used for measurements. All potentials reported in this work are *vs.* NHE.

A working disk polycrystalline gold electrode with geometrical area of 0.02 cm^2, received from Bioanalytical Systems (West Lafayette, IN, USA), was mainly used in experiments. For surface – enhanced Raman spectroscopy measurements the flat circular gold electrode with geometrical area of 0.196 cm^2, press - fitted into a Teflon rod, was employed. During the cleaning electrodes were polished with a 0.3 µm alumina suspension to obtain smooth surface, then rinsed with pure H_2O and sonicated for 10 min. The electrodes were additionally cleaned by about 5 - 10 CV scans at a 0.2 V/s scan rate between 0 and 1.9 V *vs.* NHE in 0.5 M H_2SO_4, then rinsed thoroughly with H_2O.

For the experiments where electrochemical systems containing AuNPs and multicopper oxidases were studied, gold electrode was modified by AuNPs – about 10 µl of stock AuNP solution was added on the tip of electrode, then the electrode was allowed to dry and has been rinsed thoroughly with Milipore-H_2O. Secondly, about 10 µl of concentrated laccase or Cp solution was placed on the gold surface. . The electrode was then allowed to dry, and rinsed with Millipore H_2O before measurements.

In several experiments, the correct concentration and amount of AuNP and enzyme solutions were adjusted to get the desired AuNP – enzyme ratio, and the amounts of adsorbed AuNPs or enzymes were calculated as a relative of maximum possible amount of material for full monolayer coverage. In case of AuNPs, the calculations were based on assumption that the nanoparticles arrange into two dimensional hexagonal packing monolayer structure (Evans 1993). As for *Trametes hirsuta* laccase solutions, from the analysis of published PDB structure (PDB ID: 3FPX) by RasMol software it was assumed that enzyme covers the ellipsoid with diameters 6.4 and 5.4 nm, if T1 copper active site would be closest to gold surface. The monolayer percentage was calculated as a ratio of total enzyme area to total surface area.

CV was the main tool employed to directly observe direct electron transfer (DET) bioelectrocatalysis of multicopper oxidases adsorbed on AuNP covered electrodes. CV experiments were usually conducted by scanning the electrode potential from 1000 to 200 mV *vs.* NHE and back at the specific scan speed (5 or 10 mV/s). When screening electrodes containing multicopper oxidases, three situations should be considered in respect to buffer solution used for experiment – a) regular buffer solution, b) solution with air removed by N_2 or Ar c) solution with inhibitor present (usually 1 – 5 mM NaF). The removal of oxygen from the solution or addition of enzyme inhibitor should result in disappearance of the reductive peak responsible for DET oxygen bioreduction. The reductive peak should not be observed if the nanoparticle modified electrode wouldn't be additionally modified with multicopper oxidase. Such results would confirm that the current is due to the multicopper oxidase catalysed heterogeneous electroreduction of oxygen.

2.5.2. Rotating disk electrode voltammetry

A rotating disk electrode (RDE) is a hydrodynamic working electrode used in a three electrode system. The electrode rotates during experiments inducing a flux of analyte to the electrode. These working electrodes are used in electrochemical studies when investigating reaction mechanisms related to redox chemistry, among other chemical phenomena.

As the disk turns, some of the solution described as the hydrodynamic boundary layer is dragged by the spinning disk and the resulting centrifugal force flings the solution away from the centre of the electrode. Solution flows up, perpendicular to the electrode, from the bulk to replace the boundary layer. The sum result is a laminar flow of solution towards and across the electrode. The rate of the solution flow can be controlled by the electrode's angular velocity and modelled mathematically. This flow can quickly achieve conditions in which the steady-state current is controlled by the solution flow rather than diffusion. This is a contrast to still and unstirred experiments such

as cyclic voltammetry where the steady-state current is limited by the diffusion of substrate.

By running CV and other experiments at various rotation rates, different electrochemical phenomena can be investigated, including multi-electron transfer, the kinetics of a slow electron transfer, adsorption/desorption steps, and electrochemical reaction mechanisms (Bard and Faulkner 2000).

Rotating disc gold electrodes with adsorbed AuNPs and multicopper oxidases were used in DET bioelectrocatalysis research utilizing CV experiments. The experiments conditions were as described in 2.5.1., except that the rotating disk gold surface electrode had geometrical area of 0.071 cm^2 and saturated silver chloride electrode (Ag/AgCl/sat. KCl (201 mV *vs.* NHE, as stated in electrode commercial data sheet)) was used as reference electrode.

The RDE voltammetry was used in research because it contains a wealth of information on the electron transport processes from AuNP surface to oxygen via enzyme active centre. In order to establish a basis for interpreting the results, it is first of all necessary to formulate a "skeleton" model which can be elaborated to account for all aspects of the observed behaviour. Let us focus upon this task by considering the system to be resolvable into three separate, independent processes as illustrated in Fig. 2.2.
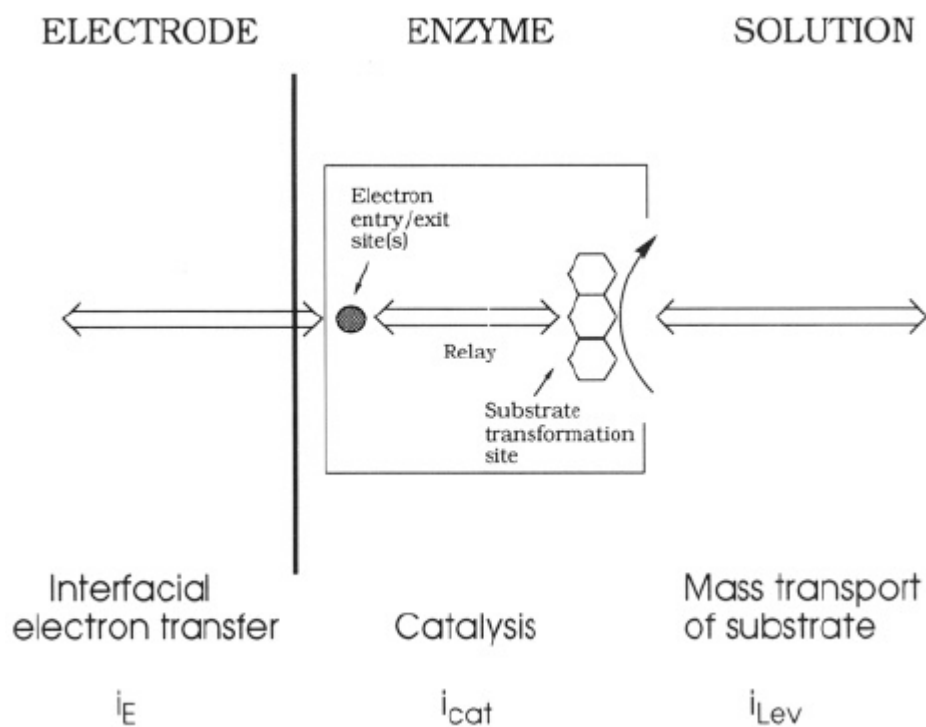
ELECTRODE   ENZYME   SOLUTION

Electron entry/exit site(s)

Relay

Substrate transformation site

Interfacial electron transfer
i_E

Catalysis
i_{cat}

Mass transport of substrate
i_{Lev}

Fig. 2.2. Scheme showing the sequence of steps in electron transport between electrode and substrate molecules during catalysis by an enzyme molecule adsorbed at the electrode surface (Sucheta, Cammack et al. 1993).

Under steady-state conditions such a reaction scheme gives rise to Eq. 2.2, which is analogous to an expression giving the resultant conductance (reciprocal resistance) of a group of resistors connected in series.

$$\frac{1}{i} = \frac{1}{i_{Lev}} + \frac{1}{i_E} + \frac{1}{i_{cat}}$$ (2.2)

The first term deals with transport of substrate molecules between the enzyme and bulk solution. This process is addressed by examining the rotation rate dependence of the current, which for a diffusion-controlled reaction is described by the Levich equation:

$$i_{Lev} = 0.62nFAD^{2/3}Cv^{-1/6}\omega^{1/2}$$ (2.3)

Here, A is the electrode surface area, C is the bulk concentration of substrate (mol per unit volume), D is the diffusion coefficient of substrate, v is the kinematic viscosity of the solution (a typical value for aqueous solutions - 0.01 cm^2/s at 25 °C), and ω is the electrode rotation rate (specifically, the angular

frequency in rad/s). In the limit of an electrode reaction occurring under such conditions that it is entirely diffusion - controlled, only this term contributes and the limiting current is directly proportional to the square root of ω (Levich and Spalding 1977)

The second term is the "exchange current" contribution due to interfacial electron transfer between the electrode and the primary electron entry/exit site on the enzyme. The potential dependence of i_E is given by the current-potential characteristic shown by Eq. 2.4.

$$i_E = nFAk_S[\Gamma_O \exp\left\{-\frac{\alpha nF(E-E°\prime)}{RT}\right\} - \Gamma_R \exp\left\{\frac{(1-\alpha)nF(E-E°\prime)}{RT}\right\}]$$ (2.4)

Here, Γ_O and Γ_R are the respective surface concentrations of the oxidized and the reduced form of the enzyme (expressed as mol per unit surface area), α is the transfer coefficient, n is the number of electrons transferred in the transition state, E is the applied electrode potential, and $E^{o\prime}$ is the appropriate apparent standard reduction potential of the system. The *standard* first-order rate constant, k_S (the *exchange* rate constant), reflects the ease of moving electrons between the electrode and the enzyme. At applied potentials much more positive or negative than $E^{o\prime}$, only oxidation or reduction components (respectively) become significant. Eq. 2.5 shows how the potential-dependent terms i_E and k_E (the first-order electrochemical rate constant) are interrelated.

$$|i_E| = nFA\Gamma k_E$$ (2.5)

The quantity Γ is the total number of enzyme molecules adsorbed per unit area of electrode and thus equals $\Gamma_O + \Gamma_R$.

The third term of Eq. 2.2 describes the intrinsic catalytic properties of the enzyme in its reaction with substrate and is assumed to be independent of driving force and electrode rotation rate. It can be expressed as an electrochemical form of the Michaelis - Menten expression:

$$i_{cat} = nFA\Gamma k_{cat}C/(C + K_M)$$ (2.6)

The quantities K_M and k_{cat} are the apparent Michaelis - Menten parameters, which are assumed to be independent of applied potential. In the limit of $C \gg K_M$, i_{cat} becomes independent of C (Sucheta, Cammack et al. 1993).

The detailed description of electron transfer processes by Eq. 2.2. – 2.6 was considered in the research, as we would observe systems comprising of AuNPs and multicopper oxidases in RDE experiment conditions, when electrode spins at sufficient angular frequency ω where i_{cat} becomes the limiting factor in Eq 2.1., and the amount of electrons transferred from electrode surface to dioxygen would relate to enzyme turnover rate.

2.5.3. Spectroelectrochemistry

An electrochemical cell and appropriate devices are required to run electrochemical experiments, whereas spectrophotometric measurements require a spectrophotometer and a spectrophotometric cuvette. However, the two methods should often be used simultaneously. For example, redox titration of proteins having active centre with different optical properties depending on oxidation state requires both reduced and oxidized forms of the proteins to be determined. Spectrophotometric methods are most commonly used in these experiments (Shleev, Kuznetsov et al. 2000).

The design and procedure for use of a bioelectrochemical cell were described by Taylor and Hastings in 1939 (Taylor and Hastings 1939). A similar cell was designed by Henderson and Rawlinson in 1956 (Henderson and Rawlinson 1956). A manual spectroscope with a special lamp installed behind the spectroscopic cell containing a sample was used to record the absorption spectra of heme - containing proteins (Henderson and Appleby 1972). However, there are some methodological problems with the use of the cells, particularly when the sample must be examined under anaerobic conditions.

The use of spectroelectrochemical cells allows one to avoid methodological disadvantages such as analyte or solution exposure to air during its transfer from one vessel to another and time delays in sample collection during kinetic measurements (Shleev, Kuznetsov et al. 2000).

In our research spectroelectrochemical cell was employed for estimation of redox potential of *Trichaptum abietinum* laccase T1 site. For such task a common T1 copper site redox titration method was used exploiting reduced mediator $K_4[Mo(CN)_8]$ (Xu, Brown et al. 1996). In all these experiments a 0.1 ml spectroelectrochemical cell setup was used, the design of the cell and the technique of titration have been described previously (Shleev, Kuznetsov et al. 2000).For the electrochemical measurement in this case, a two-electrode voltmeter (Ionomer I-130.1, Russia) was used. The reference electrode was an Ag|AgCl|KClsat electrode (201 ± 2 mV *vs.* NHE). The capillary gold electrode was used as a working electrode; platinum wire was used as the counter electrode. The gold electrode was kept at piranha solution for 24 hours, the cleaned by electrochemical cycling in 0.5 M sulphuric acid, with a scan rate of 0.05 V/s between 0.2 and 1.9 V *vs.* NHE (5 scans), and finally rinsed with Millipore water. The titration procedure was started with addition of 100 µl of laccase solution (10.38 mg/ml) into the cell containing 0.5 mM of mediator and using 10 mM phosphate solution at pH 7.0 as a buffer. The redox potential was registered on the gold electrode after equilibrium was established (40 min from initial solution application) - beginning at 500 mV *vs.* NHE, then potential was gradually increased by 50 mV steps, let to stay for 5 min, then the absorbance spectra were recorded. Such procedure was repeated until the potential has reached 1000 mV (oxidative scan) and dropped back to 500 mV (reductive scan). The light passage had been being closed between spectra recordings in order to avoid unnecessary heating of the laccase solution in the cell. The oxygen was assumed as depleted in the solution, since the presence of laccase and mediator in the cell under low potential and 40 min of equilibration time are good conditions for complete oxygen reduction to water.

To determine the redox potential of the T1 site, the dependence of absorbance values at 602 nm (peak maximum) on the applied cell potential was taken into consideration. The data points were approximated with Nernst equation:

$$E_i = E_{redox} + \frac{R \times T}{n_e \times F} ln \left(\frac{rAbs_i}{1 - rAbs_i} \right) \qquad (2.7)$$

where E_i – applied potential at the i step, E_{redox} – redox potential of T1 site, n_e – number of electrons involved in the redox process, $rAbs_i$ – relative absorption at the i step, calculated as:

$$rAbs_i = \frac{Abs_i - Abs_{min}}{Abs_{max} - Abs_{min}} \qquad (2.8)$$

where Abs_i – absorbance value at the i step, Abs_{max} and Abs_{min} – maximal in minimal absorbance values.

2.6. Gold nanoparticles synthesis and characterization

2.6.1. Gold nanoparticles synthesis

Bioelectrocatalytic systems containing AuNPs produced by tetrachloroauric acid reduction by trisodium citrate in aqueous have been examined in our research. AuNPs were synthesized as reviewed elsewhere (Schmid and Corain 2003). Briefly, 50 ml of 1 mM $HAuCl_4$ solution in water was heated to about 90° C while stirring. Then, 1 to 4 ml of 1% trisodium citrate solution was added to $HAuCl_4$ solution. The heating was continued for 15 min with stirring, and 10 min without stirring. After that the solution was left to cool down to room temperature and then excessive citrate was removed by dialysis using cellulose membrane with a cut-off size 12 - 14 kDa against ultrapure H_2O at the volume ratio 1:200 for 12 h. However, the dialysis procedure has not been applied in all cases. The solutions were stored in +4 ºC.

As stated before, the amount of citrate used during AuNP synthesis determines the final NP size (Schmid and Corain 2003) (Fig. 2.3).
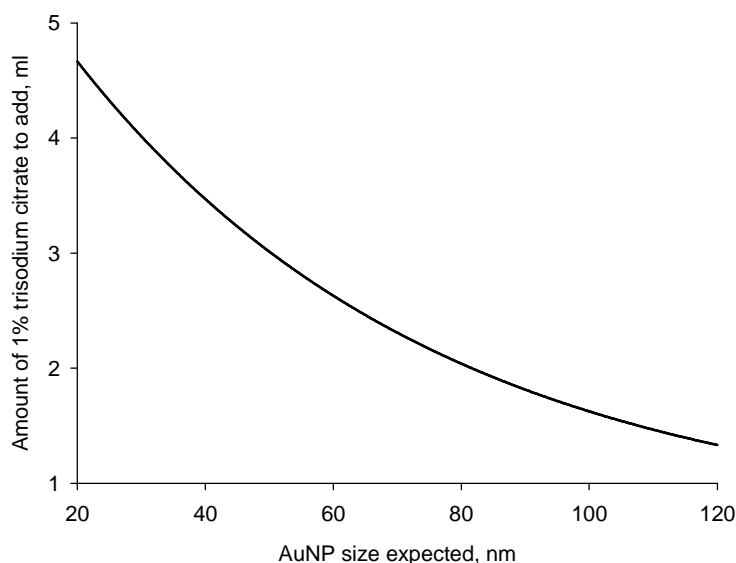
Fig. 2.3. Graph for selection how much of trisodium citrate solution (1% w/w) volume is needed to add to 50 ml of 1 mM HauCl$_4$ solution to get the desired size AuNPs. The method was derived using initial guidelines provided in (Turkevich 1985)

However due to possibility of experimental errors, associated with dilution of solutions, evaporation of reaction solution during heating, unknown water amount in weighted samples of HAuCl$_4$ x 3 H$_2$O and trisodium citrate due to exposure to air, it is hard to predict the exact size or concentration of AuNP after the synthesis just by the amount of citrate used. The size and concentration was additionally determined by various direct and indirect methods.

2.6.2. Gold nanoparticle analysis by spectrophotometry

A prominent spectroscopic feature of noble metal nanoparticles is the so - called surface plasmon resonance, which gives rise to a sharp and intense absorption band in the visible range. The physical origin of the absorption is a collective resonant oscillation of the free electrons of the conduction band of the metal.

For a spherical nanoparticle that is much smaller than the wavelength of the incident light its response to the oscillating electric field can be described by the so - called dipole approximation of Mie theory (Mulvaney 1996). This

theory is employed in Mie scattering algorithm, i.e., *MiePlot* software, which could be found as a freeware at http://www.philiplaven.com/mieplot.htm.

To determine the size of AuNPs the optical absorption spectra of their colloidal dispersions were recorded using Thermo Spectronics *Helios Beta* computer-assisted spectrophotometer. The wavelength, λ_{max}, corresponding to the maximum absorption due to surface plasmon absorbance of AuNPs in the spectrum, was determined. By comparing λ_{max} with the theoretically expected λ_{max} the diameter of the NPs has been defined. Theoretical λ_{max} values for different diameters of the particles were obtained from spectra generated by using the software, the parameters were chosen as follows: monodisperse, the refractive indexes of of medium (water) – 1.3313847, gold sphere real – 0.1557086, gold sphere imaginary – 3.6016265 at 23ºC, as suggested by software. The output was set to generate extinction efficiency, Q_{ext}, *vs.* wavelength, λ. Depending on the size of NPs, the shape of spectrum and absorption peak maximum is different, and the properties of theoretical spectrum should be close to the spectrum of the AuNPs solution if the size of AuNPs set up in the algorithm is the same as in the real solution.

The concentration of AuNPs in the dispersion can be also assessed by using MiePlot software according to this formula:

$$C_{AuNP_{real}} = \frac{A_{max} * \ln(10)}{C_{ext_{max}} * 10 * l * N_A} \qquad (2.9)$$

where $C_{ext_{max}}$ – parameter depicting maximum absorbance of one AuNP in 1 ml of solution, obtained from *MiePlot*, A_{max} – maximum absorbance of measured spectrum AuNP solution, l – length of cuvette (cm), N_A – Avogadro constant.

Additionally, AuNP can be calculated by consideration of geometrical dimensions of AuNPs. This was done by taking into account the amount of $HAuCl_4$ used in AuNP synthesis and dividing this by a number of gold atoms, N_{Au}, constituting the AuNP. The later was calculated by using the equation:

$$N_{Au} = \frac{4}{3} k_{comp} \pi \left(\frac{R_{NP}}{R_{Au}} \right)^3 \qquad\qquad (2.10)$$

where k_{comp} – atomic packing factor of the nanoparticles composed of face-centred cubic crystal (FCC) structures, taken as 0.74 , R_{NP} – radius of NP, R_{Au} – covalent radius of gold atom (0.144 nm (Nyholm 1961)). However, this method would valid if the yield of tetrachloroauric acid reduction reaction would be 100%, and it is evident that some of the reactants adsorb on the walls of reaction beaker. By combining two concentration determination methods, the reaction yield could be calculated:

$$yield = \frac{C_{Mie}}{C_{geom}} * 100\% \qquad\qquad (2.11)$$

where C_{Mie} and C_{geom} – AuNP concentrations determined by *MiePlot* calculations and by consideration of estimated AuNP size, respectively.

2.6.3. Gold nanoparticle size analysis by dynamic light scattering

Dynamic light scattering (DLS) also known as Photon Correlation Spectroscopy or Quasi-Elastic Light Scattering is one of the most popular light scattering techniques because it allows particle sizing down to 1 nm diameter. Typical applications are emulsions, micelles, polymers, proteins, nanoparticles or colloids. The basic principle is simple: the sample is illuminated by a laser beam and the fluctuations of the scattered light are detected at a known scattering angle θ by a fast photon detector (Fig 2.4). Simple DLS instruments that measure at a fixed angle can determine the mean particle size in a limited size range. More elaborated multi-angle instruments can determine the full particle size distribution.
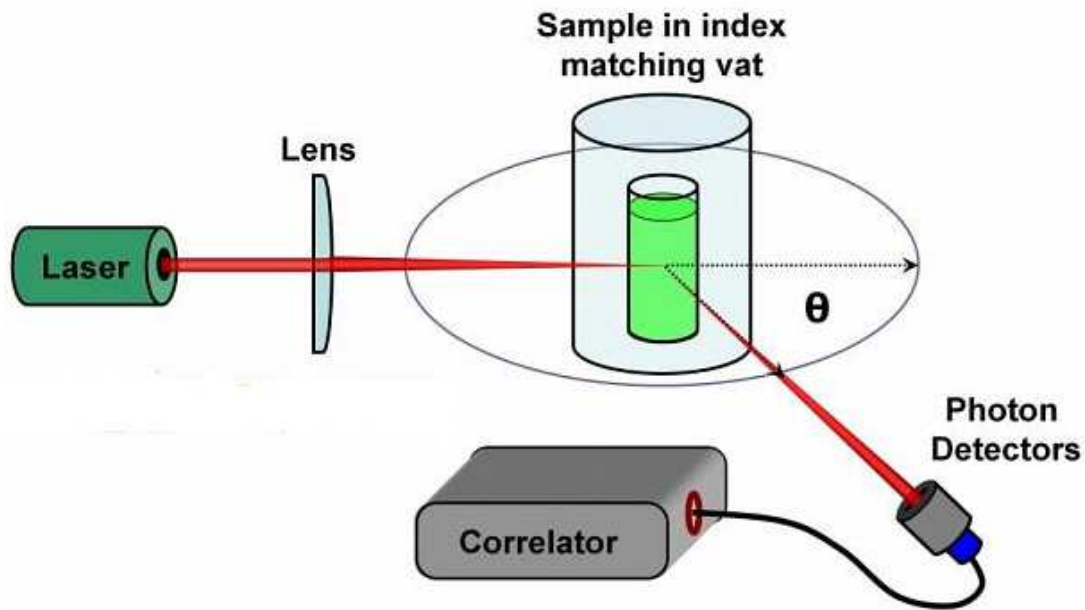
Fig. 2.4. Principle of operation of dynamic light scattering equipment.

From a microscopic point of view the particles scatter the light and thereby imprint information about their motion. Analysis of the fluctuation of the scattered light thus yields information about the particles. Experimentally one characterizes intensity fluctuations by computing the intensity correlation function $g_2(t)$, whose analysis provides the diffusion coefficient of the particles (also known as diffusion constant) (Fig. 2.5).
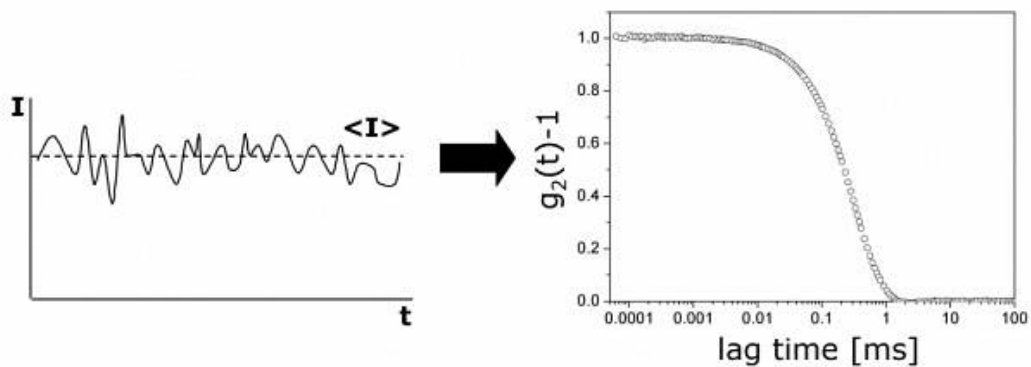

Fig. 2.5. Graphic explanation of intensity correlation function $g_2(t)$ calculation from the intensity fluctuations in time $I(t)$.

The diffusion coefficient D is then related to the radius R of the particles by means of the Stokes-Einstein Equation:

$$D = \frac{kT}{6\pi R\eta}$$
(2.12)

where k is the Boltzmann constant, T - temperature and η - viscosity.

The correlation of the intensity can be performed by electronic hardware or software analysis of the photon statistics. Because fluctuations are typically in the range of nanoseconds to milliseconds, electronic hardware is typically faster and more reliable at this job.

To obtain the diffusion coefficient the intensity correlation function must be analysed. The standard procedure for this is the application of the cumulative method. By fitting a polynomial of third degree to the logarithm of the intensity correlation function, the decay rate Γ is obtained (for single cumulate). The decay rate is directly related to the diffusion coefficient D:

$$\Gamma = q^2 D$$
(2.13)

where is q is the wave vector, which is dependent of the scattering angle.

Higher orders of the fitting result (2nd and 3rd cumulate) give the polydispersity index of the sample. Modern dynamic light scattering instruments perform cumulative analysis automatically (Berne and Pecora 2000).

In our research, the diameters of AuNPs were determined using a NICOMP^{TM} submicron particle sizer, Nicomp 380 ZLS (Santa Barbara, California). The particle sizer was set to a fixed angle of 90° in dynamic light scattering mode with a 300 kHz set point for sensitivity and auto set parameters for channel width and baseline adjustment. UHQ water was used as the solvent in all DLS experiments. Measurements were performed at 23°C and the viscosity of the solvent was found to be $9.533 \cdot 10^{-4}$ kg/m*s at said temperature and used in DLS parameter's setup. The solvent of different batches were found to have similar

viscosity with negligible differences. Data was calculated with intensity weighting, using both Gaussian and NICOMP distribution. AuNP suspensions were diluted 1:10 in UHQ water prior to application.

2.6.4. Gold nanoparticle size analysis by scanning electron microscopy

In our research SEM was used to image AuNP used and, more importantly, to check their size. The research was conducted by using EVO$^®$ SEM platform for Life Science LS10, produced by Carl Zeiss SMT. For the SEM a LaB$_6$ filament was used at 2nd peak (1.96 A) in high vacuum. Depending on the individual sample, electron high tension parameter was set to 8-10 kV, working distance to 5-7 mm, SEI collector bias to + 350-400 V and I$_{probe}$ between 10-100 pA. A thin layer of carbon epoxy was applied to the sample holder prior to the deposition of the AuNP dispersion droplets. The droplets were covered to prevent evaporation and were rinsed off with water after 15-20 minutes. When the sample was dry it was inserted into the SEM carousel.

2.7. Analysis of enzyme – gold nanoparticle interactions

2.7.1. Surface enhanced Raman spectroscopy

Surface enhanced Raman spectroscopy or surface enhanced Raman scattering (SERS) is a surface-sensitive technique that enhances Raman scattering by molecules adsorbed on rough metal surfaces. The enhancement factor can be as much as 10^{10} to 10^{11} (Blackie, Ru et al. 2009), which means the technique may detect single molecules. The increase in intensity of the Raman signal for adsorbates on particular surfaces occurs because of an enhancement in the electric field provided by the surface. When the incident light in the experiment strikes the surface, localized surface plasmons are excited. The field enhancement is greatest when the plasmon frequency is in resonance with the radiation. In order for scattering to occur, the plasmon oscillations must be perpendicular to the surface; if they are in-plane with the surface, no scattering

will occur. It is because of this requirement that roughened surfaces or arrangements of nanoparticles such as AuNPs are typically employed in SERS experiments as these surfaces provide an area on which these localized collective oscillations can occur (Smith and Dent 2005).

The light incident on the surface can excite a variety of phenomena in the surface, yet the complexity of this situation can be minimized by surfaces with features much smaller than the wavelength of the light, as only the dipolar contribution will be recognized by the system. The dipolar term contributes to the plasmon oscillations, which leads to the enhancement. The SERS effect is so pronounced because the field enhancement occurs twice. First, the field enhancement magnifies the intensity of incident light which will excite the Raman modes of the molecule being studied, therefore increasing the signal of the Raman scattering. The Raman signal is then further magnified by the surface due to the same mechanism which excited the incident light, resulting in a greater increase in the total output (Kneipp, Moskovits et al. 2006).

The choice of surface metal is dictated by the plasmon resonance frequency. Visible and near-infrared radiation (NIR) is used to excite Raman modes. Silver and gold are typical metals for SERS experiments because their plasmon resonance frequencies fall within these wavelength ranges, providing maximal enhancement for visible and NIR light (Creighton and Eadon 1991).

In our experiments SERS effect from AuNP surface was examined, which is relevant only at specific distance from the surface (Fig. 2.6).
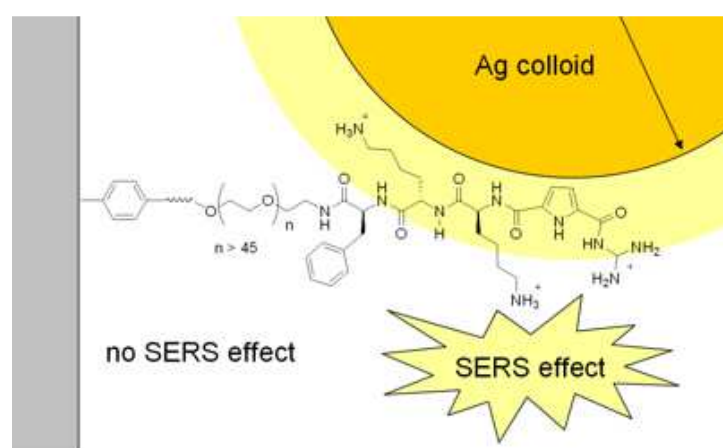

Fig. 2.6. Picture explaining that SERS effect is registered for the substances close to AuNP surface.

It was demonstrated both experimentally and theoretically that SERS intensity (*I*) from adsorbed species rapidly decreases with increasing of the adsorbate - surface distance (*d*). Theoretical analysis has indicated that another important parameter is the radius of curvature (*r*) of the nanostructure generating the surface enhancement (Murray and Allara 1982; Kovacs, Loutfy et al. 1986; Kennedy, Spaeth et al. 1999):
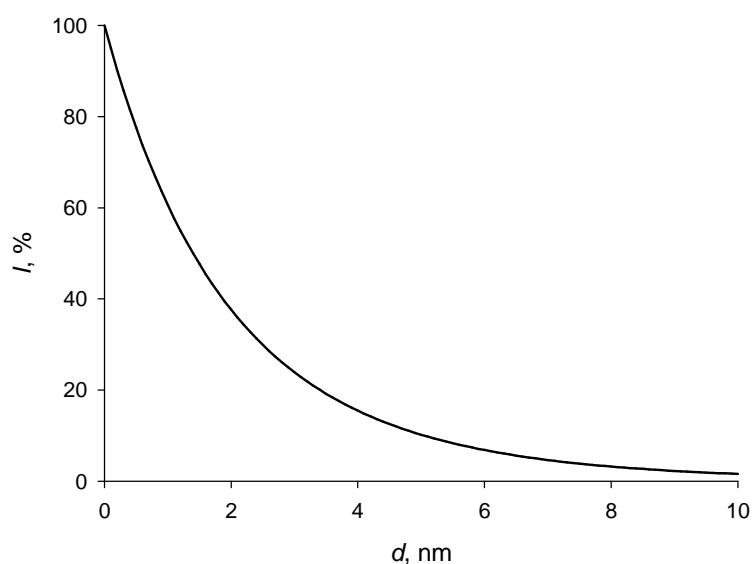
$$I = \left(\frac{r+d}{r}\right)^{-10} \qquad\qquad (2.14)$$

Fig. 2.7. Dependence of SERS intensity (*I*) on distance from AuNP surface (*d*), when round shape AuNPs of 39 nm diameter would be used, according to Eq. 2.14 .

In the research the working gold electrode containing 39 nm diameter AuNPs and laccase was prepared as described in 2.5.1. NIR Raman spectra were recorded using Echelle type spectrometer RamanFlex 400 (PerkinElmer, Inc.) equipped with thermoelectrically cooled (-50 $^{\circ}$C) CCD camera and fibre-optic cable for excitation and collection of the Raman spectra. The 785 nm beam of the diode laser was used as the excitation source. The 180° scattering geometry was employed. The laser power at the sample was restricted to 30 mW and the beam was focused to a 200 μm diameter spot on the electrode. The integration time was 10 s. Each spectrum was recorded by accumulation of 30 scans.

Spectroelectrochemical measurements were carried out in a cylinder-shaped three electrode moving cell, arranged with a, as a working electrode, platinum wire as a counter electrode, and a KCl saturated Ag/AgCl reference electrode. During the experiment solution was continuously bubbling by ultra-pure Ar gas to remove dissolved oxygen. The working electrode was placed at approx. 3 mm distance from the cell window. In order to reduce photo- and thermo effects, the cell together with the electrodes was moved linearly with respect to the laser beam with the rate of about 15 - 25 mm/s (Niaura, Gaigalas et al. 1997; Bulovas, Dirvianskyte et al. 2006). The Raman frequencies were calibrated using the polystyrene standard (ASTM E 1840) spectrum. Intensities were calibrated by NIST intensity standard (SRM 2241). Experiments were conducted at 20° C temperature.

Potential dependent SERS spectra were recorded starting from 0.8 V to 0 V and back to 0.8 V (*vs.* NHE) electrode potentials.

2.7.2. Quartz crystal microbalance with dissipation monitoring

A quartz crystal microbalance (QCM) is a technique that measures a mass per unit area by measuring the change in frequency of a quartz crystal resonator. The resonance is disturbed by the addition or removal of a small mass due to oxide growth/decay or film deposition at the surface of the acoustic resonator. The QCM can be used under vacuum, in gas phase and more recently in liquid environments. It is useful for monitoring the rate of deposition in thin film deposition systems under vacuum. In liquid, it is highly effective at determining the affinity of molecules (proteins, in particular) to surfaces functionalized with recognition sites. Larger entities such as viruses or polymers are investigated, as well. QCM has also been used to investigate interactions between biomolecules. Frequency measurements are easily made to high precision; hence, it is easy to measure mass densities down to a level of below 1 μg/cm^2 (Sauerbrey 1959).

Traditional QCM has been used for more than 50 years to analyse mass changes on rigid surfaces, most effectively in air or vacuum. QCM relies on a

voltage being applied to a quartz crystal causing it to oscillate at a specific frequency. Changes in mass on the quartz surface are related to changes in frequency of the oscillating crystal through the Sauerbrey relationship:

$$\Delta m = -\frac{C \Delta f}{n} \qquad (2.15)$$

where C – 17.7 ng Hz^{-1}cm^{-2} for a 5 MHz quartz crystal, Δf – change in resonance frequency, n – overtone number (1, 3, 5, 7). The Sauerbrey relation is valid for rigid, evenly distributed, and sufficiently thin adsorbed layers. However, for soft or viscoelastic films that do not fully couple to the oscillating crystal, the Sauerbrey relationship underestimates the mass.

QCM with dissipation monitoring (QCM-D) measures both frequency and dissipation of the quartz crystal. Dissipation occurs when the driving voltage to the crystal is shut off and the energy from the oscillating crystal dissipates from the system. D is defined as:

$$D = \frac{E_{lost}}{2\pi E_{stored}} \qquad (2.16)$$

where E_{lost} is the energy lost (dissipated) during one oscillation cycle and E_{stored} is the total energy stored in the oscillator (Dixon 2008). Figure 2.8 shows how the frequency of the oscillating quartz crystal changes with the mass on the sensor. Figure 2.9 shows the dissipation for a soft (green) and rigid (red) film when the driving voltage is turned off.
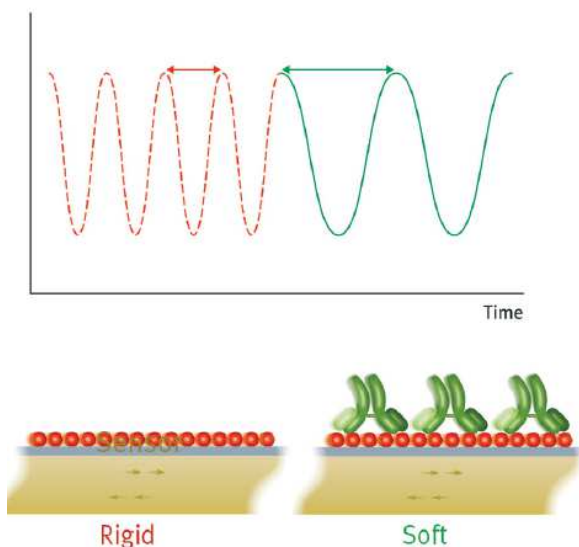
Fig. 2.8. The top diagram illustrates how the frequency of the oscillating sensor crystal (gold) changes when the mass is increased by addition of a molecular layer. Here antibodies (green) are added to a layer of protein (red).
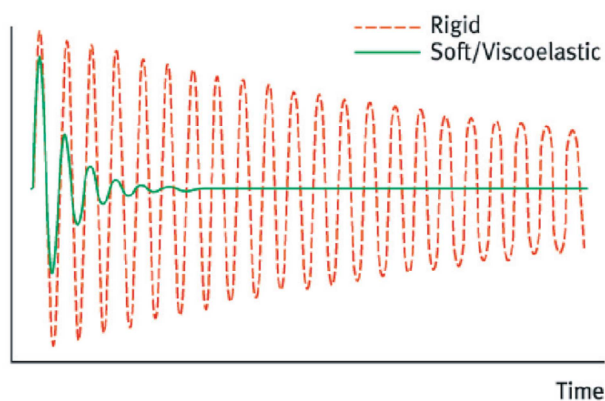

Fig. 2.9. Diagram illustrating the difference in dissipation signal generated by a rigid (red) and soft (green) molecular layer on the sensor crystal.

When molecules adsorb to an oscillating quartz crystal, water (or other liquid) couples to the adsorbed material as an additional dynamic mass via direct hydration and/or entrapment within the adsorbed film. Thus, the layer is sensed as a viscoelastic "hydrogel" composed of the molecules and the coupled water. By measuring the dissipation, one can determine if the adsorbed film is rigid or viscoelastic (soft). The amount of water in an adsorbed film can be as high as 95% depending on the type of material and the surface being studied.

Dissipation measurements enable qualitative analysis of the structural properties of adsorbed molecular layers. QCM-D technology allows quantitative analysis of the thickness, shear elastic modulus, and viscosity of the adsorbed films whereas these measurements are well beyond the Sauerbrey regime. This is achieved by combining frequency (*f*) and dissipation (*D*)

measurements from multiple harmonics (overtones) and applying simulations using a Voigt-based viscoelastic model:

$$\Delta f \approx -\frac{1}{2\pi\rho_0 h_0}\left\{\frac{\eta_3}{\delta_3} + \sum_{j=1,2}\left[h_j\rho_j\omega - 2h_j\left(\frac{\eta_3}{\delta_3}\right)^2\frac{n_j\omega^2}{\mu_j^2+\omega^2\eta_j^2}\right]\right\} \tag{2.17}$$

$$\Delta D \approx \frac{1}{2\pi f\rho_0 h_0}\left\{\frac{\eta_3}{\delta_3} + \sum_{j=1,2}\left[2h_j\left(\frac{\eta_3}{\delta_3}\right)^2\frac{\mu_j\omega}{\mu_j^2+\omega^2\eta_j^2}\right]\right\} \tag{2.18}$$

which describes acoustic response of quartz crystal (index "0") covered by two thin viscoelastic overlayers (j = 1,2) under a bulk Newtonian liquid (index „3"), where ρ is layer of liquid density, h – thickness, μ – elastic shear modulus, η – shear viscosity, δ – viscous penetration depth and ω – natural frequency of quartz crystal ($\omega = 2\pi f$), the indexes are specified accordingly (Voinova, Rodahl et al. 1999). Thus, if the adsorbed film is assumed to have a uniform thickness and density, Δf and ΔD can be described as functions of: n – overtone number, d – thickness, ρ – density, η – viscosity and μ – elasticity. By fitting experimental frequency and dissipation data from 2 or more harmonics, the unknown parameters can be extracted. This model has been successfully used in many publications studying a variety of experimental systems; however, it is important to note that it is a model with certain assumptions being made (Q-Sense). The bulk liquid should conform as Newtonian fluid where stress versus strain rate curve is linear (Batchelor 2000).

Q-Sense[®] (BiolinScientific AB, Sweden) has developed a patented QCM-D technology for surface analysis, enabling real-time, label free measurements of molecular adsorption and/or interactions on various surface with mass sensitivity of several ng/cm^2.

Fig. 2.10. Quartz sensor with gold surface, provided by Q-Sense® and used in the research.

The Q-Sense QWEM401 Electrochemistry Module allows simultaneous QCM-D electrochemistry measurements. The design enables flow measurements, which is important for well - controlled experiments. Also, the module withstands the harsh conditions necessary for some electrochemistry applications. The QCM-D sensor doubles as a working electrode for electrochemistry measurements. A platinum counter-electrode also acting as the top wall of the chamber reduces the volume above the sensor to about 100 μl. A low-leak reference electrode from WPI (essentially saturated silver chloride electrode) is included and is fixed in the outlet flow channel.

QCM-D experiments were carried out in our research in order to estimate the amount of AuNPs and laccase molecules attached to the surface, and to evaluate the bioelectrocatalytic properties of AuNP – laccase layer on a planar electrode. All measurements were made at 23 ± 0.02 °C temperature controlled by Peltier elements included in QWEM401 module. The QCM-D sensor surface was modified with poly-L-lysine (PLL), AuNPs and the enzyme by the following procedure. PLL was adsorbed on the QCM-D sensor and then laccase was deposited. After that an AuNP layer was adsorbed followed by adsorption of laccase. We assume that this final laccase adsorption step resulted into the enzyme adsorption only on AuNPs since adsorption of laccase directly on PLL covered gold sensor was already blocked by the first laccase adsorption step. After each adsorption step the characteristics of the resulting surface structures were assessed by QCM-D and electrochemistry.

Experiment initiation procedure was as follows. The flow cell was cleaned by consequent purge of Hellmanex® II solution (received from LabShop) and pure water. QCM-D gold sensor was rinsed with 99.5% pure ethanol and Millipore water, then dried under a flow of nitrogen gas, and placed in a Harrick plasma cleaner, model PDC-32G, for 10 min at the highest plasma intensity setting. For measurements the sensor was mounted into a QCM-D cell module and a stable baseline, i.e., Δf and ΔD response *vs.* time, was obtained in distilled water at a fixed flow rate of 100 µl/min and maintained the same all the time. The external potentiostat, Ivium CompactStat (Eindhoven, Netherlands), was set to record CVs starting from 1000 to 400 mV *vs.* NHE and back at the speed of 5 mV/s. The flow sequence was as follows - 0.002 % PLL solution in water (w/v) for 5 min, water for 10 min, buffer solution for 20 min, 50 µg/ml laccase solution for 10 min, buffer solution until the stable frequency, CV recorded, then water for 10 min, AuNP solution for ~3 h in order to get the fullest possible layer of nanoparticles, water for 2 min, buffer solution for 20 min until the stable frequency, CV recorded, 50 µg/ml laccase solution for 10 min, buffer solution for 20 min until stable frequency, CV recorded, buffer solution with inhibitor (1 mM NaF for *Trametes hirsuta*, 5 mM NaF for *Trichaptum abietinum* laccase assays) for 5 min and final CV recorded.

For adsorption of PLL layer on surface the Δf was relatively small and ΔD was negligible. During the enzyme and AuNP adsorption measurements with QCM-D fairly large Δf and ΔD were observed. Relatively large values of ΔD indicate that the adsorbed Lc and AuNP layer was viscoelastic and that the adsorbed mass was not linearly proportional to the change of the normalized frequency as assumed by Sauerbrey equation. During the viscoelastic modeling the adsorbed layer density (or thickness) and two viscoelastic parameters, *i.e.*, shear viscosity and shear modulus, were set as fitting parameters. The fluid density ($\rho = 1$ g/cm^3), fluid viscosity ($\mu = 1$ g/ms), and thickness (or density) of adsorbed layer were set constant. The modeling was performed with QTools software using the 3rd, 5th, and 7th overtones.

The mass of the enzyme layer on the PLL treated QCM-D sensor was calculated as a mass difference of the total mass of PLL and laccase layer minus the mass of PLL layer measured before enzyme adsorption.

In order to fit the data of the adsorbed AuNP and laccase layers, having extremely different properties, modeling was performed using a two-layer system. First layer corresponded to a structure PLL - laccase and second layer consisted of the AuNP layer in the structure PLL – laccase - AuNP. In order to evaluate the viscoelastic properties and thickness of the PLL - laccase layer, it was assumed that the density of the adsorbed protein layer was 1.20 g/cm^3 (Rodahl, Hook et al. 1997). All modeled first layer parameters were set as constant parameters, then second layer was included and the properties of the AuNP layer were modeled. The thickness, *i.e.*, the diameter of AuNPs used, measured in nm, was set as a constant parameter of the modeled AuNP layer. For the evaluation of the thickness of the enzymatic layer adsorbed on AuNPs, similarly as in the previous modeling analysis, the fitted viscoelastic properties and thickness of the PLL - laccase - AuNP layer were used for modeling as fixed parameters.

The best fit between the Voigt model and the experimental data for all the overtones was obtained considering the minimum value of the error function χ^2. The mass (g/cm^2) was obtained after multiplying the modeled values of density and thickness.

The experimental number of adsorbed AuNPs and laccase molecules per geometric area was estimated by dividing the sensed mass by the mass of a one AuNP or the mass of enzyme molecule, respectively. The mass of one AuNP was obtained by calculating the mass of a sphere with a determined diameter and density of 19.3 g/cm^3. The maximum possible monolayer coverage of AuNPs was established in assessment that AuNPs arrange into two-dimensional hexagonal packing monolayer structure (Evans 1993).

The QCM-D experiments were primarily used in order to establish the heterogeneous electron transfer constants between the active centres of laccases (both *Trametes hirsuta* and *Trichaptum abietinum*) and the surface of

AuNP. The average difference between cathodic current strength in the interval of 0.4 to 0.5 V *vs.* NHE from CV measurements of PLL – laccase – Au-NP – laccase multilayer assembly and the same after injection of buffer solution containing the inhibitor was taken into consideration. After establishing the number of laccase molecules on the sensor surface, the heterogeneous electron transfer constant, which accounts for amount of electrons passed through one enzyme molecule per second, was calculated:

$$k_{obs} = \frac{-\Delta I_{cat}}{N_A \times e \times n_{lac}} \qquad\qquad (2.19)$$

where k_{obs} – turnover constant (s^{-1}), ΔI_{cat} – cathodic current strength difference between working and inhibited systems (A), N_A – Avogadro constant, e – elementary charge, n_{lac} – amount of laccase present on the sensor surface (mol).

2.7.3. Null ellipsometry

As mentioned in 2.7.2., in the QCM-D measurements, water (or any other liquid or solvent molecules) couples to analysed protein film as an additional mass via direct hydration, viscous drag, or entrapment in cavities in the adsorbed film. This means that the layer is essentially sensed as a viscoelastic "hydrogel" composed of the macromolecules and the coupled water (Höök, Kasemo et al. 2001). Therefore, the water amount in the protein film adsorbed on AuNP needs to be established by other means for accurate estimation of number of laccase molecules on the AuNP surface.

Such tool chosen for the research is ellipsometry - an optical technique able to detect changes in the polarization state of light when it is reflected at the interface between two media with different optical properties: solid-air, solid-liquid, air-liquid or liquid-liquid. If the surface is optically modified, e.g., by protein adsorption, the associated change in polarization is detected (Tiberg and Landgren 1993; Tiberg 1996).

To describe the changes in polarization it is very common to use the so called ellipsometric angles psi, ψ, and delta, Δ. The first one describes the relative change in amplitude between the perpendicular and parallel components of light (with respect to the surface), p and s respectively in Figure 2.11. The latter is related to the phase shift between them.
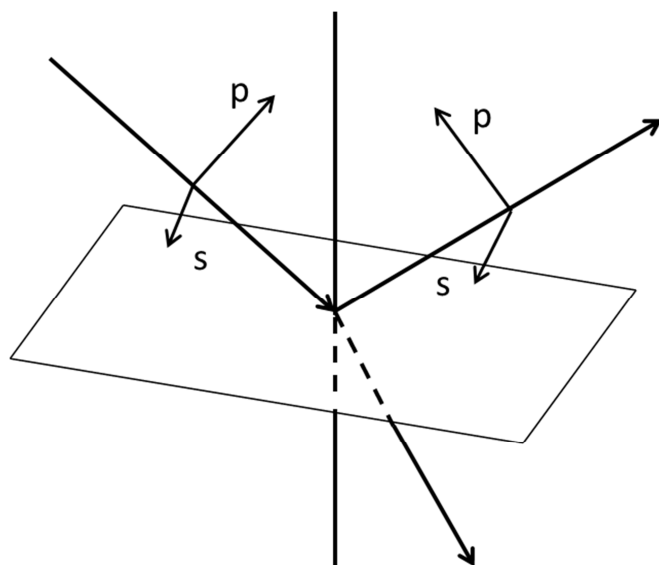

Fig. 2.11. Principle of ellipsometry, depicting relation between the perpendicular and parallel components of light.

In order to simplify calculations ψ and Δ are combined to form a single complex number, ρ:

$$\rho = \tan(\psi)\, e^{i\Delta} \hspace{3cm} (2.20)$$

Null ellipsometry is one of the methods used to experimentally obtain the ellipsometric angles. In Figure 2.12 the set-up of a null ellipsometer in the PCSA configuration is described.
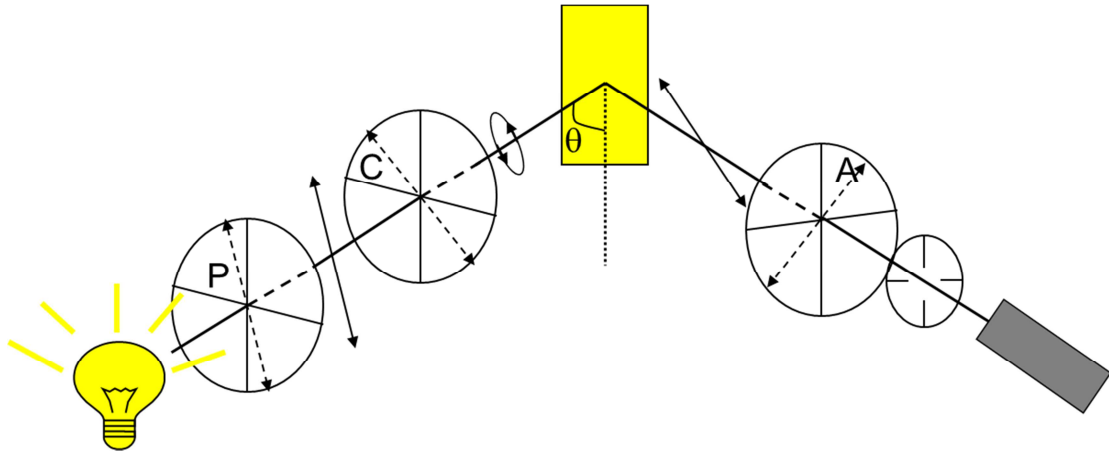
Fig. 2.12. Null ellipsometer in PCSA configuration

As illustrated, light coming from the source first passes through a polarizer (P), then, it goes through a retardation plate or compensator (C) and is reflected upon the sample, finally, it passes through a second polarizer, denoted analyser (A), and is detected by a photodetector. The method is called null ellipsometry because the components are set so as to produce a minimum in the transmitted light. In other words, light is extinguished at the analyser. The output parameters obtained are the angular positions for the polarizer and the analyser that result in light extinction. As the compensator can have its fast axis oriented at ± 45° relative to the plane of incidence, there are 4 possible relative positions (or zones) for P and A that allow the null condition, and for each of these relative positions there one expression that relates ψ with A and Δ with P:

	Compensator angle	ψ	Δ
Zone 1	- 45°	A	2P + 90°
Zone 2	- 45°	A	- 2P - 90°
Zone 3	+ 45°	180° - A	2P - 90°
Zone 4	+ 45°	180° - A	- 2P + 90°

In order to obtain the optical properties of the gold surface a two-layer model, gold surface-ambient, has to be applied. The input data are the experimentally determined ψ and Δ needed to solve Equation 2.20, and the refractive index for

the ambient medium, n_0, and the angle of incidence of light Θ, that together with the value obtained for ρ, are inserted in this equation:

$$n_{Au} = n_0 \tan\theta_0 \sqrt{\left(1 - \frac{4\,\rho}{(1+\rho)^2}\sin\theta_0\right)} \qquad (2.21)$$

where n_{Au} corresponds to the complex refractive index of the gold surface.

To be able to calculate the adsorbed amount of protein, Γ, calculated as mg/m^2, of the enzyme the optical properties of the enzyme layer (refractive index, n_f, and thickness, d) should be determined. To do so, a three layers model has to be used, and the layer is assumed to be homogeneous and plane parallel. No analytical expression can be obtained, and an iterative procedure has to be performed in order to obtain the refractive index and the layer thickness. Once these parameters are known, the adsorbed amount is calculated by using this equation:

$$\Gamma = \frac{n_f - n_0}{\frac{dn}{dc}}d \qquad (2.22)$$

where *dn/dc* reflects the dependence of the refractive index with the concentration of enzyme in solution (0.18 ml/g) (De Feijter, Benjamins et al. 1978).

3. RESULTS AND DISCUSSION

3.1. Kinetics of *Trichaptum abietinum* laccase in solution

Before the synthesis and research of bioelectrocatalytic systems consisting of AuNPs and laccases, the biochemical properties of newly purified *Trichaptum abietinum* laccase had to be established. Particularly interesting was establishment of kinetic parameters of inorganic and organic substance oxidation catalysis and also determination of laccase T1 active centre redox potential. Obtained results were compared to known parameters of *Trametes hirsuta* laccase.

As described in 2.4.2., the oxidation of the various substrates in solution catalysed by *Trichaptum abietinum* laccase was analysed spectrophotometrically and by using a homemade computer-assisted membrane oxygen electrode. Calculated kinetic parameters are presented in Table 3.1. and 3.2.

Table 3.1. Spectrophometricaly determined kinetic parameters of *Trichaptum abietinum* laccase catalysed substrates oxidation at pH 4.0 and 5.5 at 25 $^\circ$C.

Substrate	pH	K_M, μM	V_{max}, μM/s	k_{cat}, s^{-1}	k_{ox}, μM^{-1}·s^{-1}
ABTS	5.5	42 ± 7	0.056 ± 0.004	87 ± 6	2.1 ± 0.3
ABTS	4.0	110 ± 8	0.25 ± 0.02	390 ± 30	3.5 ± 0.5
K$_4$[Fe(CN)$_6$]	5.5	5.5 ± 0.7	0.132 ± 0.004	110 ± 3	19 ± 2
K$_4$[Fe(CN)$_6$]	4.0	5.4 ± 1.2	0.088 ± 0.005	680 ± 40	130 ± 20
PYR	5.5	620 ± 250	0.45 ± 0.12	62 ± 17	0.11 ± 0.01
HQU	5.5	390 ± 100	0.15 ± 0.02	22 ± 3	0.06 ± 0.01
SYR	5.5	15 ± 2	0.063 ± 0.005	21 ± 2	1.4 ± 0.1

Table 3.2. Kinetic characteristics of substrates oxidation catalysed by *Trichaptum abietinum* laccase (according to oxygen consumption)

Substrate	pH	K_M, µM	V_{max}, µM/s	k_{cat}, s^{-1}	k_{ox}, µM^{-1}·s^{-1}
ABTS	5.5	140 ± 20	0.20 ± 0.01	32 ± 2	0.22 ± 0.03
ABTS	4.0	180 ± 40	0.27 ± 0.01	140 ± 10	0.82 ± 0.16
$K_4[Fe(CN)_6]$	5.5	250 ± 90	0.42 ± 0.06	67 ± 2	0.26 ± 0.11
$K_4[Fe(CN)_6]$	4.0	46 ± 10	0.19 ± 0.01	480 ± 30	10 ± 2
PYR	5.5	1360 ± 160	0.43 ± 0.03	34 ± 2	0.03 ± 0.01
HQU	5.5	320 ± 40	0.44 ± 0.02	7.0 ± 0.3	0.022 ± 0.002
SYR	5.5	3.0 ± 1.0	0.0084 ± 0.0005	0.27 ± 0.02	0.09 ± 0.03

Unlike *Trametes hirsuta* laccase, described in 1.1.2., this new laccase poorly catalyses oxidation of organic compounds, meanwhile exhibiting fast catalysis of oxidation of inorganic substance ferocyanide. Since we currently don't have an established 3D structure of *Trichaptum abietinum* laccase for detailed insight, this result could lead into speculation that surface area of T1 active centre of the new laccase has a larger surface charge (possibly positive, since ferocyanide ion is negative), thus posing difficulties for hydrophobic organic substances to reach the catalytic centre.

Spectroelectrochemical T1 copper site titration of *Trichaptum abietinum* laccase was performed as described in 2.5.3, the results are presented in Fig. 3.1. and Table 3.3.
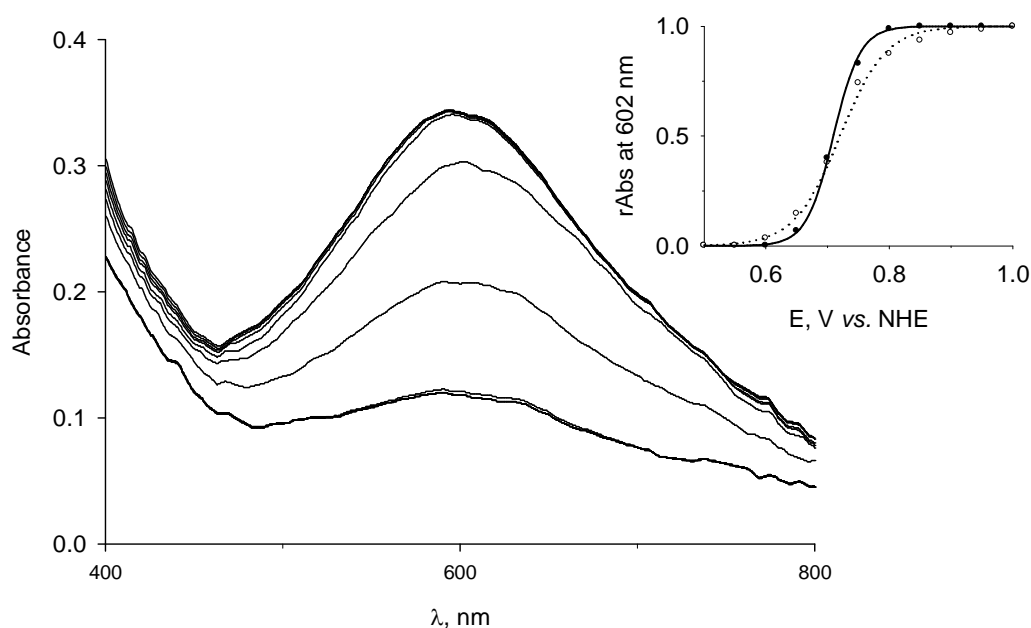
Fig 3.1. Redox titration of the T1 copper site of laccase from *Trichaptum abietinum* using the redox mediator $K_4[Mo(CN)_8]$. The inset shows dependence of relative absorption at 602 nm on the electrode potential, calculated by Eq. 2.8. The curves connecting points are drawn following model, described by Eq. 2.6 - 2.8; solid curve represents oxidative, dotted curve – reductive scan direction.

Table 3.3. Estimated redox potential of the T1 site of *Trichaptum abietinum* laccase and number of electrons involved in the redox process, as described in 2.5.3.

|	E_{redox}, mV *vs.* NHE	n_e
Anodic scan	709 ± 4	1.161 ± 0.007
Cathodic scan	720 ± 7	0.688 ± 0.007
Average	714 ± 12	0.92 ± 0.24

It can be observed that estimated redox potential of *Trichaptum abietinum* laccase (714 mV *vs.* NHE) is lower than redox potential of *Trametes hirsuta* laccase (780 mV *vs.* NHE (Shleev, Morozova et al. 2004)). Both enzymes could be considered as high – potential laccases.

3.2. Size and concentration of gold nanoparticles

AuNPs were synthesized as described in 2.6.1. The batch solutions were kept refrigerated at 4ºC before the use in construction of bioelectrocatalytic assays.

The solutions proved to be stable throughout time; however, batches older than 6 months were discarded from experiments.

Some of the AuNPs used in the experiments that had their size estimated using different techniques, described in 2.6.2, 2.6.3, 2.6.4; the results are compared in Table 3.4. The exemplary SEM pictures of several AuNPs are shown in Fig. 3.2, and DLS analysis of several AuNPs using the NICOMP distribution algorithm is depicted in Fig. 3.3. DLS results obtained by Gaussian distribution algorithm are also presented – this method is traditionally employed in DLS data analysis, whereas Particle Sizing Systems® regards their patented NICOMP distribution algorithm superior than Gaussian distribution algorithm.
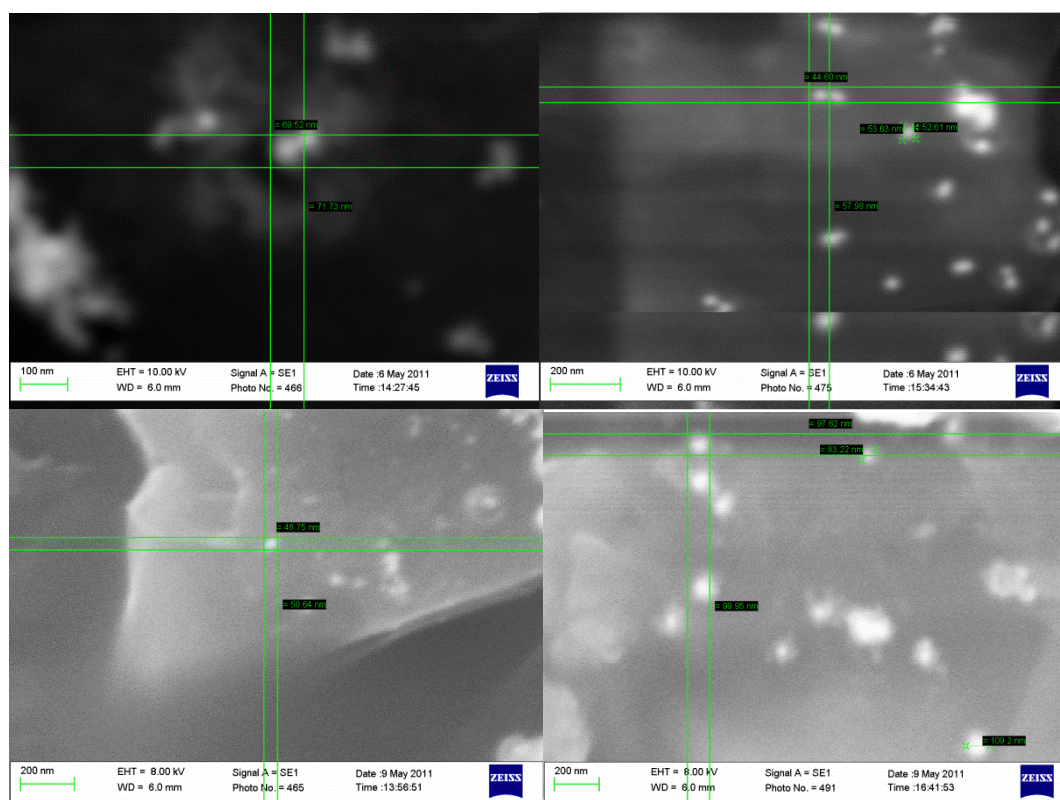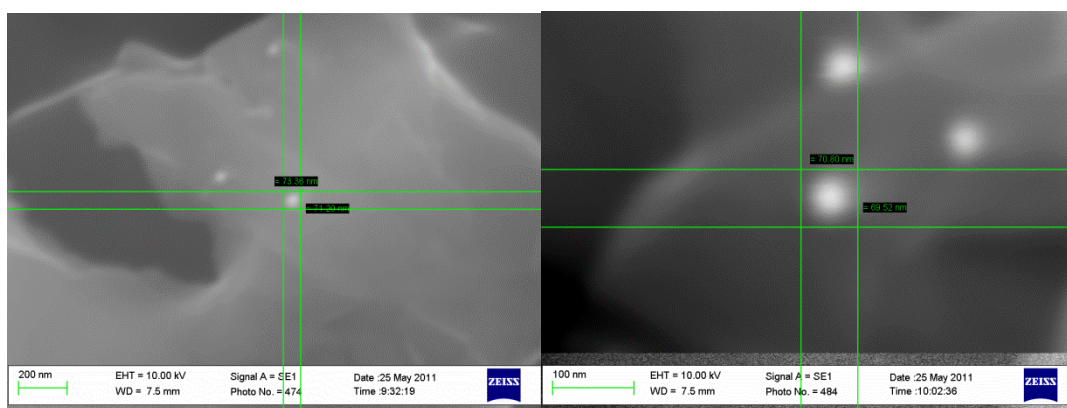
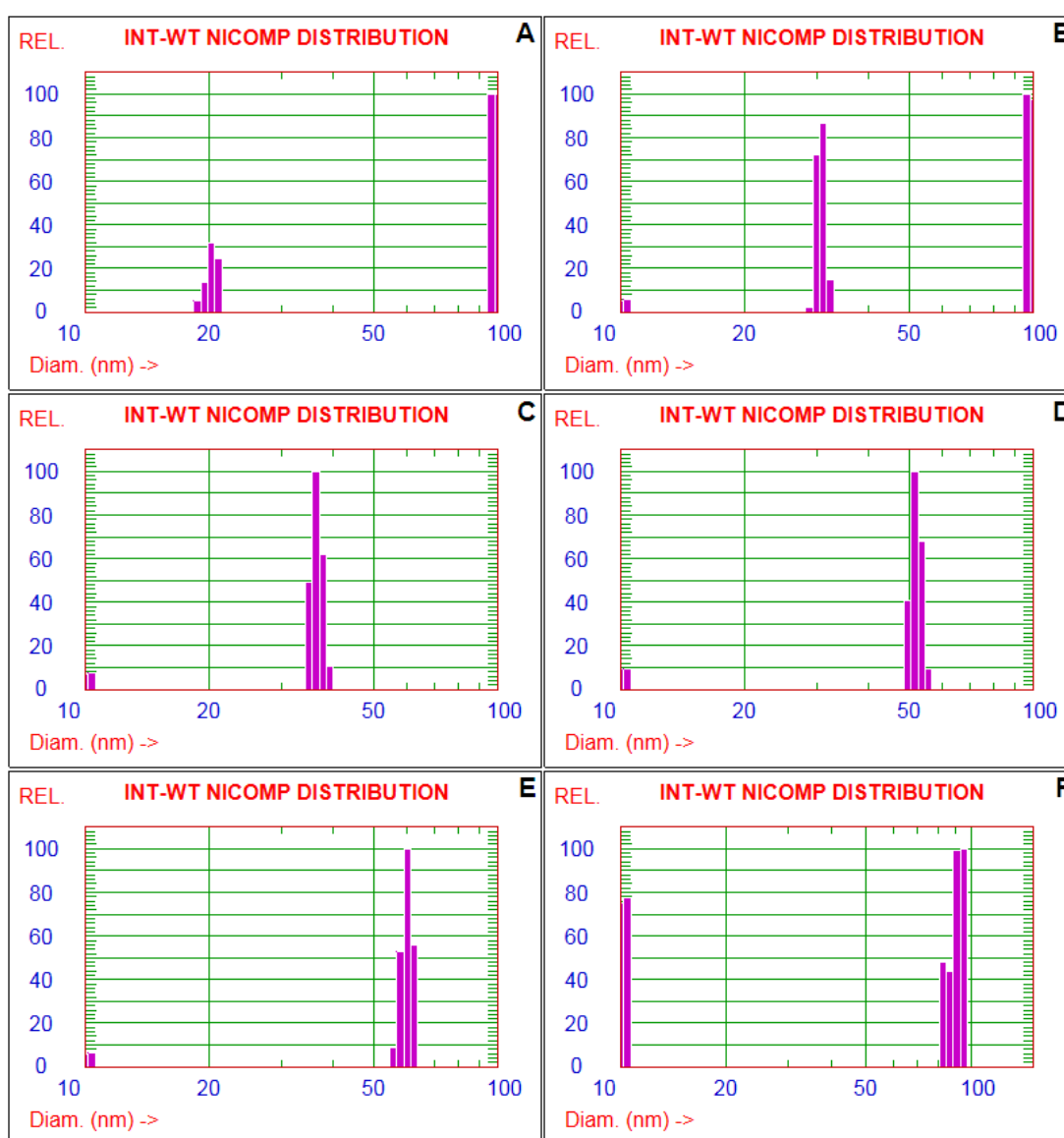**Fig. 3.2.** SEM images of several batches of AuNPs used in research.

Fig. 3.3. Diameters of AuNPs measured with DLS. Minimum diameter was set to 10 nm, Plot size to 60, Smoothing to 2, and Plot range to 10 for **A-E**. Plot range for **F** had to be set higher

(15) due to the diameter of the particles. Diameters are; **A**: 20.2 nm, **B**: 30.6 nm, **C**: 36.5 nm, **D**: 52.0 nm, **E**: 60.1 nm, **F**: 91.6 nm.

Table 3.4. Estimated and measured diameters of some of AuNP suspensions. The errors calculated in SEM analysis were attributed by visual assessment of AuNPs (see Fig. 3.2.).

AuNP Batch Nr.	Expected diameter, nm	d_{SPA}, nm	d_{SEM}, nm	d_{DLS}, nm	
				NICOMP dist.	Gaussian dist.
1	15	≤20	33.3 ± 2.4	20.2 ± 0.8	79.5 ± 69.5
2	15	≤20	41.3 ± 2.9	30.6 ± 0.7	62.5 ± 45.3
3	20	35	57.7 ± 5.9	35.6 ± 1.0	33.9 ± 14.0
4	20	28	51.2 ± 3.9	36.5 ± 1.4	32.8 ± 9.8
5	20	32	50.0 ± 4.9	39.3 ± 1.6	25.4 ± 8.2
6	30	39	58.2 ± 4.0	45.4 ± 1.1	24.0 ± 9.2
7	60	49	61.3 ± 6.6	46.9 ± 1.4	31.0 ± 9.9
8	70	54	70.2 ± 1.0	52.0 ± 1.8	44.7 ± 16.6
9	70	52	74.2 ± 3.9	60.1 ± 1.6	68.5 ± 43.1
10	75	64	103.9 ± 10.9	91.6 ± 3.1	32.3 ± 23.6

The sizes measured with DLS are larger than the size for the same particle batches measured with the spectrophotometer (Table 3.4.). However, differences in diameters using surface plasmon absorbance and DLS methods are not entirely unexpected. The DLS is based on the diffusion properties of the particles and measures how fast the particles are moving through the solvent. The actual size obtained from these measurements is the hydrodynamic radius, or Stokes radius R_S (Berne and Pecora 2000):

$$R_S = \frac{k_B T}{6\pi\eta D}$$

(3.1)

where D is the diffusion coefficient, k_B is the Boltzmann constant, η is the viscosity and T the absolute temperature. The actual shape (not perfectly round) of the particles would influence the diameter derived through Stokes radius. In case of AuNP obtained through the citrate reduction method the

thickness of the hydrodynamic layer is considered too thin to have an impact on the results.

In all DLS measurements a large amount of artefacts were visible at 5 - 10 nm in the spectrum, using the NICOMP distribution algorithm (intensity weighted) (Fig. 3.3). Whether these artefacts were due to interference, contamination, or aggregates of non - reacted compounds from the synthesis is unknown.

When absorbing particles on surface, it is very likely that the particles will arrange in a way that assures maximum surface binding energy. Hence, the same particle suspension may yield different diameters using techniques that measures different properties of the sample. In case of citrate reduced AuNPs, the measurements could be further complicated due to accumulation of substances present in solution.

SEM was used to view the shape of the particle adsorbed on a carbon surface. This was used as a reference to the other sizing techniques. While the SEM most likely views the "flattest" side of the particles, citrate in the solvent may also absorb on the particles and yield a structure that looks bigger. However, the differences between DLS, SPA and SEM diameters were consistent, as seen in Fig. 3.4.

One technique cannot be deemed inadequate or erroneous, simply because the resulting diameters are different compared to those of other techniques. Discrepancy in diameters between two or more techniques should instead be seen as a potential tool for evaluating the three - dimensional shape or roughness of AuNPs. It could be concluded that it is best to use several methods to determine the exact size of AuNPs. It is important that the results obtained by several methods correlate, so for the matter of simplicity, we used AuNP size measurements results obtained by DLS utilizing NICOMP particle distribution algorithm (Table 3.4 and Fig. 3.3) in further experiments and references, unless stated otherwise.

The concentrations of each AuNP batch were calculated as described in 2.6.2. by using Eq. 2.9 – 2.11. Typically, AuNPs of apparent diameter between 40 and 50 nm resulted in concentrations of about 0.2 – 0.4 nM (the smaller the

size, the higher the concentration), and the yield of reactions were about 70 – 80 %. The yield results were not reproducible and had no relation to obtained AuNP size.
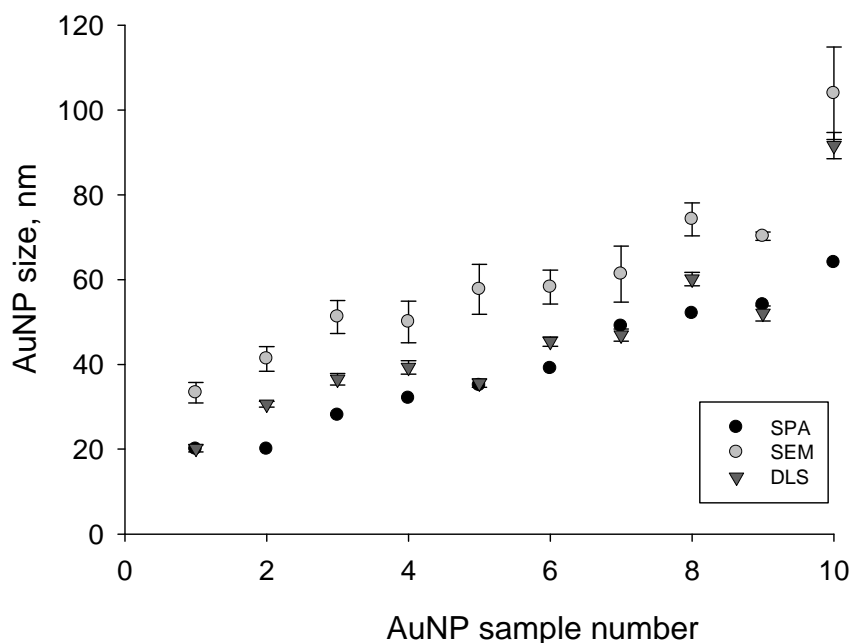

Fig. 3.4. Comparison graph correlating AuNP sizes obtained through DLS, SEM and SPA techniques.

3.3. Interaction between gold nanoparticles and *Trametes hirsuta* laccase

Before the DET bioelectrochemical research, AuNP and laccase interactions in the buffer solution were studied. Two aspects of laccase – AuNP interaction were addressed – the enzymatic activity of the mixture in respect to the size of nanoparticles, and the activity change over time. If AuNP surface would completely or partially block T1 copper site of laccase, we could see the drop of laccase enzymatic activity in catalysis of ABTS oxidation by oxygen. The influence of AuNP to the activity of laccase was investigated according to the method for determination of k_{obs} described in 2.4.2. In order to have the maximum number of enzymes in solution to be connected to AuNP, the ratio of enzyme – AuNPs was adjusted so that 30% of the NP surface would be covered by enzyme. After immediate mixing the enzyme activities usually stayed between 54 and 73% compared to native activity, and after 20h the

activity dropped to 30 - 49% (Fig. 3.5). The k_{obs} of pure *Trametes hirsuta* laccase after thawing from -20°C to room temperature was 140 ± 10 s^{-1} (mean value of five measurements), and after keeping in 4°C for 20h (as well as laccase – gold NPs mixture) – 130 ± 20 s^{-1}.
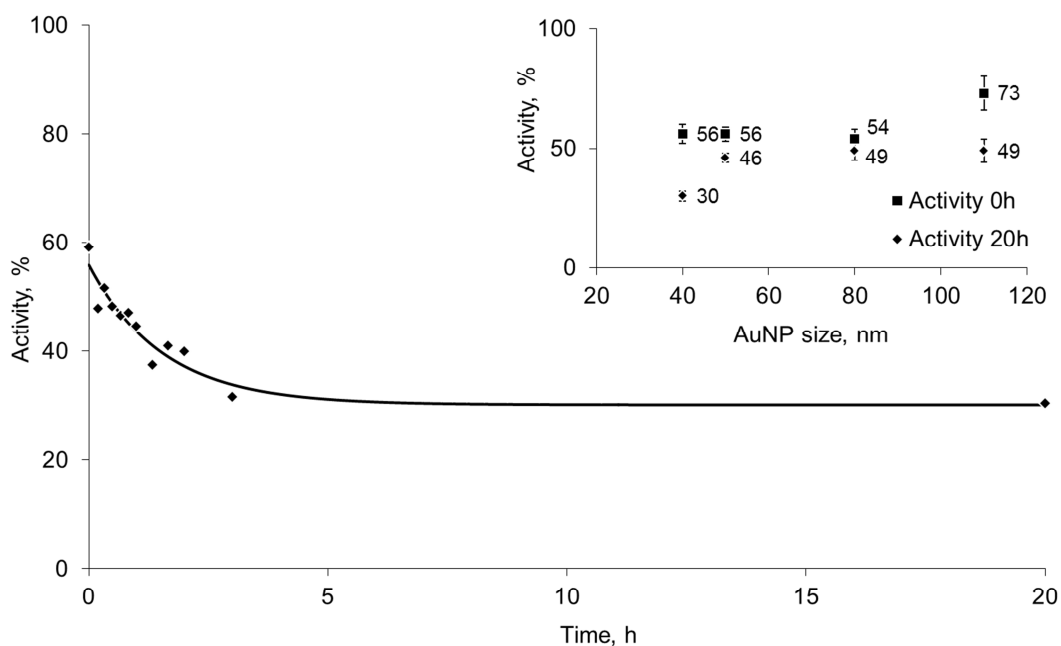

Fig. 3.5. The relative activitiy of 40 nm AuNP – laccase mixture dependence on time after mixing. 100% stands for the k_{obs} of laccase solution at the same time. The exponential model implies that initial relative activity of the mixture is 56 ± 4 % at the beginning and 30 ± 2 % after 20h. The inset shows such values of relative activities when using different size AuNP in the mixture.

Apparent laccase activity on AuNPs could be altered by various means, such as enzyme denaturation on metallic surface, decrease of substrate diffusion to active centre of enzyme, etc. Thus, this research was used only as incitement to further electrochemical analysis of AuNP and laccase DET bioelectrocatalytic systems.

3.4. Direct electron transfer of multicopper oxidases on gold nanoparticles

3.4.1. Gold nanoparticle and laccase electrochemistry

After observation that AuNP interact with the *Trametes hirsuta* laccase, the experimental work was directed to investigate the effect of AuNP on heterogeneous ET of this enzyme. AuNPs were deposited on the surface of solid gold electrode and the laccase was adsorbed. The laccase ability for DET at these electrodes has been studied by running CV experiments. The experimental results are shown in Fig. 3.6.
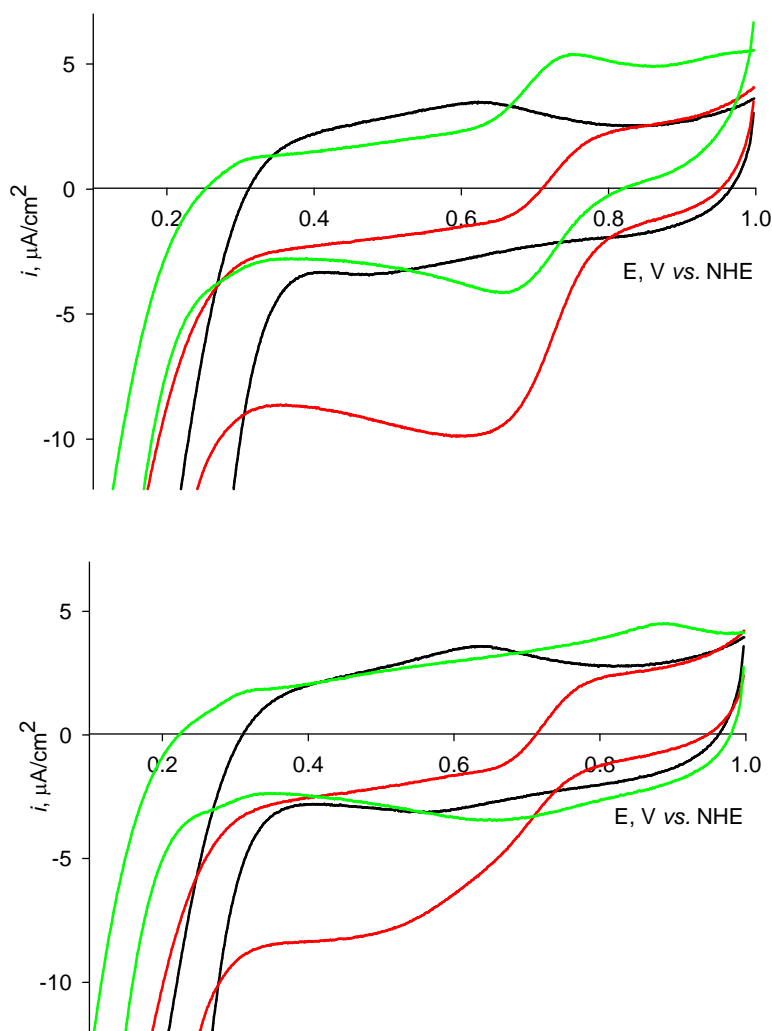

Fig. 3.6. CVs of *Trametes hirsuta* laccase immobilized on gold electrodes modified with 40 nm (top) and 50 nm (bottom) AuNPs. The black line represents CV of bare gold electrode with AuNPs, red line – the same electrode with laccase adsorbed on the surface, green line –

the electrode modified with AuNPs and laccase in the presence of 1mM NaF. CVs were recorded at 10mV/s potential scan rate. Buffer solution was 50 mM Na_2HPO_4 with 0.1 M Na_2SO_4, pH 4.0, adjusted by citric acid.

From Fig. 3.6 it can be seen that by gradually lowering an applied potential (starting at 1 V) the reduction current begins to increase at approximately 850 mV and levels off at the potentials below 650 mV (in the case of 40 nm AuNP system). The current is observed due to the bioelectrocatalytic reduction of oxygen at laccase - AuNP modified electrode. The removal of oxygen from the solution resulted in the disappearance of the bioelectrocatalysis (data not shown). Additionally, the current (Fig. 3.6, green line) was strongly suppressed in the presence of NaF. The bioelectrocatalytic current was not observed if the AuNP modified electrode was not additionally modified with the laccase (fig. 3.6, black line). These controls confirm that the current is due to the laccase catalysed heterogeneous electroreduction of oxygen. In agreement with many other experiments (Shleev, Christenson et al. 2005; Shleev and Ruzgas 2008) it was not possible to observe any substantial oxygen bioelectroreduction at laccase modified planar gold electrodes (data not shown). Thus, the modification of the electrode with AuNPs is of key importance for enabling the bioelectrocatalysis of oxygen at the electrodes modified with the laccase.

It is obvious that the bioelectrocatalysis is due to DET between the laccase and AuNP modified surface since no any ET mediators are present in solution or are confined to the surface. It can be argued that the electrons are transferred from the AuNP modified electrode surface to the T1 copper site and further onto the T2/T3 copper cluster where the oxygen is reduced to water. The proposed electron transfer mechanism is schematically depicted in Fig. 3.7.
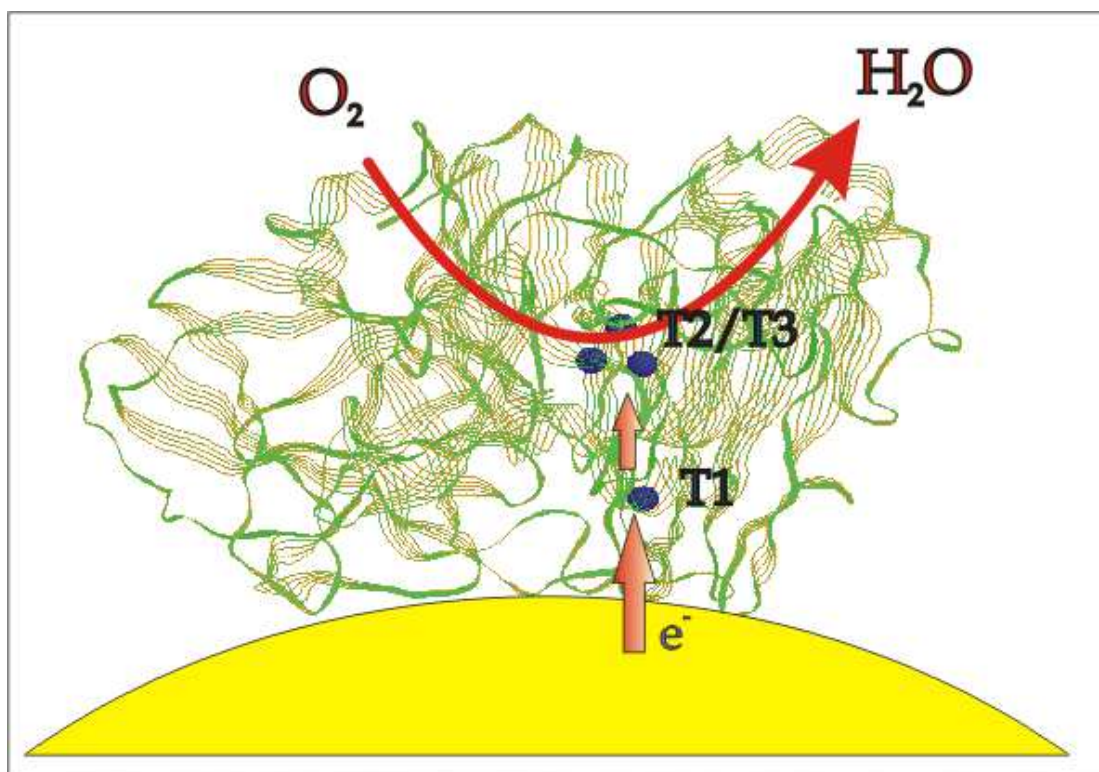
Fig. 3.7. The proposed mechanism of direct ET of laccase at gold nanoparticle modified electrodes. The T1 and T2/T3 copper sites are presented in blue spheres. Red arrows represent the direction of heterogeneous ET and the reaction of oxygen reduction to water when the applied potential is below 850 mV (see Fig. 3.5).

The conclusion, that the T1 site accepts the electrons from the electrode first, is based on several facts. First, the midpoint potential of LSV (Fig. 3.6, red line, 730 mV) is sufficiently close to the formal potential of the T1 copper in *Trametes hirsuta* laccase, i.e., 780 mV (Shleev, Christenson et al. 2005). Secondly, the midpoint potential in LSVs remains practically the same in the absence and presence of fluoride ions (Fig. 3.6). It is known that fluoride complexes at the T2/T3 copper site and blocks catalytic oxygen reduction (Shleev, Christenson et al. 2005). Additionally, DET between the T2/T3 copper site of high potential laccases and the electrode surfaces was previously postulated to appear at much lower potentials, specifically, at 300-400 mV (Shleev, Christenson et al. 2005; Ramírez, Mano et al. 2008). All this supports the heterogeneous electron transfer mechanism depicted in Fig. 3.7.

Based on the provided explanations and experimental results presented in Fig. 3.6 it can be concluded for the first time that oxygen electroreduction catalysed by laccases is possible on gold, i.e., metal, electrodes following the mechanism schematically presented in Fig. 3.7. The efficient bioelectrocatalysis seems to require nanostructured gold surface. Additionally, by comparing the results presented in Fig. 3.5 to the bioelectrochemical laccase investigation on carbon electrodes (Shleev, Jarosz-Wilkolazka et al. 2005) it is possible to state that the laccase-catalysed electroreduction of oxygen on AuNP modified electrode is similar to the well know oxygen bioelectrocatalysis on laccase modified carbon surfaces. At this point, a detailed molecular model of the laccase - AuNP interaction is not clear. The experimental results indicate that AuNP might enable shorter electron transfer distance between the electrode and the T1 copper site (Fig. 3.7).

Further experiments involved DET bioelectrocatalytic systems with newly purified *Trichaptum abietinum* laccase. The CVs of gold RDE, covered by AuNPs and *Trichaptum abietinum* laccase, as described in 2.5.2, were recorded and analysed. From Fig. 3.8 it can be seen that by gradually lowering an applied potential (starting at 1 V) the reduction current begins to increase at approximately 900 mV and levels off at the potentials below 700 mV. The current is observed due to the bioelectrocatalytic reduction of oxygen at AuNP and laccase modified electrode.

The removal of oxygen from the solution resulted in the disappearance of the bioelectrocatalysis (data not shown). Additionally, the current (Fig. 3.8, green line) was strongly suppressed in the presence of NaF. The bioelectrocatalytic current was not observed if the AuNP modified electrode was not additionally modified with the laccase (Fig. 3.8, black line). These controls confirm that the current is due to the laccase catalysed heterogeneous electron transfer based bioreduction of oxygen. The bioelectrocatalytic current was the highest ever recorded for such laccase – AuNP system, reaching >200 µA/cm2. Since the current doesn't change significantly at potentials lower than 700 mV, we

assume the process is limited by enzyme turnover, because: a) the current doesn't increase by increasing RDE rotation rate, so oxygen diffusion is not the limiting factor, and b) higher overpotential does not lead to higher current density, as it would in case the process would be limited by heterogeneous electron transfer between electrode surface and enzyme (refer to 2.5.2). .
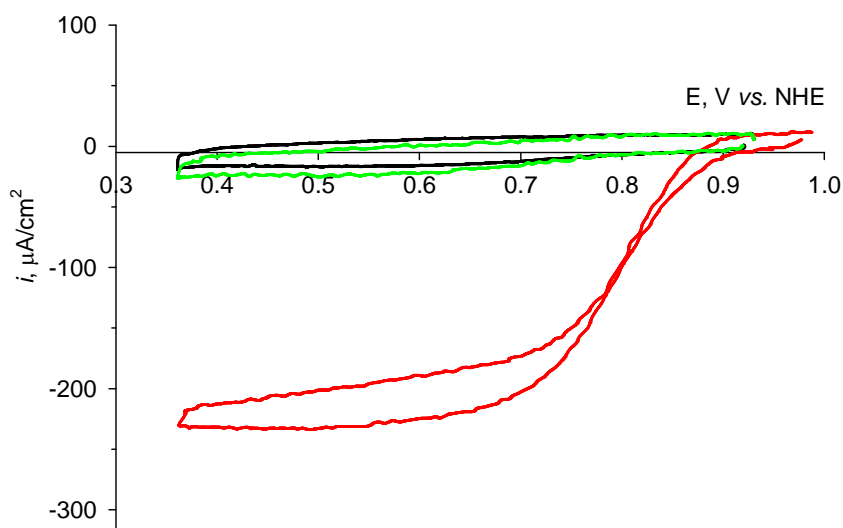

Fig. 3.8. CVs of *Trichaptum abietinum* laccase adsorbed on gold electrodes, modified with AuNPs. Black curve represents CV recorded with a gold electrode modified with AuNPs, red curve – same electrode after addition adsorption of laccase, green curve – the same electrode in the presence of laccase inhibitor, 2 mM NaF. CVs were recorded at 5 mV/s by using RDE, spinning at 400 rpm.

Similar RDE CV experiments carried out with DET bioelectrocatalytic systems consisting of AuNPs and *Trametes hirsuta* laccase showed that current density does not increase with increasing electrode rotation speed (data not shown), implying that the current density is limited either by heterogeneous ET between enzyme active centre and AuNP or by catalytic activity of the immobilized enzyme.

The RDE CV experiments for AuNP size effect to bioelectrocatalytic current output were also carried out. Amount of AuNP for electrode coverage was selected so that the number of used AuNP would be enough to form a

monolayer of AuNPs on gold electrode surface, as described in 2.5.1. The results are presented in Fig. 3.9.
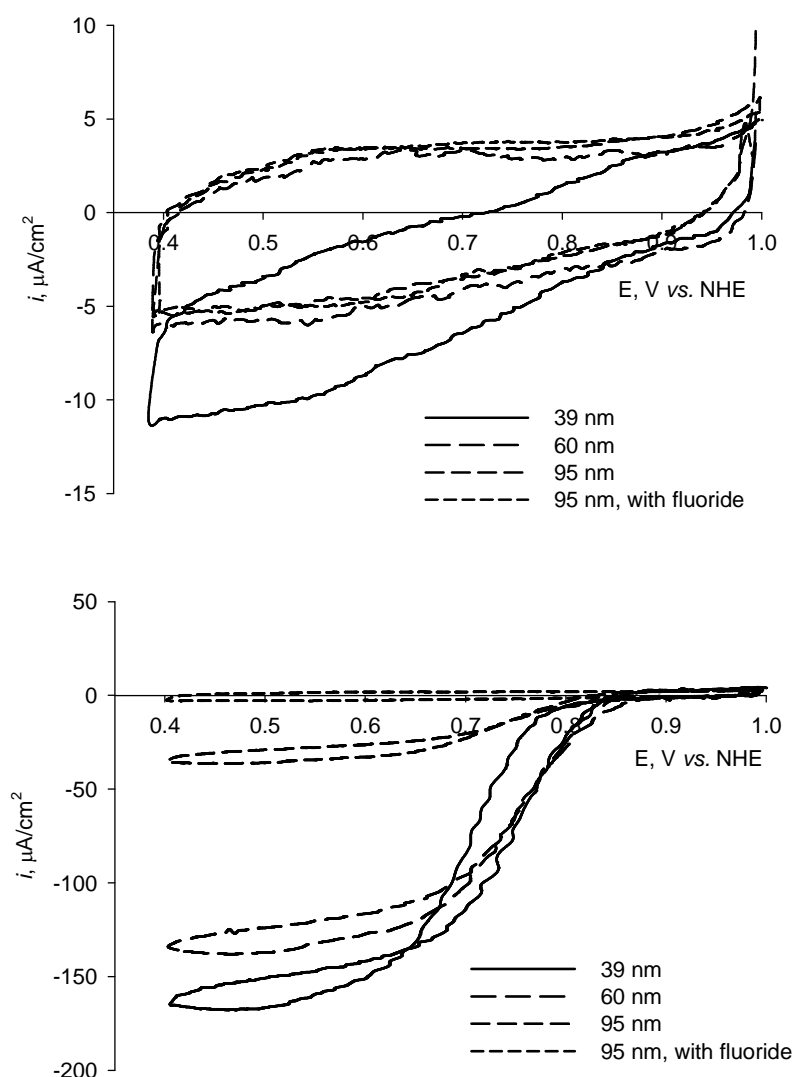

Fig. 3.9. CVs of *Trametes hirsuta* (top) and *Trichaptum abietinum* (bottom) laccases adsorbed on RDE gold electrodes modified with different size AuNPs. CVs recorded after fluoride addition to solution are shown for 95 nm Au-NPs' systems, in case of other size Au-NPs the CVs are very similar.

The results indicate that smaller diameter AuNP contribute to higher current density output of laccase – AuNP DET bioelectrocatalytic system. However, this research could be considered only as advisory, since adsorption of needed amount of AuNPs in orderly monolayer manner on electrode surface cannot be

controlled. The results proposed idea for QCM-D AuNP – laccase interaction experiments.

The effect of fluoride and chloride addition to the bioelectrocatalytic system was analysed. In these experiments 0.4 V *vs.* NHE potential was applied to the prepared RDE gold electrode spun at 400 rpm, the current change over time was analysed during consequent addition of inhibitor to the reaction solution (Fig. 3.10 - 3.11). Since the time required obtaining the steady current at each inhibitor addition step would be quite long (usually more than 15 minutes), the simple exponential growth model was used for data fitting:

$$i_i = a \times e^{b \times t_i} + c \qquad\qquad (3.2)$$

where i_i and t_i – current density and time values at the i step. The offset c is considered as the last - point current density value. The dependence of such values on the inhibitor concentration present in the buffer solution was analysed. In the case of fluoride addition, non - competitive inhibition model was considered, and in the case of chloride the competitive model was applied to the data (Dixon 1953). The inhibition research result comparison is presented in Table 3.5.
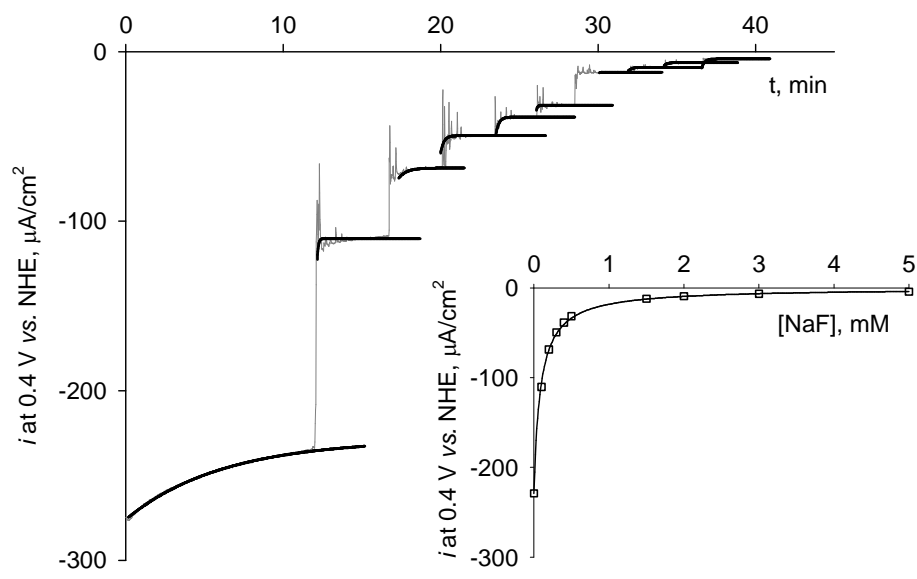
Fig 3.10. Effect of fluoride addition to the solution on biocathodic current density of gold electrode coated with AuNPs and *Trichaptum abietinum* laccase at 0.4 V *vs.* NHE. The simple exponential growth models are presented over the data points. The inset shows current response dependence on fluoride concentration in the solution, non - competitive inhibition model curve when K_i equals 87 µM of NaF is drawn over the data points.
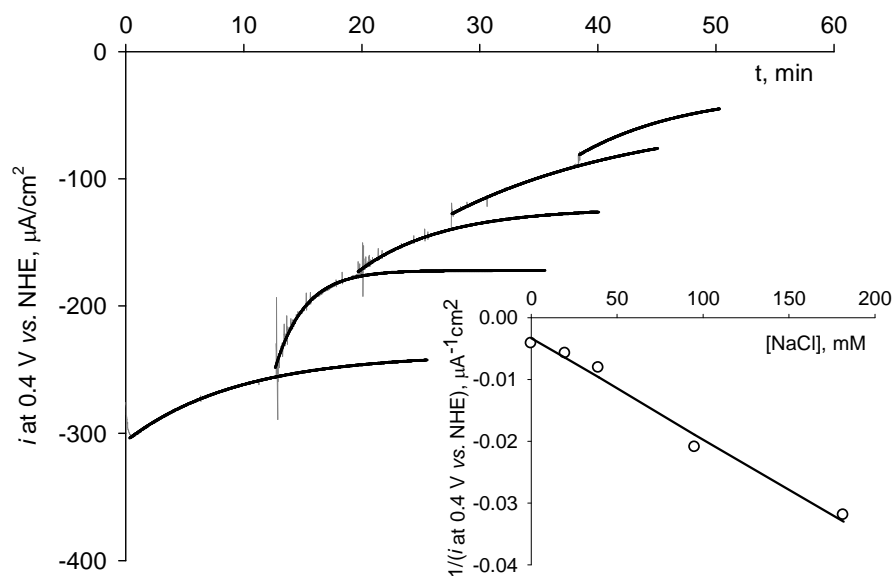

Fig 3.11. Effect of chloride addition to the solution on biocathodic current density of gold electrode coated with AuNPs and *Trichaptum abietinum* laccase at 0.4 V *vs.* NHE. The simple exponential growth models are presented over the data points. The inset shows inverted current response dependence on chloride concentration in the solution, competitive inhibition model line when K_i equals 5.6 mM of NaCl is drawn over the data points.

Table 3.5. Comparison of laccase inhibition constants (K_i, mM) in either homogenous (in solution with 2 mM ABTS) and heterogenous (on AuNP modified gold electrode) systems. Buffer solutions used in measurements were the same.

Laccase	NaCl (competitive inhibition)		NaF (non – competitive inhibition)	
	In solution	On electrode	In solution	On electrode
Trichaptum abietinum	20.2 ± 2.6	5.6 ± 1.1	12.4 ± 2.0	0.087 ± 0.003
Trametes hirsuta	8.8 ± 3.7	13.8 ± 5.7	0.037 ± 0.009	0.071 ± 0.007

The experiments revealed that *Trichaptum abietinum* laccase, which is resistant to NaF in homogeneous system in comparison to *Trametes hirsuta* laccase, loses resistance to NaF in AuNP – laccase DET bioelectrocatalytic system, possibly after adsorption on AuNP surface. The reasons of this behaviour remain unclear; however, we speculate that T2/T3 site of *Trichaptum abietinum* laccase experience structural changes upon adsorption on gold surface, meanwhile such effect is not observed when *Trametes hirsuta* laccase is used.

3.4.2. Gold nanoparticle and human ceruloplasmin electrochemistry

The possibility of working heterogeneous DET bioelectrocatalytic system containing human ceruloplasmin (Cp) and AuNPs was studied. AuNPs were deposited on the surface of solid gold electrode and Cp was adsorbed. The Cp ability for DET at these electrodes has been studied by running CV experiments. Electrode modification procedure was as follows. Firstly, gold electrodes were modified with AuNPs. 10 μl of a solution containing 50 nm AuNPs was added on the top of the electrode, after which the electrode was allowed to dry and then rinsed thoroughly with Milipore water. Secondly, 10 μl of Cp (10 mg/ml in 10mM phosphate buffer, pH 6.0) was placed on the gold surface. The electrode was covered to avoid evaporation and left to react for 90 min.

The CVs of AuNP modified gold electrodes with adsorbed Cp in the presence and absence of NaF are shown in Fig. 3.12.
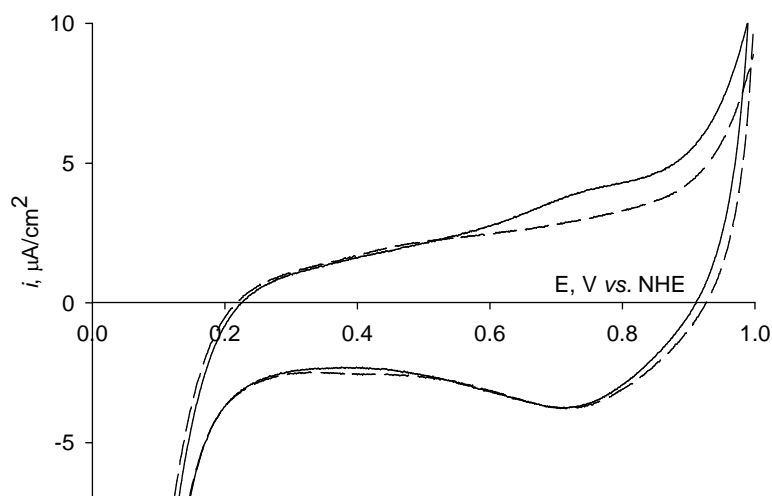

Fig. 3.12. CVs of gold electrode modified with AuNPs and Cp in the absence (solid line) and presence (dashed line) of 1 mM NaF. Conditions - 0.1 M phosphate buffer solution, pH 7.4, scan rate 10 mV/s, starting potential - 1 V.

An electrochemical process at about 730 mV *vs.* NHE could be seen. This process could be assigned to the redox transformation of Cp though not with certainty. The graph indicates that Cp exhibit DET on AuNP but without significant oxygen bioreduction. No clear conclusions about which of the copper active sites of Cp come into contact could have been made. The results were included to a study exploiting advances in surface nanotechnology, where Cp was immobilized on different electrodes: bare and carbon nanotube modified glassy carbon; spectrographic graphite; bare, thiol- and AuNP modified gold. In no case, however, was DET based bioelectrocatalytic reduction of O_2 by Cp was registered. It was concluded that based on a comprehensive picture of the thermodynamics and kinetics of the mechanism of Cp function, the bioelectrocatalytic inertness of Cp is associated with a very complicated mechanism of intramolecular ET in this complex redox protein. The study was published in (Haberska, Vaz-Domínguez et al. 2009).

3.5. Laccase T1 site detection on gold nanoparticle surface

Surface enhanced Raman spectroscopy measurements (SERS) were performed on AuNP and *Trametes hirsuta* laccase modified gold electrode. The idea behind these experiments was an attempt to obtain any SERS signal of laccase T1 copper centre at AuNP and laccase interface. T1 copper centre usually exhibits intense resonance Raman feature near 415 - 430 cm^{-1} (Augustine, Kragh et al. 2008) excited with red laser line, for example at the wavelength of 647 nm. Pre-resonance enhancement is expected for spectra recorded with near-infrared (785 nm) excitation. Indeed, Fig. 3.13 clearly demonstrates enhancement of predominantly Cu - S_{Cys} stretching vibrations coupled to Cys deformation motion at 367, 388, 409, 428, and 494 cm^{-1} (Han, Adman et al. 1991).
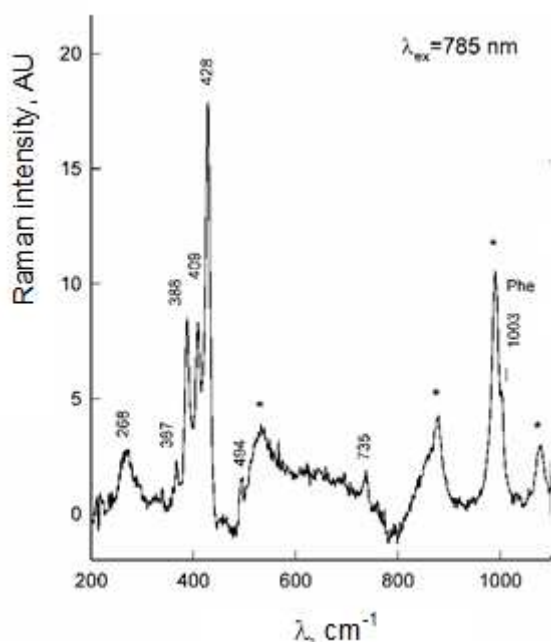

Fig. 3.13. Raman spectrum of *Trametes hirsuta* laccase in buffer solution. Raman bands of phosphate anions present in buffer solution are indicated by asterisks. Measurement conditions: excitation wavelength - 785 nm, laser power at the sample - 100 mW, total integration time - 2000 s.

The broad mode near 268 cm^{-1} contains high contribution from the Cu - His stretching vibration (Han, Adman et al. 1991). The low intensity feature at 735 cm^{-1} is associated with C–S_{Cys} stretching vibration of Cys residue ligated to Cu center (Blair, Campbell et al. 1985; Andrew, Yeom et al. 1994). However, vibrations associated not only with the T1 center are visible in the Raman spectrum excited with 785 nm radiation. The shoulder near 1003 cm^{-1} corresponds to ring stretching vibration of Phe residues (v_{12}). We have

estimated the relative intensity I_{428}/I_{phe} of the T1 center and Phe bands located at 428 and 1003 cm^{-1}, respectively, after decomposition of the experimental contours into the mixed Gaussian - Lorentzian shape components. The estimated intensity ratio I_{428}/I_{phe}=6.8 clearly demonstrates preresonant enhancement of the T1 center bands upon excitation at 785 nm wavelength.

Fig. 3.14 shows SERS spectra of adsorbed *Trametes hirsuta* laccase at gold electrode covered by AuNPs in the 300 - 1800 cm^{-1} and 2600 - 3200 cm^{-1} spectral region, respectively. Potential dependent SERS spectra were recorded starting from 0.8 V to 0 V and back to 0.8 V (*vs.* NHE) electrode potentials. Presence of adsorbed protein is clearly evidenced from the sharp Phe ring stretching peak near 1004 cm^{-1} (Fig. 3.13, left) and aromatic ring ν(=C–H) stretching vibration at 3059 cm^{-1} (Fig. 3.13, right). Sharp 1004 cm^{-1} band broadens and shifts to lower wavenumbers (1001 cm^{-1}) at more negative electrode potentials, while the high frequency component at 3059 cm^{-1} completely disappears at 0 V. These findings indicate that potential dependent reorientation of adsorbed protein takes place so that the domain rich with Phe residues moves away from the electrode surface at more negative potentials.

It should be noted that at relatively more negative electrode potentials high frequency SERS spectra exhibit shoulder near 2820 cm^{-1} (Fig. 3.14, left, d, e) assigned previously to „soft" C–H stretching mode of methylene groups directly contacting the metal surface (Razmute-Razme, Kuodis et al. 2010). Thus reorientation of the protein takes place at more negative potentials so that the methylene groups of amino acid residues directly contact the AuNP surface. SERS bands of adsorbed protein are visible at all studied potentials and reversible changes take place when electrode potential was switched back to 0.8 V after excursion to more negative values indicating irreversible adsorption of biomolecule (Fig. 3.15, Table 3.6). Bands from other amino acid residues and amide bonds are also visible in the spectra. Tentative assignments of the SERS bands based on references (Wen 2007; Misiūnas, Talaikytė et al. 2008; Podstawka, Niaura et al. 2009) are listed in the Table 3.7.
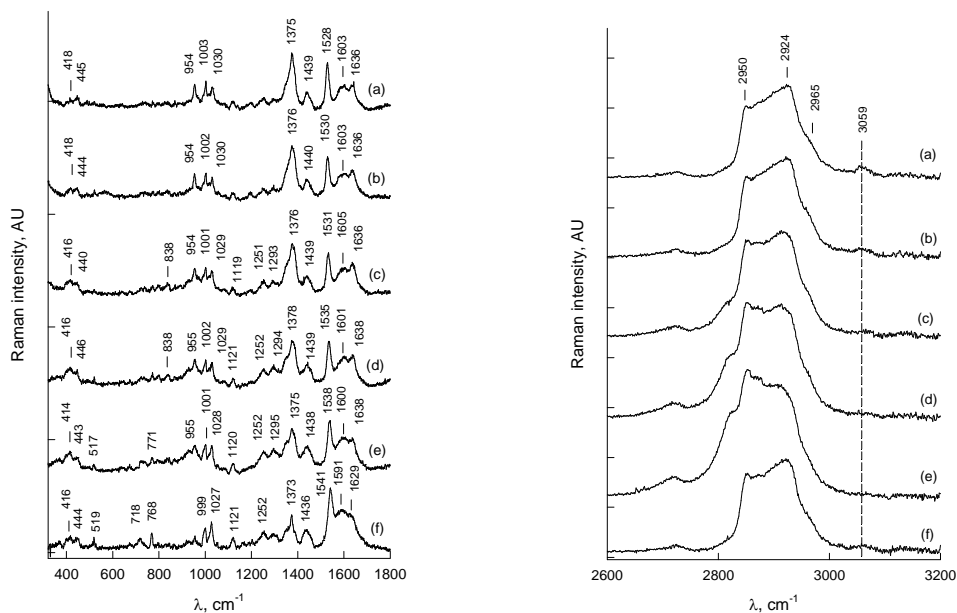
Fig. 3.14. SERS spectra of *Trametes hirsuta* laccase, immobilized on gold electrode covered by AuNPs at 0.8 V (a), 0.6 V (b), 0.4 V (c), 0.2 V (d), 0 V (e), and 0.8 V (f) potentials (*vs.* NHE) in the frequency regions 300-1800 cm^{-1} (left) and 2600-3200 cm^{-1} (right). Measurement conditions: excitation wavelength, 785 nm; laser power at the sample, 30 mW; total integration time, 300 s. One increment of Raman intensity equals to 100 AU.
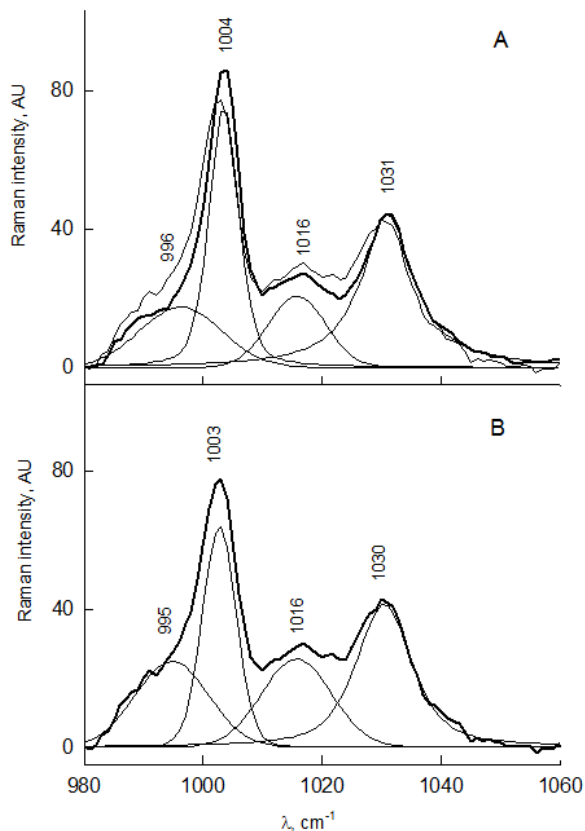

Fig. 3.15. Phe ring vibration spectral region of adsorbed *Trametes hirsuta* laccase on AuNP surface at 0.8 V electrode potential before (A) and after (B) excursion to 0 V with added Gaussian - Lorentzian curve fitting. Conditions: total experimental time - 70 min, excitation wavelength - 785 nm, laser power at the sample - 30 mW, total integration time - 300 s.

Table 3.6. Parameters of the Gausian - Lorentzian components of SERS spectra in Phe ring vibrational region 980-1060 cm^{-1}, related to adsorbed *Trametes hirsuta* laccase on AuNP surface. Total experiment time – 70 min.

Experimental conditions	Peak position, cm^{-1}	Area, AU	Intensity, AU	Full width at half maximum, cm^{-1}
0.8 V, before excursion to 0 V	1003.5	543	76	6
	1031	668	44	10.4
0.8 V, after excursion to 0 V	1002.7	471	64	6.7
	1030.4	597	41	11.2

Table 3.7. Tentative assignments of the SERS bands. Abbreviations: ν, stretching; δ, deformation; ν_s, symmetric stretching; ν_{as}, asymmetric stretching; t, twisting; w, wagging.

Frequency, cm^{-1}	Assignment	Frequency, cm^{-1}	Assignment
729	$\nu(X-\Sigma)$	1440	$\delta(XH_2)$
824	Tyr,	1532	$\nu_{as}(XOO)$, $\delta(NH_2)$
868	Trp	1595	$\nu_{as}(XOO)$, $\delta(NH_2)$
1004	Phe	1663	Amide I
1031	Phe	2950	$\nu_s(XH_2)$
1237	Amide III	2924	$\nu(XH_2)$
1304	w(CH$_2$), t(CH$_2$)	2965	$\nu_{as}(XH_3)$
1372	ν_s(COO), citrate	3059	$\nu(=X-H)$, aromatic

Coadsorbed citrate anions are visible from the 1372 cm^{-1} band (Munro, Smith et al. 1995), and, probably, from the strong 1532 and broad 1595 cm^{-1} SERS features. . The 1372 cm^{-1} band belongs to symmetric stretching vibration of COO groups. Its frequency is lowered as comparing with citrate solution spectrum (1417 cm^{-1}) (Munro, Smith et al. 1995) and provides evidence for direct interaction of carboxylate groups with the gold electrode surface. The bands at 1532 and 1595 cm^{-1} might be associated with asymmetric stretching vibration of carboxyl group or due to vibrations of citrate decomposition products (acetonedicarboxylic and acetoacetic acids) (Munro, Smith et al. 1995).

It should be noted that we were not able to observe SERS bands from the copper centre T1 in our spectra. Low frequency bands at 416 and 444 cm^{-1} cannot be attributed to T1 centre because:

- Position of the bands does not correspond to the most intense mode observed in the solution spectrum at 428 cm^{-1} (Fig. 3.13);
- Intensity of the bands increase at more negative potentials where T1 centre must be reduced resulting in loss of preresonant Raman enhancement (Gaigalas and Niaura 1997).

Absence of enhanced T1 bands indicates that *Trametes hirsuta* laccase adsorbs in such the geometry that the copper center is not located in the close proximity to the electrode surface.

Also, SERS spectra of *Trichaptum abietinum* laccase adsorbed on AuNPs in the middle and high frequency spectral regions have been recorded. The main spectral pattern is rather similar comparing with *Trametes hirsuta* laccase. However, intensity of the surface bound citrate band near 1375 cm^{-1} is higher *Trichaptum abietinum* laccase at the similar electrode potentials, while protein bands are of lower intensity.

In conclusion, SERS spectra provided evidence for irreversible adsorption of protein at AuNP interface. Comparison of areas of *Phe* ring stretching mode at 1004 cm^{-1} at 0.8 V before and after excursion to 0 V (Table 3.6) showed that ~ 87 % of proteins remain adsorbed at AuNP surface during electrode polarization. Also, the potential dependent reorientation of adsorbed protein at Au/Au NP interface was detected in the potential region from 0.8 V to 0 V. Presence of "soft" C–H stretching mode (2820 cm^{-1}) at more negative electrode potentials indicates direct contact of protein side chain methylene groups with the AuNP surface. Citrate anions are found to be coadsorbed at the AuNP surface with the protein molecules.

Failure to observe T1 copper site signal could mean that T1 site is farther AuNP surface. Fig. 2.7 indicates that SERS signal would be lost at a distance of 2 – 4 nm when 39 nm size AuNP are used in measurements. This would

mean that both laccases work under mixed type ET mechanism in bioelectrocatalytic systems.

3.6. Heterogeneous electron transfer at gold nanoparticle and laccase interface

3.6.1. Water element in protein films

Before the QCM-D measurements of AuNP and laccase multilayer systems, the water content in laccase protein film has been estimated. As stated in 2.7.2., when QCM-D technique is used to measure mass changes of protein films, the calculated mass of the films corresponds to collective amount of protein and the entrapped water. So in order to accurately weigh the laccase content in such film one should know how much water such film contains.

In this research the ratio of protein film masses established by combining ellipsometry that measures „dry" protein build-up on surfaces and QCM-D technique. The combination would provide the water mass ratio in laccase film, under provision that both experiment are carried out in the same conditions. So in QCM-D measurements the plasma – cleaned gold sensor was set up to the flow cell, cleaned as stated in 2.7.2., buffer solution flow was initiated at 100 µl/min and maintained throughout the experiment, temperature was set at 23 ℃. Then 50 µg/ml of laccase solution was flown at the same speed. By using *Qtools* software, provided by Q-Sense, the amount of "wet" laccase present on the surface of the sensor in relation to time was determined. In ellipsometry measurement the plasma cleaned gold surface was used in the cell, temperature was set at 23 ℃, and laccase solution of the same concentration was poured into the cell with gentle stirring. The protein mass build-up in relation to time was determined. The data from both measurements were fitted to simple exponential growth model:

$$m_{lac} = x_1 e^{x_2 * t} + x_3 \qquad\qquad (3.3)$$

where m_{lac} – adsorbed laccase mass in the time t, x_1, x_2 and x_3 are modelled parameters. Since experiments were done in different setups, the laccase mass build up speed was different. Since x_2 relates to the laccase mass growth rate, the following models were considered:

$$m_{qcm} = xq_1 * e^{(xq_2+xe_2)/2*t_{qcm}} + xq_3 \qquad (3.4)$$

$$m_{el} = xe_1 * e^{(xq_2+xe_2)/2*t_{el}} + xe_3 \qquad (3.5)$$

where m_{qcm} and m_{el} correspond to adsorbed laccase mass in time t_{qcm} and t_{el} obtained from QCM-D and ellipsometry measurements, respectively, xq_1, xq_2, xq_3 and xe_1, xe_2, xe_3 are x_1, x_2, x_3 parameters modelled from QCM-D and ellipsometry, respectively. Then by diving m_{el} to m_{qcm} the water percentage in the protein film was established.
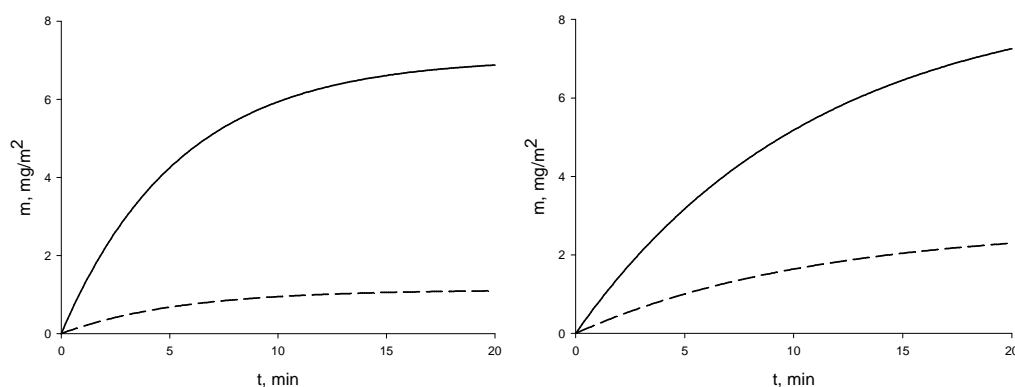

Fig. 3.16. Modelled dependence of adsorbed protein mass versus time plots of *Trametes hirsuta* (left) and *Trichaptum abietinum* (right) laccase on gold surface in QCM-D (solid line) and ellipsometry (dashed line) measurements.

As seen from Fig. 3.16., m_{qcm} is significantly higher than m_{el}, indicating that indeed protein films have significant amount of water entrapped that is detected by QCM-D. Calculated percentage of water (w/w) in *Trametes hirsuta* laccase film was $84 \pm 5\%$, and in *Trichaptum abietinum* laccase film – $68 \pm 2\%$. The "dry" protein mass in the film is recalculated accordingly in further experiments.

It is worth to emphasize that such experiment was done by adsorbing laccases on flat gold surface, not the nanoparticle surface, which would be difficult to simulate in the grounds of ellipsometry experiments. Protein films on AuNP surface probably have different amount of water entrapped, but ellipsometry experiments with laccase adsorbed on AuNP for analysis of protein film properties are complicated.

3.6.2. Analysis using quartz crystal microbalance

Simultaneous QCM-D and electrochemical experiments were conducted as described in 2.7.2. The consecutive gold sensor modification procedure involved flowing different solutions over assembled QCM-D electrochemical cell – PLL, laccase, AuNPs and again laccase. The first layer of laccase was used to cover the PLL layer, so that after AuNP adsorption most of the enzyme film would accumulate on AuNP surface only.

The measurement of PLL adsorption onto a gold surface quartz crystal sensor by QCM-D showed very small changes in frequency and no any observable variation in dissipation. The adsorbed PLL mass, calculated using QTools software at 5th, 7th and 9th overtones was statistically the same and equal to 74 $\pm$ 39 ng/cm^2. It could be stated that the dry mass of the adsorbed PLL practically must be less than estimated, if taking into account that the mass usually measured by QCM-D also accounts for water coupled to the layer (Halthur and Elofsson 2004). A low surface concentration and very small $\Delta D/\Delta f$ ratio indicate that PLL molecules should adsorb in a flat, rod-like conformation. Such PLL structure in the film can be explained by a strong PLL interaction with the gold surface and high electrostatic repulsion between the positively charged lysine monomers in PLL, particularly because PLL was adsorbed from water.

After the PLL layer had been adsorbed on the surface of a gold sensor and rinsed with water the sensor was exposed to either *Trametes hirsuta* or *Trichaptum abietinum* laccase solutions. QCM-D measurements revealed that Trametes hirsuta laccase adsorbed on top of PLL and probably also directly on

the PLL unoccupied gold surface. The surface mass of the *Trametes hirsuta* laccase film including the entrapped water was calculated as 440 ± 250 ng/cm^2, and in case of *Trichaptum abietinum* laccase – 50 ± 32 ng/cm^2.

After the sensor surface was pre-treated with PLL and laccase, the layer of AuNPs was assembled on the sensor surface. The AuNPs assembled in the way that nanoparticle packing density was lower than monolayer of hexagonal packing. The results are presented in Fig. 3.17.
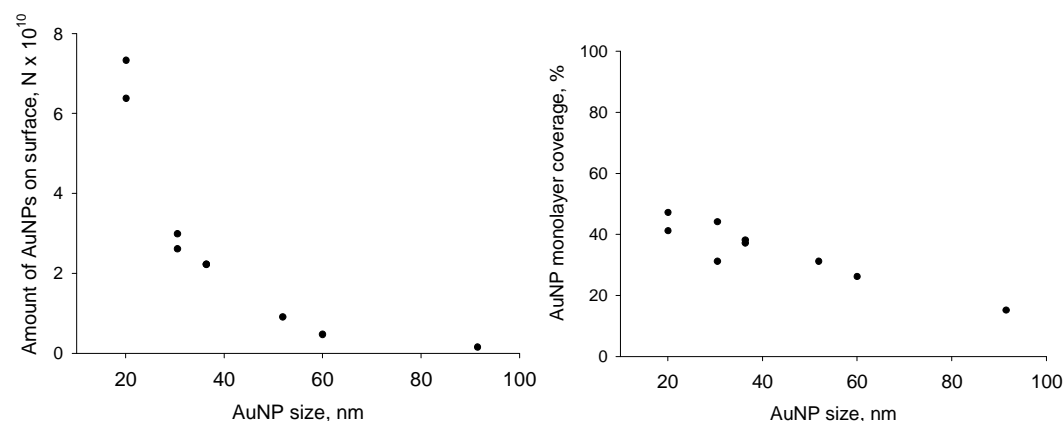

Fig. 3.17. Amount of AuNPs adsorbed on sensor surface (left) and AuNP monolayer coverage percentage (right) in relation to AuNP size, data collected from several experiments.

After AuNP addition, the procedure was completed by adsorbing the second layer of laccase on AuNP surface. Laccase solution was flown over the sensor for exactly 10 min, followed by rinsing with buffer solution. The results of „dry" mass of the enzyme, obtained by including the water content calculations presented in 3.6.1., are depicted in Fig. 3.18 – 3.19. The data indicate that *Trichaptum abietinum* laccase accumulates faster on AuNP surface, when considering that the protein solution flow over sensor time was similar. This is expected, since it was shown that *Trametes hirsuta* laccase entraps more water in the protein film (as discussed in 3.6.1.).
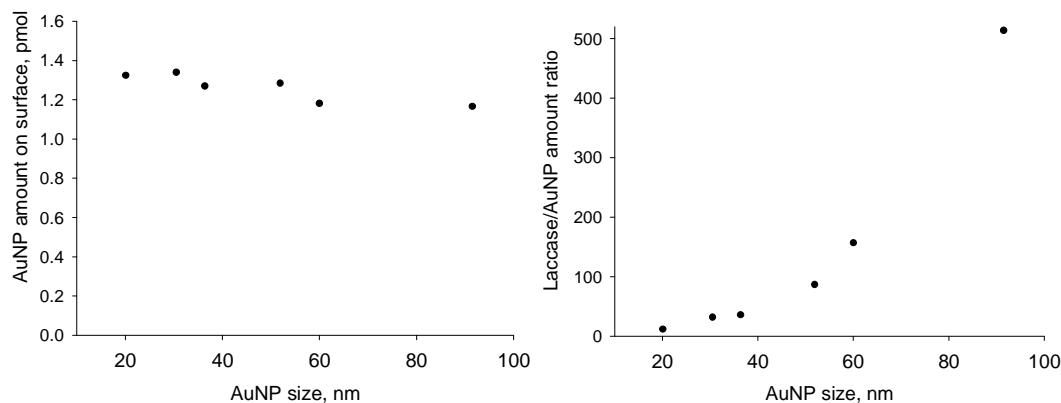
Fig. 3.18. Dependence of *Trametes hirsuta* laccase amount adsorbed on AuNP on sensor surface (left) and laccase – AuNP amount ratio (right) in relation to AuNP size. Presented values refer to „dry" amount of protein.

Fig. 3.19. Dependence of *Trichaptum abietinum* laccase amount adsorbed on AuNP on sensor surface (left) and laccase – AuNP amount ratio (right) in relation to AuNP size. Presented values refer to „dry" amount of protein.
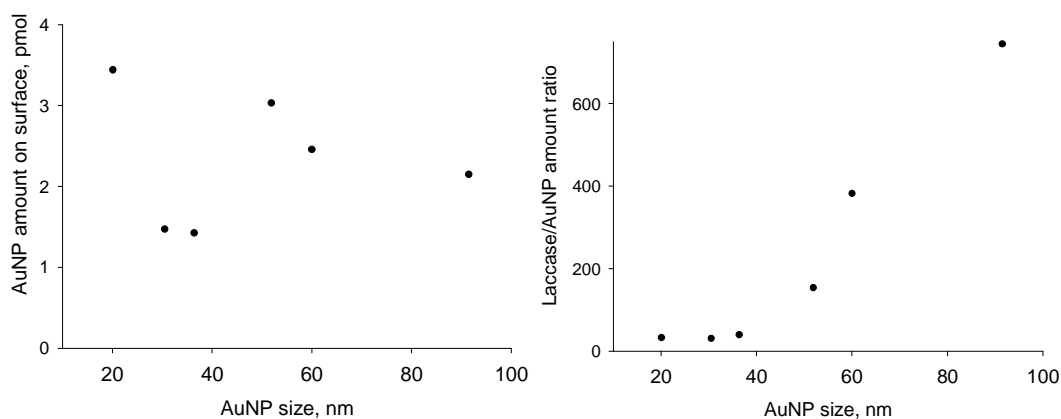
After establishing the number of laccase molecules on the sensor surface and CV analysis of resultant PLL – laccase – AuNP – laccase film (with presence and absence of 5 mM NaF in buffer solution), the heterogeneous electron transfer constant k_{obs}, which accounts for amount of electrons passed through one enzyme molecule per second, was calculated following the technique described in 2.7.2., were made. The results are depicted in Fig. 3.20.
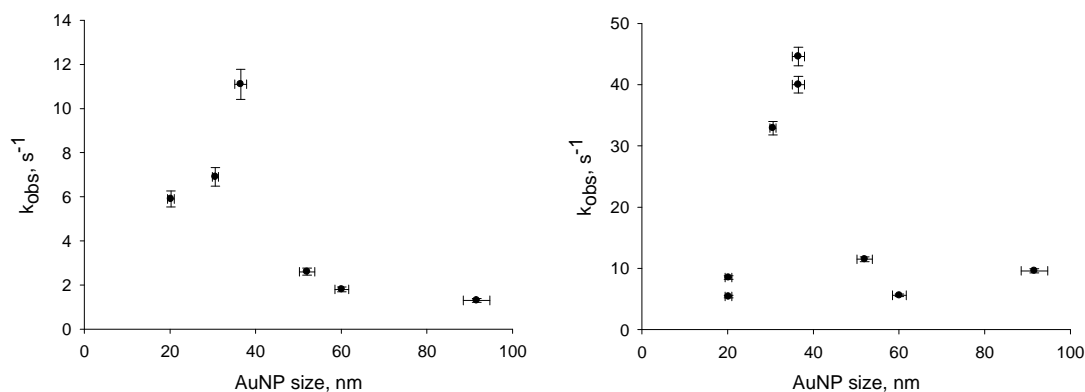
Fig. 3.20. Dependences of turnover constants k_{obs} on AuNP size for *Trametes hirsuta* (left) and *Trichaptum abietinum* (right) laccases. AuNP size errors correspond to errors of AuNP size establishment by DLS as described in 3.2., k_{obs} errors are calculated taken into consideration of "dry" protein amount in film error described in 3.6.1.

QCM-D experiments revealed that AuNP size readily affects the enzyme turnover rate based on DET bioelectrocatalysis. As expected, laccases adsorbed on smaller size AuNPs facilitate faster enzyme turnover rate. However, it is interesting to notice that enzymes adsorbed on small AuNPs (~20 nm) exhibit lower enzyme turnover rate as the ones adsorbed on medium size AuNPs (~30 – 40 nm). Further experiments were carried out to clarify this effect.

3.6.3. Gold nanoparticle - gold surface contact quality

After several attempts to reveal any irregularities in QCM-D experiments, the idea was proposed that it could be reasoned that PLL layer responsible for AuNP adhesion to sensor surface provide poorer contact between small size AuNPs and gold surface. In other words, maybe it is possible that some of AuNPs cannot "sink" deep enough into PLL layer to provide good contact. In this case, provided that average protein coverage of every AuNP is thorough and consistent, a relative amount of laccases remain out of contact with sensor surface. Then the relative amount of "disconnected" AuNP and laccases should be similar.

Further calculations were conducted by comparing the results of integration of background currents voltammograms obtained of CVs analysing PLL - AuNP surfaces. The integrated area, correlating to relative amount of total AuNP amount connected to sensor surface, was divided by AuNP amount obtained from QCM-D modelling; the result corresponds to real area of single AuNP. The data was plotted against theoretical relationship between AuNP surface area and AuNP size (Fig. 3.21).
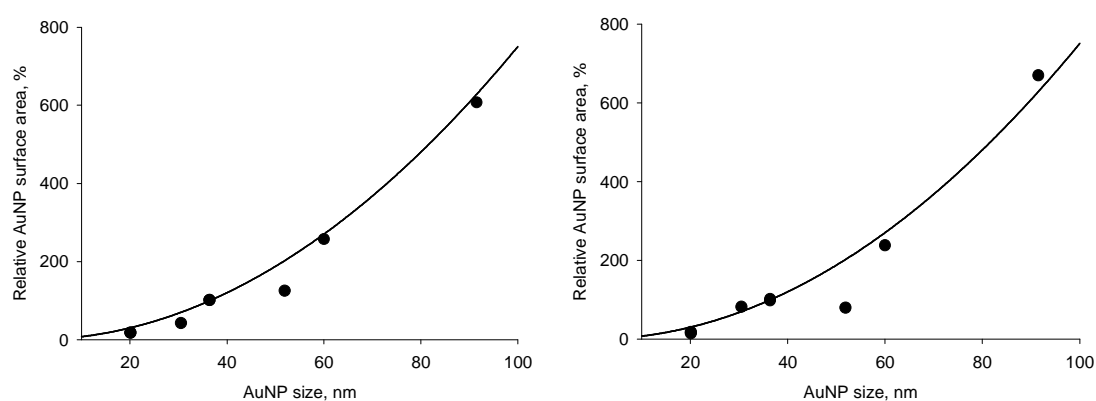

Fig. 3.21. Dependences of relative surface area for single AuNP on AuNP size, 100% - surface area of 36.5 nm size AuNP. Solid dots represent data from PLL – AuNP QCM-D modelling results, which belong to *Trametes hirsuta* (left) or *Trichaptum abietinum* (right) laccase experiments and represent real relative AuNP area, if 100% is taken as an area of 36.5 nm sized AuNPs.

The enzyme turnover constants depicted in Fig. 3.20 were recalculated accordingly – k_{obs} at AuNP size of 36.5 have been taken as reference. The recalculation results are depicted in Fig. 3.22.
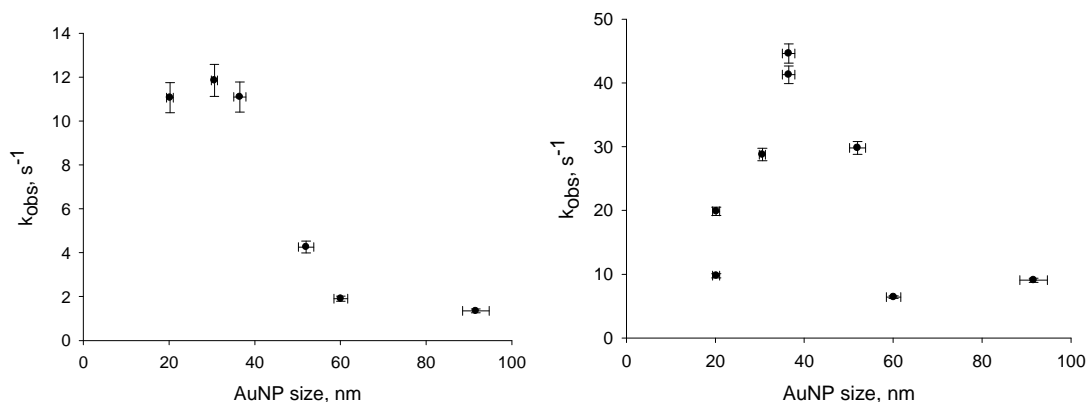
Fig. 3.22. Dependences of turnover constants k_{obs} on AuNP size for *Trametes hirsuta* (left) and *Trichaptum abietinum* (right) laccases after recalculations in respect to AuNP connection to sensor surface. AuNP size errors correspond to errors of AuNP size establishment by DLS as described in 3.2., k_{obs} errors are calculated taken into consideration of "dry" protein amount in film error described in 3.6.1.

The results indicate that in case of *Trametes hirsuta* laccase system small AuNPs (~20 nm) are responsible for similar heterogeneous ET constant values as medium size AuNPs (~30 – 40 nm). However, the principle that enzymes adsorbed on small AuNPs exhibit lower enzyme turnover rate as the ones adsorbed on medium size AuNPs is still relevant to *Trichaptum abietinum* laccase systems. Maximum heterogeneous electron transfer constant k_{obs} for *Trametes hirsuta* laccase system reached 12 s^{-1}; while its activity in homogeneous solution was about 200 s^{-1}. In comparison, *Trichaptum abietinum* laccase reached k_{obs} of 45 s^{-1}, when its activity in homogeneous solution was about 300 s^{-1}, depending on enzyme batch used. It is interesting to note that the best AuNP size for both laccases proved to be the same – 36.5 ± 1.4 nm as determined by DLS technique using NICOMP size distribution algorithm.

3.6.4. Gold nanoparticle size effect to electron transfer

After observation that AuNP size influences k_{obs}, the hypothesis was proposed that it is possible that different AuNP curvatures could lead to different orientation of adsorbed enzymes. This should result in changes of direct and

mediated electron transfer rates, as in average situation the T1 copper active site of laccase would get closer or further from AuNP surface depending on AuNP size.

In order to test this hypothesis, QCM-D experiment was performed again using *Trichaptum abietinum* laccase and various size AuNPs with some changes – no laccase was adsorbed before addition of AuNP. This resulted in PLL – AuNP – laccase multilayer structure. ABTS was chosen as an electron mediator between T1 copper centre and AuNP surface. Such multilayer approach ensured that all the laccases involved in mediated current output are quantified by QCM-D analysis. This was not necessary in previous QCM-D experiments, where only DET bioelectrocatalytic current output was registered.

The potentiostat was set to record chronoamperometry at 500 mV *vs.* NHE, then buffer solution was flown over sensor surface to record DET bioelectrocatalysis based current density, after which buffer solution containing 2 mM ABTS was flown while recording current density based on either ABTS partial reduction by electrode surface and/or ABTS mediated electron transfer based oxygen reduction by adsorbed laccase molecules. Current density attributed to reduction of oxidized ABTS form by electrode surface was determined by flowing 2 mM ABTS solution containing 2 mM NaF over the sensor surface and was subtracted from total current in presence of ABTS without inhibitor to calculate total MET current density. The exemplary chronoamperometry experiment is depicted in Fig. 3.23.
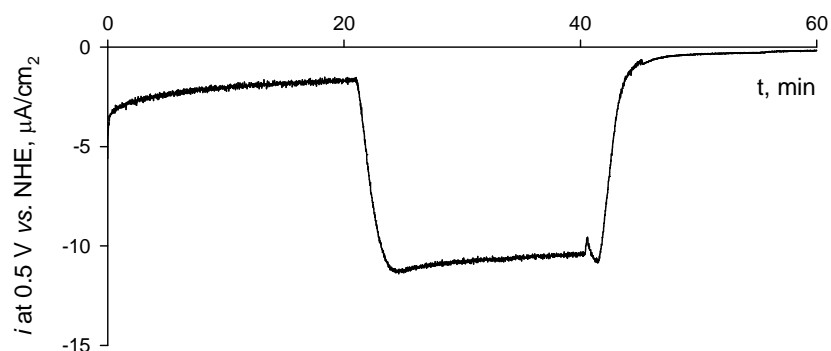
Fig. 3.23. Example of chronoamperometric measurements of *Trichaptum abietinum* laccase adsorbed on QCM-D sensor with 20.2 nm size AuNPs. First DET oxygen bioreduction current density is registered, then after addition of 2 mM ABTS the total mediated ET current is registered, and after addition of 2mM NaF the current related to electrochemical ABTS oxidation on electrode surface is registered. The potential was set at 500 mV *vs.* NHE. Simple exponential growth model was used in data analysis to determine last point current density values.

After establishing the adsorbed laccase mass by QTools software according to methods of previous QCM-D measurements, the current densities were recalculated to represent current density facilitated by 1 ng of enzyme. The results are depicted in Table 3.8.

Table 3.8. DET and total bioelectrocatalytic current density dependence on AuNP size, recalculated to represent the current output provided by 1 ng of laccase. The errors are calculated in respect to water content in protein film error as determined in 3.6.1.

AuNP size, nm	DET current density, $\mu A/cm^2$	MET current density, $\mu A/cm^2$	DET/MET current density ratio, %	AuNPs surface area vs total area, %
20.2 ± 0.8	3.8 ± 0.1	24.9 ± 0.2	15.4 ± 0.6	56
36.5 ± 1.4	9.3 ± 0.1	34.3 ± 0.2	26.9 ± 0.4	55
91.6 ± 3.1	1.28 ± 0.03	27.0 ± 0.3	4.7 ± 0.1	27

The results indicate that middle size AuNPs in bioelectrocatalytic systems contribute to highest DET and MET current densities. Highest DET could

indicate that middle size AuNPs contribute to most optimal connection of laccase active centre to AuNP surface. Highest MET could mean that laccases adsorbed on middle size AuNPs are least denatured, provided that substrate diffusion had no influence in current output.

3.7. Discussion

The most interesting find of this study is revelation that laccases are capable of efficient oxygen bioelectroreduction of gold nanoparticle (AuNP) surface without the need of additional redox active substances or polymers. By the time of our publication describing direct electron transfer (DET) bioelectrocatalytic system consisting of *Trametes hirsuta* laccase and 40 – 50 nm size AuNPs at the year of 2010, the modification of electrodes with AuNPs was shown to enable DET of cytochrome c (Ju, Liu et al. 2002),myoglobin (Liu and Ju 2003), horseradish peroxidase (Zhao, Henkens et al. 1992), superoxide dismutase (El-Deab and Ohsaka 2007) and bilirubin oxidase (Murata, Kajiya et al. 2009). Despite the fact that laccase was the first enzyme for which DET was discovered on carbon electrodes (Berezin, Bogdanovskaya et al. 1978), no efficient DET bioelectrocatalysis has been realized at metal electrodes (Shleev, Christenson et al. 2005; Shleev and Ruzgas 2008) before our research.

It was obvious that DET bioelectrocatalysis of oxygen reduction in *Trametes hirsuta* laccase – AuNP system was efficient, as in CV experiments the reduction current begins to increase at approximately 850 mV (vs. NHE) and levels off at the potentials below 650 mV, while the redox potential of the laccase was estimated as 780 mV (Shleev, Morozova et al. 2004). However, the achievable current densities in these systems, when AuNP amount on gold electrode was enough to form a two dimensional hexagonal packed monolayer, failed to achieve the values higher than 15 $\mu A/cm^2$. Later it became known that this laccase has to be in the right orientation in respect to gold surface – further study by our research colleagues and their partners revealed that by using gold surface modified with a mixed monolayer of an aromatic diazonium salt

derivative and 6-mercapto-1-hexanol to immobilize *Trametes hirsuta* laccase it is possible to achieve current densities up to 40 μA/cm^2 (Pita, Gutierrez-Sanchez et al. 2011). Laccase orientation on AuNP surface could possibly be changed by AuNP surface modification with different coating ligands, or directed mutagenesis of enzyme itself to introduce new surface amino acids with affinity toward gold surface, however, this strategy was not pursued. Instead, we tried using different multicopper oxidases to obtain high current density DET bioelectrocatalytic systems with AuNPs.

Two more multicopper oxidases proved to exhibit DET on AuNPs. One enzyme was human ceruloplasmin, which showed an electrochemical process at about 730 mV in AuNP – enzyme DET bioelectrocatalytic system. This process could be assigned to the redox transformation of the enzyme but without certainty. No efficient DET oxygen bioreduction was observed. Another enzyme – laccase purified from *Trichaptum abietinum* – has been revealed as much more capable of generating high current densities on AuNP covered gold electrodes even than *Trametes hirsuta* laccase. Gold electrodes covered by monolayer amount of AuNPs and this new enzyme were capable of generating current densities up to 170 μA/cm^2 when solution flow towards the electrode surface was enhanced by using rotating gold disk electrode system. The DET process was apparently limited by enzyme turnover rate.

The special interest was to analyse why *Trichaptum abietinum* laccase systems are superior to analogical *Trametes hirsuta* laccase systems. The redox potential of the new laccase has been established as 714 mV, which is lower than redox potential of *Trametes hirsuta* laccase 780 mV (Shleev, Morozova et al. 2004), however both enzymes could be considered as high potential laccases. Unlike *Trametes hirsuta* laccase, the new laccase loses its native resistance to NaF (non – competitive T2/T3 copper site inhibitor) when attached to AuNP by about 140 times, meanwhile maintaining high sensitivity to NaCl (competitive T1 copper site inhibitor). Also, in comparison to *Trametes hirsuta* laccase, the new laccase exhibit poor catalysis of organic compounds oxidation, meanwhile exhibiting fast catalysis of oxidation of

inorganic substance ferocyanide. Since we currently don't have an established PDB structure of *Trichaptum abietinum* laccase for detailed insight, this result could lead into speculation that surface area of T1 active centre of the new laccase has a larger surface charge (possibly more positive, since ferocyanide ion is negative), thus posing difficulties for hydrophobic organic substances to reach the catalytic centre. If this speculation would be true, it could lead to further thinking that maybe the positively charged T1 copper site of this laccase interact better with negatively charged AuNP surface thus providing shorter distance between T1 copper and gold surface. The crystal structure of *Trichaptum abietinum* laccase is being analysed, and possibly further studies would provide more answers.

However, the importance of close proximity of T1 copper site to AuNP surface is debatable. In surface enhanced Raman spectroscopy we were unable to detect T1 copper signal in AuNP – laccase DET systems for either laccase, even though potential dependent enzyme reorientation was observed. Moreover, addition of ABTS, which act as electron mediator between electrode surface and T1 copper site, increased the reductive current in AuNP – laccase bioelectrocatalytic system, which means that in average T1 copper site is exposed to solvent. This is in agreement with (Shleev, Jarosz-Wilkolazka et al. 2005), where the authors speculated that not the T1 but rather the T2 site of the enzyme was in electric contact with the gold surface. As mentioned, *Trichaptum abietinum*, unlike *Trametes hirsuta* laccase, loses resistance to NaF when adsorbed on AuNP surface, which could lead to speculation that maybe AuNP adsorption process has something to do with T2/T3 copper site changes. In that case, T2/T3 copper site of *Trichaptum abietinum* laccase should have gotten closer to surface than *Trametes hirsuta* laccase, thus leading to higher current output.

Another interesting find of this work – heterogeneous electron transfer (ET) rate of both laccases adsorbed on AuNPs depend on AuNP size. It was revealed that using middle size (40 – 50 nm) AuNPs lead to higher ET rates in respect to single average laccase molecule than in case of using large size (70 –

90 nm) AuNPs. Usage of optimal AuNP size ensures the most efficient DET and the least denaturation or degradation of the enzyme. The reasons of this phenomenon are speculative. To our best knowledge, currently there are no clear studies leading to explanation of AuNP crystal structure in sizes of 10 – 100 nm. There were successful attempts to produce DET systems of enzymes adsorbed on monocrystalline Au(111) surfaces (González Arzola, Gimeno et al. 2010). However, if AuNP structure would appear to be monocrystalline, probably there would be no clear distinction between AuNP size and heterogeneous ET rates provided the surface area of AuNPs are kept similar. If AuNPs are in fact polycrystalline, we could speculate that probably the optimal curvature of AuNPs is responsible for proper alignment of multicopper oxidase active centres, ensuring the shortest distance for heterogeneous electron transfer. Recent study (Suzuki, Murata et al. 2012) has revealed opposite effect – in AuNP – bilirubin oxidase DET systems the usage of 70 nm AuNPs lead to higher current densities than in case of 7 and 15 nm AuNPs. This would probably support the idea that the optimum AuNP curvature is responsible for optimal heterogeneous ET between enzyme active centre and AuNP.

CONCLUSIONS

1. Newly extracted and purified laccase from *Trichaptum abietinum* is a high redox potential laccase with the T1 copper site redox potential of 714 ± 12 mV *vs.* NHE.

2. Laccases from *Trametes hirsuta and Trichaptum abietinum*, as well as human ceruloplasmin, are capable of exhibit direct electron transfer between active centre and gold nanoparticle.

3. Surface enhanced Raman spectroscopy indicate that some amino acid residues of adsorbed *Trametes hirsuta* laccase change orientation during electrode potential change but SERS of T1 copper site had not been produced.

4. Electron transfer rate depends on size of gold nanoparticles. In general, laccases adsorbed on large diameter (60 – 90 nm) gold nanoparticles exhibit slower rate in comparison to ones adsorbed on medium sized (40 – 50 nm) gold nanoparticles. Heterogeneous electron transfer rate constants can reach value as high as 45 s^{-1} and 11 s^{-1} if *Trichaptum abietinum* and *Trametes hirsuta* laccase were used, respectively.

5. Laccases from *Trametes hirsuta and Trichaptum abietinum* catalyses oxygen reduction when adsorbed on gold nanoparticles. The maximum biocatalytical current is limited by enzyme turnover rate or by interfacial electron transfer for *Trichaptum abietinum* laccase or *Trametes hirsuta* laccase, respectively. In contrast to homogeneous solution, bioelectrocatalytical system containing *Trichaptum abietinum* laccase is strongly inhibited by fluoride ions.

PUBLICATIONS

The results of investigations were published in:

1. Haberska, K.; Vaz-Domínguez, C.; De Lacey, A.L.; Dagys, M.; Reimann, C.T.; Shleev, S. Direct electron transfer reactions between human ceruloplasmin and electrodes. *Bioelectrochemistry*. 2009, 76(1-2), 34-41.

2. Dagys, M.; Haberska, K.; Shleev, S.; Arnebrant, T.; Kulys, J.; Ruzgas, T. Laccase – gold nanoparticle assisted bioelectrocatalytic reduction of oxygen. *Electrochemistry Communications*. 2010, 12(7), 933-935.

3. Dagys, M.; Shleev, S.; Arnebrant, T.; Niaura, G.; Kulys, J.; Ruzgas, T. Bioelectrocatalysis of oxygen reduction with *Trametes hirsuta* laccase immobilized on gold nanoparticles. Oxizymes & 9th International Symposium on Peroxidases, Leipzig 2010.

4. Dagys, M.; Shleev, S.; Arnebrant, T.; Niaura, G.; Kulys, J.; Ruzgas, T. Bioelectrocatalysis of oxygen reduction with *Trametes hirsuta* laccase immobilized on gold nanoparticles. 6th Annual Workshop of Biofilms – Research Center for Biointerfaces "Biomaterials – From Fundamentals to Market Application", Malmö 2010.

5. Dagys, M.; Lamberg, P.; Shleev, S.; Niaura, G.; Bachmatova, I.; Marcinkeviciene, L.; Meskys, R.; Kulys, J.; Arnebrant, T.; Ruzgas, T. Direct electron transfer of laccase immobilized on gold nanoparticles of different diameters. 14th International Conference on Electroanalysis ESEAC 2012, Portoroz 2012.

The results of investigations were presented in international conferences (each representative speaker is underlined):

1. Dagys, M.; Haberska, K.; Shleev, S.; Arnebrant, T.; Kulys, J.; Ruzgas, T. Gold nanoparticle assisted bioelectrocatalytic reduction of oxygen by *Trametes hirsuta* laccase. 15th International Student and Young Scientists conference „Chemistry and Chemical Technology 2010". Faculty of Chemistry, Vilnius University. Vilnius, 2010 05 07.

2. Dagys, M.; Shleev, S.; Arnebrant, T.; Niaura, G.; Kulys, J.; Ruzgas, T. Bioelectrocatalysis of oxygen reduction with *Trametes hirsuta* laccase immobilized on gold nanoparticles. Oxizymes & 9th International Symposium on Peroxidases, Leipzig, Germany, 2010 06 14 – 16.

3. Dagys, M.; Shleev, S.; Arnebrant, T.; Niaura, G.; Kulys, J.; Ruzgas, T. Bioelectrocatalysis of oxygen reduction with *Trametes hirsuta* laccase immobilized on gold nanoparticles. 6th Annual Workshop of Biofilms – Research Center for Biointerfaces "Biomaterials – From Fundamentals to Market Application", Malmö, Sweden, 2010 10 13 – 15.

4. Dagys, M.; Lamberg, P.; Shleev, S.; Niaura, G.; Bachmatova, I.; Marcinkeviciene, L.; Meskys, R.; Kulys, J.; Arnebrant, T.; Ruzgas, T. Direct electron transfer of laccase immobilized on gold nanoparticles of different diameters. 14th International Conference on Electroanalysis ESEAC 2012, Portoroz, Slovenia, 2012 06 03 – 07.

ACKNOWLEDGEMENTS

REFERENCES

1. Akers, N. L., Moore, C. M. and Minteer, S. D. Development of alcohol/O$_2$ biofuel cells using salt-extracted tetrabutylammonium bromide/Nafion membranes to immobilize dehydrogenase enzymes. *Electrochimica Acta*, **2005**, 50(12), 2521-2525.

2. Ali, N. and Varfolomeev, S. D. Inhibition mechanism of Polyporus versicolor laccase by halide ions. *Biokhimiia*, **1981**, 46(9), 1694-1702.

3. Andrew, C. R., Yeom, H., Valentine, J. S., Karlsson, B. G., van Pouderoyen, G., Canters, G. W., Loehr, T. M., Sanders-Loehr, J. and Bonander, N. Raman Spectroscopy as an Indicator of Cu-S Bond Length in Type 1 and Type 2 Copper Cysteinate Proteins. *Journal of the American Chemical Society*, **1994**, 116(25), 11489-11498.

4. Augustine, A. J., Kragh, M. E., Sarangi, R., Fujii, S., Liboiron, B. D., Stoj, C. S., Kosman, D. J., Hodgson, K. O., Hedman, B. and Solomon, E. I. Spectroscopic Studies of Perturbed T1 Cu Sites in the Multicopper Oxidases *Saccharomyces cerevisiae* Fet3p and *Rhus vernicifera* Laccase: Allosteric Coupling between the T1 and Trinuclear Cu Sites. *Biochemistry*, **2008**, 47(7), 2036-2045.

5. Baldrian, P. Fungal laccases – occurrence and properties. *FEMS Microbiology Reviews*, **2006**, 30(2), 215-242.

6. Banerjee, U. C. and Vohra, R. M. Production of laccase by Curvularia sp. *Folia Microbiologica*, **1991**, 36(4), 343-346.

7. Bao, W., O'Malley, D. M., Whetten, R. and Sederoff, R. R. A Laccase Associated with Lignification in Loblolly Pine Xylem. *Science*, **1993**, 260(5108), 672-674.

8. Bard, A. J. and Faulkner, L. R. Electrochemical Methods: Fundamentals and Applications. **2000**, 2nd Edition.

9. Bartlett, P. N. Bioelectrochemistry: Fundamentals, Experimental Techniques and Applications. **2008,** John Wiley & Sons.

10. Batchelor, G. K. An Introduction to Fluid Dynamics. **2000**.

11. Berezin, I. V., Bogdanovskaya, V. A., Varfolomeev, S. D., Tarasevich, M. R. and Yaropolov, A. I. Equilibrium oxygen potential in the presence of laccase. *Doklady Akademii Nauk SSSR*, **1978**, 240, 615-618.

12. Berka, R. M., Schneider, P., Golightly, E. J., Brown, S. H., Madden, M., Brown, K. M., Halkier, T., Mondorf, K. and Xu, F. Characterization of the gene encoding an extracellular laccase of Myceliophthora thermophila and analysis of the recombinant enzyme expressed in Aspergillus oryzae. *Applied and Environmental Microbiology*, **1997**, 63(8), 3151-3157.

13. Berne, B. J. and Pecora, R. Dynamic Light Scattering: With Applications to Chemistry, Biology, and Physics. **2000**, Dover Publications.

14. Bhattacharya, R. and Mukherjee, P. Biological properties of "naked" metal nanoparticles. *Advanced Drug Delivery Reviews*, **2008**, 60(11), 1289-1306.

15. Blackie, E. J., Ru, E. C. L. and Etchegoin, P. G. Single-Molecule Surface-Enhanced Raman Spectroscopy of Nonresonant Molecules. *Journal of the American Chemical Society*, **2009**, 131(40), 14466-14472.

16. Blair, D. F., Campbell, G. W., Cho, W. K., English, A. M., Fry, H. A., Lum, V., Norton, K. A., Schoonover, J. R. and Chan, S. I. Resonance Raman studies of blue copper proteins: effects of temperature and isotopic substitutions. Structural and thermodynamic implications. *Journal of the American Chemical Society*, **1985**, 107(20), 5755-5766.

17. Bollag, J. M. and Leonowicz, A. Comparative studies of extracellular fungal laccases. *Appl Environ Microbiol*, **1984**, 48(4), 849-854.

18. Bond, D. R. and Lovley, D. R. Evidence for Involvement of an Electron Shuttle in Electricity Generation by Geothrix fermentans. *Applied and Environmental Microbiology*, **2005**, 71(4), 2186-2189.

19. Brust, M., Walker, M., Bethell, D., Schiffrin, D. J. and Whyman, R. Synthesis of thiol-derivatised gold nanoparticles in a two-phase Liquid-

Liquid system. *Journal of the Chemical Society, Chemical Communications*, **1994**, (7), 801-802.

20. Bucak, S., Jones, D. A., Laibinis, P. E. and Hatton, T. A. Protein Separations Using Colloidal Magnetic Nanoparticles. *Biotechnology Progress*, **2003**, 19(2), 477-484.

21. Bulovas, A., Dirvianskyte, N., Talaikyte, Z., Niaura, G., Valentukonyte, S., Butkus, E. and Razumas, V. Electrochemical and structural properties of self-assembled monolayers of 2-methyl-3-([omega]-mercaptoalkyl)-1,4-naphthoquinones on gold. *Journal of Electroanalytical Chemistry*, **2006**, 591(2), 175-188.

22. Burda, C., Chen, X., Narayanan, R. and El-Sayed, M. A. Chemistry and Properties of Nanocrystals of Different Shapes. *Chemical Reviews*, **2005**, 105(4), 1025-1102.

23. Calabrese Barton, S., Gallaway, J. and Atanassov, P. Enzymatic Biofuel Cells for Implantable and Microscale Devices. *Chemical Reviews*, **2004**, 104(10), 4867-4886.

24. Chaudhuri, B. and Raychaudhuri, S. Manufacturing high-quality gold sol. **2001**.

25. Chefetz, B., Chen, Y. and Hadar, Y. Purification and characterization of laccase from Chaetomium thermophilium and its role in humification. *Applied and Environmental Microbiology*, **1998**, 64(9), 3175-3179.

26. Childs, R. E. and Bardsley, W. G. The steady-state kinetics of peroxidase with 2,2'-azino-di-(3-ethyl-benzthiazoline-6-sulphonic acid) as chromogen. *Biochemical Journal*, **1975**, 145(1), 93-103.

27. Chirea, M., Garcia-Morales, V., Manzanares, J. A., Pereira, C., Gulaboski, R. and Silva, F. Electrochemical Characterization of Polyelectrolyte/Gold Nanoparticle Multilayers Self-Assembled on Gold Electrodes. *Journal of Physical Chemistry B*, **2005**, 109(46), 21808-21817.

28. Chirea, M., Pereira, C. M. and Silva, F. Catalytic effect of gold nanoparticles self-assembled in multilayered polyelectrolyte films. *Journal of Physical Chemistry C*, **2007**, 111(26), 9255-9266.

29. Christenson, A., Dimcheva, N., Ferapontova, E. E., Gorton, L., Ruzgas, T., Stoica, L., Shleev, S., Yaropolov, A. I., Haltrich, D., Thorneley, R. N. F. and Aust, S. D. Direct Electron Transfer Between Ligninolytic Redox Enzymes and Electrodes. *Electroanalysis*, **2004**, 16(13-14), 1074-1092.

30. Coll, P. M., Tabernero, C., Santamaria, R. and Perez, P. Characterization and structural analysis of the laccase I gene from the newly isolated ligninolytic basidiomycete PM1 (CECT 2971). *Applied and Environmental Microbiology*, **1993**, 59(12), 4129-4135.

31. Coman, V., Vaz-Dominguez, C., Ludwig, R., Harreither, W., Haltrich, D., De Lacey, A. L., Ruzgas, T., Gorton, L. and Shleev, S. A membrane-, mediator-, cofactor-less glucose/oxygen biofuel cell. *Physical Chemistry Chemical Physics*, **2008**, 10(40), 6093-6096.

32. Creighton, J. A. and Eadon, D. G. Ultraviolet-visible absorption spectra of the colloidal metallic elements. *Journal of the Chemical Society, Faraday Transactions*, **1991**, 87(24), 3881-3891.

33. Cushing, B. L., Kolesnichenko, V. L. and O'Connor, C. J. Recent Advances in the Liquid-Phase Syntheses of Inorganic Nanoparticles. *Chemical Reviews*, **2004**, 104(9), 3893-3946.

34. De Feijter, J. A., Benjamins, J. and Veer, F. A. Ellipsometry as a tool to study the adsorption behavior of synthetic and biopolymers at the air–water interface. *Biopolymers*, **1978**, 17(7), 1759-1772.

35. Deinum, J. and Vänngård, T. The stoichiometry of the paramagnetic copper and the oxidation-reduction potentials of type I copper in human ceruloplasmin. *Biochimica et Biophysica Acta (BBA) - Protein Structure*, **1973**, 310(2), 321-330.

36. Dixon, M. The determination of enzyme inhibitor constants. *Biochemical Journal*, **1953**, 55(1), 170-171.

37.   Dixon, M. C. Quartz Crystal Microbalance with Dissipation Monitoring: Enabling Real-Time Characterization of Biological Materials and Their Interactions. *Journal of Biomolecular Techniques*, **2008**, 19, 151–158.

38.   Duran, N., Rosa, M. A., D'Annibale, A. and Gianfreda, L. Applications of laccases and tyrosinases (phenoloxidases) immobilized on different supports: a review. *Enzyme and Microbial Technology*, **2002**, 31(7), 907-931.

39.   Eddowes, M. J. and Hill, H. A. O. Novel method for the investigation of the electrochemistry of metalloproteins: cytochrome c. *Journal of the Chemical Society, Chemical Communications*, **1977**, (21), 771b-772.

40.   Ehresmann, B., Imbault, P. and Weil, J. H. Spectrophotometric determination of protein concentration in cell extracts containing tRNA and rRNA. *Analytical Biochemistry*, **1973**, 54(2), 454-463.

41.   El-Deab, M. S. and Ohsaka, T. Direct electron transfer of copper–zinc superoxide dismutase (SOD) on crystallographically oriented Au nanoparticles. *Electrochemistry Communications*, **2007**, 9(4), 651-656.

42.   Elghanian, R., Storhoff, J. J., Mucic, R. C., Letsinger, R. L. and Mirkin, C. A. Selective colorimetric detection of polynucleotides based on the distance-dependent optical properties of gold nanoparticles. *Science*, **1997**, 277(5329), 1078-1081.

43.   Enguita, F. J., Martins, L. O., Henriques, A. O. and Carrondo, M. A. Crystal Structure of a Bacterial Endospore Coat Component. *Journal of Biological Chemistry*, **2003**, 278(21), 19416-19425.

44.   Evans, J. W. Random and cooperative sequential adsorption. *Reviews of Modern Physics*, **1993**, 65(4), 1281-1329.

45.   Freire, R. S., Pessoa, C. A., Mello, L. D. and Kubota, L. T. Direct electron transfer: an approach for electrochemical biosensors with higher selectivity and sensitivity. *Journal of the Brazilian Chemical Society*, **2003**, 14, 230-243.

46. Frens, G. Controlled nucleation for the regulation of the particle size in monodisperse gold suspensions. *Nature (London), Physical Science*, **1973**, 241, 20-22.

47. Gaigalas, A. K. and Niaura, G. Measurement of Electron Transfer Rates between Adsorbed Azurin and a Gold Electrode Modified with a Hexanethiol Layer. *Journal of Colloid and Interface Science*, **1997**, 193(1), 60-70.

48. Gallaway, J., Wheeldon, I., Rincon, R., Atanassov, P., Banta, S. and Barton, S. C. Oxygen-reducing enzyme cathodes produced from SLAC, a small laccase from Streptomyces coelicolor. *Biosensors and Bioelectronics*, **2008**, 23(8), 1229-1235.

49. Gallaway, J. W. and Calabrese Barton, S. A. Effect of redox polymer synthesis on the performance of a mediated laccase oxygen cathode. *Journal of Electroanalytical Chemistry*, **2009**, 626(1-2), 149-155.

50. Gao, X., Chan, W. C. W. and Nie, S. Quantum-dot nanocrystals for ultrasensitive biological labeling and multicolor optical encoding. *Journal of Biomedical Optics*, **2002**, 7(4), 532-537.

51. Geoghegan, W. D. The effect of three variables on adsorption of rabbit *IgG* to colloidal gold. *Journal of Histochemistry & Cytochemistry*, **1988**, 36(4), 401-407.

52. Gianfreda, L., Xu, F. and Bollag, J.-M. Laccases: A Useful Group of Oxidoreductive Enzymes. *Bioremediation Journal*, **1999**, 3(1), 1-26.

53. Giardina, P., Palmieri, G., Scaloni, A., Fontanella, B., Faraco, V., Cennamo, G. and Sannia, G. Protein and gene structure of a blue laccase from *Pleurotus ostreatus*. *Biochemical Journal*, **1999**, 341(Pt 3), 655-663.

54. Gilardi, G. and Fantuzzi, A. Manipulating redox systems: application to nanotechnology. *Trends in Biotechnology*, **2001**, 19(11), 468-476.

55. Gole, A., Dash, C., Ramakrishnan, V., Sainkar, S. R., Mandale, A. B., Rao, M. and Sastry, M. Pepsin−Gold Colloid Conjugates: Preparation,

Characterization, and Enzymatic Activity. *Langmuir*, **2001**, 17(5), 1674-1679.

56. González Arzola, K., Gimeno, Y., Arévalo, M. C., Falcón, M. A. and Hernández Creus, A. Electrochemical and AFM characterization on gold and carbon electrodes of a high redox potential laccase from Fusarium proliferatum. *Bioelectrochemistry*, **2010**, 79(1), 17-24.

57. Haberska, K., Vaz-Domínguez, C., De Lacey, A. L., Dagys, M., Reimann, C. T. and Shleev, S. Direct electron transfer reactions between human ceruloplasmin and electrodes. *Bioelectrochemistry*, **2009**, 76(1–2), 34-41.

58. Haghighi, B., Jarosz-Wilkolazka, A., Ruzgas, T., Gorton, L. and Leonowicz, A. Charecterization of graphite electrodes modified with laccases from Trametes hirsuta and Cerrena unicolor and their use for flow injection amperometric determination of some phenolic compounds. *International Journal of Environmental Analytical Chemistry*, **2005**, 85, 753-770.

59. Hayat, M. A. Colloidal Gold, Volume 1: Principles, Methods, and Applications. *Colloidal Gold: Principles, Methods & Application*, **1989**.

60. Halthur, T. J. and Elofsson, U. M. Multilayers of Charged Polypeptides As Studied by in Situ Ellipsometry and Quartz Crystal Microbalance with Dissipation. *Langmuir*, **2004**, 20(5), 1739-1745.

61. Han, J., Adman, E. T., Beppu, T., Codd, R., Freeman, H. C., Huq, L., Loehr, T. M. and Sanders-Loehr, J. Resonance Raman spectra of plastocyanin and pseudoazurin: evidence for conserved cysteine ligand conformations in cupredoxins (blue copper proteins). *Biochemistry*, **1991**, 30(45), 10904-10913.

62. Harkin, J. M. and Obst, J. R. Syringaldazine, an effective reagent for detecting laccase and peroxidase in fungi. *Cellular and Molecular Life Sciences*, **1973**, 29(4), 381-387.

63. Heaven, M. W., Dass, A., White, P. S., Holt, K. M. and Murray, R. W. Crystal Structure of the Gold Nanoparticle

[N(C8H17)4][Au25(SCH2CH2Ph)18]. *Journal of the American Chemical Society*, **2008**, 130(12), 3754-3755.

64. Heinze, J. Cyclic Voltammetry - "Electrochemical Spectroscopy". New Analytical Methods (25). *Angewandte Chemie International Edition in English*, **1984**, 23(11), 831-847.

65. Henderson, R. W. and Appleby, C. A. The redox potential of leghaemoglobin. *Biochimica et Biophysica Acta (BBA) - Bioenergetics*, **1972**, 283(1), 187-191.

66. Henderson, R. W. and Rawlinson, W. A. Potentiometric and other studies on preparations of cytochrome c from ox- and horse-heart muscle. *Biochemical Journal*, **1956**, 62(1), 21-29.

67. Hermanson, G. T. Bioconjugate Techniques **1996**.

68. Hicks, J. F., Seok-Shon, Y. and Murray, R. W. Layer-by-Layer Growth of Polymer/Nanoparticle Films Containing Monolayer-Protected Gold Clusters. *Langmuir : the ACS journal of surfaces and colloids*, **2002**, 18(6), 2288-2294.

69. Hyung, K. H., Jun, K. Y., Hong, H. G., Kim, H. S. and Shin, W. Immobilization of laccase onto the gold electrode using b-mercaptopropionate. *Bulletin of the Korean Chemical Society*, **1997**, 18, 564-566.

70. Höök, F., Kasemo, B., Nylander, T., Fant, C., Sott, K. and Elwing, H. Variations in Coupled Water, Viscoelastic Properties, and Film Thickness of a *Mefp-1* Protein Film during Adsorption and Cross-Linking: A Quartz Crystal Microbalance with Dissipation Monitoring, Ellipsometry, and Surface Plasmon Resonance Study. *Analytical Chemistry*, **2001**, 73(24), 5796-5804.

71. Ivnitski, D., Branch, B., Atanassov, P. and Apblett, C. Glucose oxidase anode for biofuel cell based on direct electron transfer. *Electrochemistry Communications*, **2006**, 8(8), 1204-1210.

72. Yan, Y., Su, L. and Mao, L. Multi-walled carbon nanotube-based glucose/O_2 biofuel cell with glucose oxidase and laccase as biocatalysts. *Journal of Nanoscience and Nanotechnology*, **2007**, 7(4/5), 1625-1630.

73. Yan, Y., Zheng, W., Su, L. and Mao, L. Carbon-Nanotube-Based Glucose/O_2 Biofuel Cells. *Advanced Materials*, **2006**, 18(19), 2639-2643.

74. Yanez-Sedeno, P. and Pingarron, J. M. Gold nanoparticle-based electrochemical biosensors. *Analytical and Bioanalytical Chemistry*, **2005**, 382(4), 884-886.

75. Yaropolov, A., Skorobogat'ko, O., Vartanov, S. and Varfolomeyev, S. Laccase. *Applied Biochemistry and Biotechnology*, **1994**, 49(3), 257-280.

76. Yaropolov, A. I., Kharybin, A. N., Emnéus, J., Marko-Varga, G. and Gorton, L. Electrochemical properties of some copper-containing oxidases. *Bioelectrochemistry and Bioenergetics*, **1996**, 40(1), 49-57.

77. Yeh, P. and Kuwana, T. Reversible electrode reaction of cytochrome *c*. *Chemistry Letters*, **1977**, 6(10), 1145-1148.

78. Yoshida, H. LXIII.-Chemistry of lacquer (Urushi). Part I. Communication from the Chemical Society of Tokio. *Journal of the Chemical Society, Transactions*, **1883**, 43, 472-486.

79. Yu, A., Liang, Z., Cho, J. and Caruso, F. Nanostructured Electrochemical Sensor Based on Dense Gold Nanoparticle Films. *Nano Letters*, **2003**, 3(9), 1203-1207.

80. Jadzinsky, P. D., Calero, G., Ackerson, C. J., Bushnell, D. A. and Kornberg, R. D. Structure of a Thiol Monolayer-Protected Gold Nanoparticle at 1.1 Å Resolution. *Science*, **2007**, 318(5849), 430-433.

81. Ju, H., Liu, S., Ge, B., Lisdat, F. and Scheller, F. W. Electrochemistry of Cytochrome c Immobilized on Colloidal Gold Modified Carbon Paste Electrodes and Its Electrocatalytic Activity. *Electroanalysis*, **2002**, 14(2), 141-147.

82. Katz, E., Willner, I. and Wang, J. Electroanalytical and bioelectroanalytical systems based on metal and semiconductor nanoparticles. *Electroanalysis*, **2004**, 16(1-2), 19-44.

83. Kawai, S., Umezawa, T. and Higuchi, T. Degradation mechanisms of phenolic beta-1 lignin substructure model compounds by laccase of Coriolus versicolor. *Archives of Biochemistry and Biophysics*, **1988**, 262(1), 99-110.

84. Kennedy, B. J., Spaeth, S., Dickey, M. and Carron, K. T. Determination of the Distance Dependence and Experimental Effects for Modified SERS Substrates Based on Self-Assembled Monolayers Formed Using Alkanethiols. *The Journal of Physical Chemistry B*, **1999**, 103(18), 3640-3646.

85. Kiefer-Meyer, M.-C., Gomord, V., O'Connell, A., Halpin, C. and Faye, L. Cloning and sequence analysis of laccase-encoding cDNA clones from tobacco. *Gene*, **1996**, 178(1–2), 205-207.

86. Kim, B. H., Chang, I. S., Cheol Gil, G., Park, H. S. and Kim, H. J. Novel BOD (biological oxygen demand) sensor using mediator-less microbial fuel cell. *Biotechnology Letters*, **2003**, 25(7), 541-545.

87. Kim, J., Jia, H. and Wang, P. Challenges in biocatalysis for enzyme-based biofuel cells. *Biotechnology Advances*, **2006**, 24(3), 296-308.

88. Kneipp, K., Moskovits, M. and Kneipp, H. Surface-enhanced Raman Scattering: Physics And Applications. **2006,** Springer.

89. Koppenol, W. H. and Butler, J. Energetics of Interconversion Reactions of Oxyradicals. *Advances in Free Radical Biology & Medicine*, **1985**, 1(1), 91-131.

90. Koudelka, G. B. and Ettinger, M. J. Fluoride effects on the activity of Rhus laccase and the catalytic mechanism under steady-state conditions. *Journal of Biological Chemistry*, **1988**, 263(8), 3698-3705.

91. Kovacs, G. J., Loutfy, R. O., Vincent, P. S., Jennings, C. and Aroca, R. Distance dependence of SERS enhancement factor from Langmuir-

Blodgett monolayers on metal island films: evidence for the electromagnetic mechanism. *Langmuir 2*, **1986**, 679-694.

92. Kruus, K. Laccase: a useful enzyme for industrial applications. *Kemia - Kemi*, **2000**, 27(3), 184-186.

93. Kulys, J., Bratkovskaja, I. and Vidziunaite, R. Laccase-catalysed iodide oxidation in presence of methyl syringate. *Biotechnology and Bioengineering*, **2005**, 92(1), 124-128.

94. Kumar, S., Aaron, J. and Sokolov, K. Directional conjugation of antibodies to nanoparticles for synthesis of multiplexed optical contrast agents with both delivery and targeting moieties. *Nature Protocols*, **2008**, 3(2), 314-320.

95. Kunamneni, A., Plou, F. J., Ballesteros, A. and Alcalde, M. Laccases and their applications: a patent review. *Recent Patents on Biotechnology*, **2008**, 2(1), 10-24.

96. Kuznetsov, B. A., Mestechkina, N. M. and Shumakovich, G. P. electrochemical behaviour of proteins containing coenzyme groups and metals. *Bioelectrochemistry and Bioenergetics*, **1977**, 4(1), 1-17.

97. LaFayette, P. R., Eriksson, K.-E. L. and Dean, J. F. D. Characterization and heterologous expression of laccase cDNAs from xylem tissues of yellow-poplar (Liriodendron tulipifera). *Plant Molecular Biology*, **1999**, 40(1), 23-35.

98. Lee, C.-W., Gray, H. B., Anson, F. C. and Malmström, B. G. Catalysis of the reduction of dioxygen at graphite electrodes coated with fungal laccase A. *Journal of Electroanalytical Chemistry and Interfacial Electrochemistry*, **1984**, 172(1–2), 289-300.

99. Leonowicz, A., Cho, N., Luterek, J., Wilkolazka, A., Wojtas-Wasilewska, M., Matuszewska, A., Hofrichter, M., Wesenberg, D. and Rogalski, J. Fungal laccase: properties and activity on lignin. *Journal of Basic Microbiology*, **2001**, 41(3-4), 185-227.

100. Levich, V. G. and Spalding, D. B. Physicochemical hydrodynamics: V.G. Levich festschrift. **1977**.

101. Lin, Z., Cui, S., Zhang, H., Chen, Q., Yang, B., Su, X., Zhang, J. and Jin, Q. Studies on quantum dots synthesized in aqueous solution for biological labeling via electrostatic interaction. *Analytical Biochemistry*, **2003**, 319(2), 239-243.

102. Lindley, P. F., Card, G., Zaitseva, I., Zaitsev, V., Reinhammar, B., Selin-Lindgren, E. and Yoshida, K. An X-ray structural study of human ceruloplasmin in relation to ferroxidase activity. *Journal of Biological Inorganic Chemistry*, **1997**, 2(4), 454-463.

103. Liu, S. and Ju, H. Electrocatalysis via Direct Electrochemistry of Myoglobin Immobilized on Colloidal Gold Nanoparticles. *Electroanalysis*, **2003**, 15(18), 1488-1493.

104. Liu, S., Leech, D. and Ju, H. Application of colloidal gold in protein immobilization, electron transfer, and biosensing. *Analytical Letters*, **2003**, 36(1), 1-19.

105. Liz-Marzán, L. M. and Mulvaney, P. The Assembly of Coated Nanocrystals†. *The Journal of Physical Chemistry B*, **2003**, 107(30), 7312-7326.

106. Lowry, O. H., Rosebrough, N. J., Farr, A. L. and Randall, R. J. Protein measurement with the Folin phenol reagent. *Journal of Biological Chemistry*, **1951**, 193(1), 265-275.

107. Luo, X.-L., Xu, J.-J., Du, Y. and Chen, H.-Y. A glucose biosensor based on chitosan-glucose oxidase-gold nanoparticles biocomposite formed by one-step electrodeposition. *Analytical Biochemistry*, **2004**, 334(2), 284-289.

108. Luo, X., Morrin, A., Killard, A. J. and Smyth, M. R. Application of nanoparticles in electrochemical sensors and biosensors. *Electroanalysis*, **2006**, 18(4), 319-326.

109. Machonkin, T. E. and Solomon, E. I. The Thermodynamics, Kinetics, and Molecular Mechanism of Intramolecular Electron Transfer in Human Ceruloplasmin. *Journal of the American Chemical Society*, **2000**, 122(50), 12547-12560.

110. Mafuné, F., Kohno, J.-y., Takeda, Y., Kondow, T. and Sawabe, H. Formation of Gold Nanoparticles by Laser Ablation in Aqueous Solution of Surfactant. *The Journal of Physical Chemistry B*, **2001**, 105(22), 5114-5120.

111. Mayer, A. M. and Staples, R. C. Laccase: new functions for an old enzyme. *Phytochemistry*, **2002**, 60(6), 551-565.

112. Maxwell, D. J., Taylor, J. R. and Nie, S. Self-assembled nanoparticle probes for recognition and detection of biomolecules. *Journal of American Chemical Society*, **2002**, 124(32), 9606-9612.

113. McFarland, A. D., Haynes, C. L., Mirkin, C. A., Van Duyne, R. P. and Godwin, H. A. Color My Nanoworld. *Journal of Chemical Education*, **2004**, 81(4), 544A.

114. McIlvaine, T. C. A Buffer Solution for Colorimetric Comparison. *Journal of Biological Chemistry*, **1921**, 49(1), 183-186.

115. Messerschmidt, A. ChemInform Abstract: Blue Copper Oxidases. *ChemInform*, **1994**, 25(43), no-no.

116. Messerschmidt, A., Ladenstein, R., Huber, R., Bolognesi, M., Avigliano, L., Petruzzelli, R., Rossi, A. and Finazzi-Agro, A. Refined crystal structure of ascorbate oxidase at 1.9 A resolution. *Journal of Molecular Biology*, **1992**, 224(1), 179-205.

117. Minussi, R. C., Miranda, M. A., Silva, J. A., Ferreira, C. V., Aoyama, H., Marangoni, S., Rotilio, D., Pastore, G. M. and Duran, N. Purification, characterization and application of laccase from *Trametes versicolor* for colour and phenolic removal of olive mill wastewater in the presence of 1-hydroxybenzotriazole. *African Journal of Biotechnology*, **2007**, 6(10), 1248-1254.

118. Minussi, R. C., Pastore, G. M. and Duran, N. Potential applications of laccase in the food industry. *Trends in Food Science and Technology*, **2002**, 13(6-7), 205-216.

119. Misiūnas, A., Talaikytė, Z., Niaura, G., Razumas, V. and Nylander, T. Thermomyces lanuginosus lipase in the liquid-crystalline phases of

aqueous phytantriol: X-ray diffraction and vibrational spectroscopic studies. *Biophysical Chemistry*, **2008**, 134(3), 144-156.

120. Moon, H., Chang, I. S. and Kim, B. H. Continuous electricity production from artificial wastewater using a mediator-less microbial fuel cell. *Bioresource Technology*, **2006**, 97(4), 621-627.

121. Moore, C. M., Akers, N. L., Hill, A. D., Johnson, Z. C. and Minteer, S. D. Improving the Environment for Immobilized Dehydrogenase Enzymes by Modifying Nafion with Tetraalkylammonium Bromides. *Biomacromolecules*, **2004**, 5(4), 1241-1247.

122. Morozova, O., Shumakovich, G., Shleev, S. and Yaropolov, Y. Laccase-mediator systems and their applications: A review. *Applied Biochemistry and Microbiology*, **2007**, 43(5), 523-535.

123. Mulvaney, P. Surface Plasmon Spectroscopy of Nanosized Metal Particles. *Langmuir*, **1996**, 12(3), 788-800.

124. Munro, C. H., Smith, W. E., Garner, M., Clarkson, J. and White, P. C. Characterization of the Surface of a Citrate-Reduced Colloid Optimized for Use as a Substrate for Surface-Enhanced Resonance Raman Scattering. *Langmuir*, **1995**, 11(10), 3712-3720.

125. Murata, K., Kajiya, K., Nakamura, N. and Ohno, H. Direct electrochemistry of bilirubin oxidase on three-dimensional gold nanoparticle electrodes and its application in a biofuel cell. *Energy & Environmental Science*, **2009**, 2(12), 1280-1285.

126. Murray, C. A. and Allara, D. L. Measurement of the molecule--silver separation dependence of surface enhanced Raman scattering in multilayered structures. *The Journal of Chemical Physics*, **1982**, 76(3), 1290-1303.

127. Niaura, G., Gaigalas, A. K. and Vilker, V. L. Moving spectroelectrochemical cell for surface Raman spectroscopy. *Journal of Raman Spectroscopy*, **1997**, 28(12), 1009-1011.

128. Nishizawa, Y., Nakabayashi, K. and Shinagawa, E. Purification and characterization of laccase from white rot fungus *Trametes sanguinea*

M85-2. Journal of Fermentation and Bioengineering, **1995**, 80(1), 91-93.

129. Nyholm, R. S. Chemical periodicity - By R. T. Sanderson. Pp. x + 330. Reinhold Publishing Corporation, New York; Chapman and Hall Ltd, London. 1960. 94s. net. *Endeavour*, **1961**, 20(79), 168-168.

130. Palmore, G. T. R. Biofuel Cells. Bioelectrochemistry. *John Wiley & Sons, Ltd,* **2008**: 359-375.

131. Palmore, G. T. R. and Whitesides George, M. Microbial and Enzymatic Biofuel Cells. Enzymatic Conversion of Biomass for Fuels Production. *American Chemical Society,* **1994,** 566: 271-290.

132. Petkov, V., Peng, Y., Williams, G., Huang, B., Tomalia, D. and Ren, Y. Structure of gold nanoparticles suspended in water studied by x-ray diffraction and computer simulations. *Physical Review B*, **2005**, 72(19), 195402.

133. Pingarron, J. M., Yanez-Sedeno, P. and Gonzalez-Cortes, A. Gold nanoparticle-based electrochemical biosensors. *Electrochimica Acta*, **2008**, 53(19), 5848-5866.

134. Piontek, K., Antorini, M. and Choinowski, T. Crystal Structure of a Laccase from the Fungus *Trametes versicolor* at 1.90 Å Resolution Containing a Full Complement of Coppers. *Journal of Biological Chemistry*, **2002**, 277(40), 37663-37669.

135. Pita, M., Gutierrez-Sanchez, C., Olea, D., Velez, M., Garcia-Diego, C., Shleev, S., Fernandez, V. M. and De Lacey, A. L. High Redox Potential Cathode Based on Laccase Covalently Attached to Gold Electrode. *The Journal of Physical Chemistry C*, **2011**, 115(27), 13420-13428.

136. Podstawka, E., Niaura, G. and Proniewicz, L. M. Potential-Dependent Studies on the Interaction between Phenylalanine-Substituted Bombesin Fragments and Roughened Ag, Au, and Cu Electrode Surfaces. *The Journal of Physical Chemistry B*, **2009**, 114(2), 1010-1029.

137. Pong, B.-K., Elim, H. I., Chong, J.-X., Ji, W., Trout, B. L. and Lee, J.-Y. New Insights on the Nanoparticle Growth Mechanism in the Citrate

Reduction of Gold(III) Salt: Formation of the Au Nanowire Intermediate and Its Nonlinear Optical Properties. *The Journal of Physical Chemistry C*, **2007**, 111(17), 6281-6287.

138. Q-Sense. Quarzt crystal microbalance with dissipation (QCM-D) - technology note.

139. Ramírez, P., Mano, N., Andreu, R., Ruzgas, T., Heller, A., Gorton, L. and Shleev, S. Direct electron transfer from graphite and functionalized gold electrodes to T1 and T2/T3 copper centers of bilirubin oxidase. *Biochimica et Biophysica Acta*, **2008**, 1777, 1364–1369.

140. Ranocha, P., McDougall, G., Hawkins, S., Sterjiades, R., Borderies, G., Stewart, D., Cabanes-Macheteau, M., Boudet, A.-M. and Goffner, D. Biochemical characterization, molecular cloning and expression of laccases – a divergent gene family – in poplar. *European Journal of Biochemistry*, **1999**, 259(1-2), 485-495.

141. Razmute-Razme, I., Kuodis, Z., Eicher-Lorka, O. and Niaura, G. SERS observation of soft C-H vibrational mode of bifunctional alkanethiol molecules adsorbed at Au and Ag electrodes. *Physical Chemistry Chemical Physics*, **2010**, 12(18), 4564-4568.

142. Razumas, V. J., Vidugiris, G. J. A., Zapalskyté, A. A., Gudavičius, A. V. and Kulys, J. J. 855 — Electrochemical conversion of lactoperoxidase, ceruloplasmin and alkaline phosphatase on mercury electrodes. *Bioelectrochemistry and Bioenergetics*, **1986**, 15(3), 407-415.

143. Rodahl, M., Hook, F., Fredriksson, C., A. Keller, C., Krozer, A., Brzezinski, P., Voinova, M. and Kasemo, B. Simultaneous frequency and dissipation factor QCM measurements of biomolecular adsorption and cell adhesion. *Faraday Discuss.*, **1997**, 107, 229-246.

144. Sakurai, T. Anaerobic reactions of *Rhus vernicifera* laccase and its type-2 copper-depleted derivatives with hexacyanoferrate(II). *Biochemical Journal*, **1992**, 284(Pt 3), 681-685.

145. Santucci, R., Ferri, T., Morpurgo, L., Savini, I. and Avigliano, L. Unmediated heterogeneous electron transfer reaction of ascorbate oxidase and laccase at a gold electrode. *Biochemical Journal*, **1998**, 332, 611-615.

146. Sato, Y., Wuli, B., Sederoff, R. and Whetten, R. Molecular Cloning and Expression of Eight Laccase cDNAs in Loblolly Pine (*Pinus taeda*)*. *Journal of Plant Research*, **2001**, 114(2), 147-155.

147. Sauerbrey, G. Verwendung von Schwingquarzen zur Wägung dünner Schichten und zur Mikrowägung. *Zeitschrift für Physik A Hadrons and Nuclei*, **1959**, 155(2), 206-222.

148. Schaaff, T. G., Shafigullin, M. N., Khoury, J. T., Vezmar, I., Whetten, R. L., Cullen, W. G., First, P. N., Gutiérrez-Wing, C., Ascensio, J. and Jose-Yacamán, M. J. Isolation of Smaller Nanocrystal Au Molecules: Robust Quantum Effects in Optical Spectra. *The Journal of Physical Chemistry B*, **1997**, 101(40), 7885-7891.

149. Scheinberg, I. H. and Gitlin, D. Deficiency of ceruloplasmin in patients with hepatolenticular degeneration (Wilson's disease). *Science*, **1952**, 116(3018), 484-485.

150. Schellenberg, K. A. and Hellerman, L. Oxidation of reduced diphosphopyridine nucleotide. *Journal of Biological Chemistry*, **1958**, 231(1), 547-556.

151. Schmid, G. and Corain, B. Nanoparticulated gold: syntheses, structures, electronics, and reactivities. *European Journal of Inorganic Chemistry*, **2003**, 3081-3098.

152. Schmitt, J., Decher, G., Dressick, W. J., Brandow, S. L., Geer, R. E., Shashidhar, R. and Calvert, J. M. Metal nanoparticle/polymer superlattice films. Fabrication and control of layer structure. *Advanced Materials,* **1997**, 9(1), 61-65.

153. Schneider, P., Caspersen, M. B., Mondorf, K., Halkier, T., Skov, L. K., Østergaard, P. R., Brown, K. M., Brown, S. H. and Xu, F.

Characterization of a *Coprinus cinereus* laccase. *Enzyme and Microbial Technology*, **1999**, 25(6), 502-508.

154. Shin, W., Sundaram, U. M., Cole, J. L., Zhang, H. H., Hedman, B., Hodgson, K. O. and Solomon, E. I. Chemical and Spectroscopic Definition of the Peroxide-Level Intermediate in the Multicopper Oxidases: Relevance to the Catalytic Mechanism of Dioxygen Reduction to Water. *Journal of the American Chemical Society*, **1996**, 118(13), 3202-3215.

155. Shleev, S., Andoralov, V., Falk, M., Reimann, C. T., Ruzgas, T., Srnec, M., Ryde, U. and Rulíšek, L. On the Possibility of Uphill Intramolecular Electron Transfer in Multicopper Oxidases: Electrochemical and Quantum Chemical Study of Bilirubin Oxidase. *Electroanalysis*, **2012**, 24(7), 1524-1540.

156. Shleev, S., Christenson, A., Serezhenkov, V., Burbaev, D., Yaropolov, A., Gorton, L. and Ruzgas, T. Electrochemical redox transformations of T1 and T2 copper sites in native *Trametes hirsuta* laccase at gold electrode. *Biochemical Journal*, **2005**, 385, 745–754.

157. Shleev, S., Jarosz-Wilkolazka, A., Khalunina, A., Morozova, O., Yaropolov, A., Ruzgas, T. and Gorton, L. Direct electron transfer reactions of laccases from different origins on carbon electrodes. *Bioelectrochemistry*, **2005**, 67, 115 – 124.

158. Shleev, S., Kuznetsov, S. V. and Topunov, A. F. A bioelectrochemical cell allowing simultaneous spectrophotometric control of the analyte. *Applied Biochemistry and Microbiology*, **2000**, 36(3), 306-309.

159. Shleev, S., Nikitina, O., Christenson, A., Reimann, C. T., Yaropolov, A. I., Ruzgas, T. and Gorton, L. Characterization of two new multiforms of *Trametes pubescens* laccase. *Bioorganic Chemistry*, **2007**, 35(1), 35-49.

160. Shleev, S. and Ruzgas, T. Transistor-Like Behavior of a Fungal Laccase. *Angewandte Chemie International Edition*, **2008**, 47, 7270 – 7274.

161. Shleev, S., Tkac, J., Christenson, A., Ruzgas, T., Yaropolov, A. I., Whittaker, J. W. and Gorton, L. Direct electron transfer between copper-containing proteins and electrodes. *Biosensors and Bioelectronics*, **2005**, 20(12), 2517-2554.

162. Shleev, S. V., Morozova, O. V., Nikitina, O. V., Gorshina, E. S., Rusinova, T. V., Serezhenkov, V. A., Burbaev, D. S., Gazaryan, I. G. and Yaropolov, A. I. Comparison of physico-chemical characteristics of four laccases from different basidiomycetes. *Biochimie*, **2004**, 86(9-10), 693-703.

163. Shleev, S. V., Zaitseva, E. A., Gorshina, E. S., Morozova, O. V., Serezhenkov, V. A., Burbaev, D. S., Kuznetsov, B. A. and Yaropolov, A. I. Spectral and electrochemical study of laccases from basidiomycetes. *Moscow University Chemistry Bulletin*, **2003**, 44, 35-39.

164. Smith, E. and Dent, G. Modern Raman Spectroscopy: A Practical Approach. **2005,** J. Wiley.

165. Solomon, E. I., Sundaram, U. M. and Machonkin, T. E. Multicopper Oxidases and Oxygenases. *Chemical Reviews*, **1996**, 96(7), 2563-2606.

166. Song, W.-J., Du, J.-Z., Sun, T.-M., Zhang, P.-Z. and Wang, J. Gold Nanoparticles Capped with Polyethyleneimine for Enhanced siRNA Delivery. *Small*, **2010**, 6(2), 239-246.

167. Sperling, R. A. and Parak, W. J. Surface modification, functionalization and bioconjugation of colloidal inorganic nanoparticles. *Philosophical Transactions of the Royal Society A: Mathematical, Physical and Engineering Sciences*, **2010**, 368(1915), 1333-1383.

168. Sperling, R. A., Rivera Gil, P., Zhang, F., Zanella, M. and Parak, W. J. Biological applications of gold nanoparticles. *Chemical Society Reviews*, **2008**, 37(9), 1896-1908.

169. Sterjiades, R., Dean, J. F. D. and Eriksson, K.-E. L. Laccase from Sycamore Maple (*Acer pseudoplatanus*) Polymerizes Monolignols. *Plant Physiology*, **1992**, 99(3), 1162-1168.

170. Studničková, M., Pitřincová, J. and Kovář, J. The electrochemical behaviour of copper proteins using differential pulse polarography. *Bioelectrochemistry and Bioenergetics*, **1991**, 25(1), 109-120.

171. Sucheta, A., Cammack, R., Weiner, J. and Armstrong, F. A. Reversible electrochemistry of fumarate reductase immobilized on an electrode surface. Direct voltammetric observations of redox centers and their participation in rapid catalytic electron transport. *Biochemistry*, **1993**, 32(20), 5455-5465.

172. Suzuki, M., Murata, K., Nakamura, N. and Ohno, H. The Effect of Particle Size on the Direct Electron Transfer Reactions of Metalloproteins Using Au Nanoparticle-Modified Electrodes. *Electrochemistry*, **2012**, 80(5), 337-339.

173. Taylor, J. F. and Hastings, A. B. Oxidation-reduction potentials of the methemoglobin-hemoglobin system. *Journal of Biological Chemistry*, **1939**, 131(2), 649-662.

174. Tarasevich, M. R., Bogdanovskaya, V. A. and Kuznetsova, L. N. Bioelectrocatalytic Reduction of Oxygen in the Presence of Laccase Adsorbed on Carbon Electrodes. *Russian Journal of Electrochemistry*, **2001**, 37(8), 833-837.

175. Tarasevich, M. R., Yaropolov, A. I., Bogdanovskaya, V. A. and Varfolomeev, S. D. Electrocatalysis of a cathodic oxygen reduction by laccase. *Bioelectrochemsitry and Bioenergetics*, **1979**, 6, 393-403.

176. Temp, U. and Eggert, C. Novel Interaction between Laccase and Cellobiose Dehydrogenase during Pigment Synthesis in the White Rot Fungus *Pycnoporus cinnabarinus*. *Applied and Environmental Microbiology*, **1999**, 65(2), 389-395.

177. Thurston, C. F. The structure and function of fungal laccases. *Microbiology*, **1994**, 140(1), 19-26.

178. Tiberg, F. Physical characterization of non-ionic surfactant layers adsorbed at hydrophilic and hydrophobic solid surfaces by time-

resolved ellipsometry. *Journal of the Chemical Society, Faraday Transactions*, **1996**, 92(4), 531-538.

179. Tiberg, F. and Landgren, M. Characterization of thin nonionic surfactant films at the silica/water interface by means of ellipsometry. *Langmuir*, **1993**, 9(4), 927-932.

180. Turkevich, J. Colloidal gold. Part I. *Gold Bulletin*, **1985**, 18(3), 86-91.

181. Turkevich, J., Stevenson, P. C. and Hillier, J. A study of the nucleation and growth processes in the synthesis of colloidal gold. *Discussions of the Faraday Society*, **1951**, 11, 55-75.

182. Vasil'chenko, L. G., Koroleva, O. V., Stepanova, E. V., Landesman, E. O. and Rabinovich, M. L. Isolation and characteristics of micromycetes--producers of neutral phenol oxidase from trophic soil with a high level of dioxins. *Prikladnaia Biokhimiia i Mikrobiologiia*, **2000**, 36(4), 412-421.

183. Voinova, M. V., Rodahl, M., Jonson, M. and Kasemo, B. Viscoelastic Acoustic Response of Layered Polymer Films at Fluid-Solid Interfaces: Continuum Mechanics Approach. *Physica Scripta*, **1999**, 59(5), 391.

184. Wen, Z.-Q. Raman spectroscopy of protein pharmaceuticals. *Journal of Pharmaceutical Sciences*, **2007**, 96(11), 2861-2878.

185. Wherland, S., Holwerda, R. A., Rosenberg, R. C. and Gray, H. B. Kinetic studies of the reduction of blue copper proteins by iron(EDTA)$^{2-}$. *Journal of the American Chemical Society*, **1975**, 97(18), 5260-5262.

186. Willner, B., Katz, E. and Willner, I. Electrical contacting of redox proteins by nanotechnological means. *Current Opinion in Biotechnology*, **2006**, 17(6), 589-596.

187. Xiao, Y., Patolsky, F., Katz, E., Hainfeld, J. F. and Willner, I. "Plugging into Enzymes": Nanowiring of Redox Enzymes by a Gold Nanoparticle. *Science (Washington, DC, U. S.)*, **2003**, 299(5614), 1877-1881.

188. Xu, F. Catalysis of novel enzymatic iodide oxidation by fungal laccase. *Applied Biochemistry and Biotechnology*, **1996**, 59(3), 221-230.

189. Xu, F. Oxidation of phenols, anilines, and benzenethiols by fungal laccases: correlation between activity and redox potentials as well as halide inhibition. *Biochemistry*, **1996**, 35(23), 7608-7614.

190. Xu, F. Effects of Redox Potential and Hydroxide Inhibition on the pH Activity Profile of Fungal Laccases. *Journal of Biological Chemistry*, **1997**, 272(2), 924-928.

191. Xu, F., Brown, S. H., Wahleithner, J. A., Sundaram, U. M. and Solomon, E. I. A study of a series of recombinant fungal laccases and bilirubin oxidase that exhibit significant differences in redox potential, substrate specificity, and stability. *Biochimica et Biophysica Acta*, **1996**, 1292, 303-311.

192. Zhao, J., Bradbury, C. R. and Fermin, D. J. Long-Range Electronic Communication between Metal Nanoparticles and Electrode Surfaces Separated by Polyelectrolyte Multilayer Films. *Journal of Physical Chemistry C*, **2008**, 112(17), 6832-6841.

193. Zhao, J., Henkens, R. W., Stonehuerner, J., O'Daly, J. P. and Crumbliss, A. L. Direct electron transfer at horseradish peroxidase - colloidal gold modified electrodes. *Journal of Electroanalytical Chemistry*, **1992**, 327(1–2), 109-119.

194. Zhao, J. and Kwan, H. S. Characterization, molecular cloning, and differential expression analysis of laccase genes from the edible mushroom *Lentinula edodes*. *Applied and Environmental Microbiology*, **1999**, 65(11), 4908-4913.

195. Zheng, W., Li, Q., Su, L., Yan, Y., Zhang, J. and Mao, L. Direct Electrochemistry of Multi-Copper Oxidases at Carbon Nanotubes Noncovalently Functionalized with Cellulose Derivatives. *Electroanalysis*, **2006**, 18(6), 587-594.